

RICE UNIVERSITY

**ELUCIDATION OF THE UNIQUE TRANSLATION OF  
ANGIOGENIC SIGNALING BY AORTIC VALVE CELLS**

by

**Christopher Alexander Arevalos**

A THESIS SUBMITTED  
IN PARTIAL FULFILLMENT OF THE  
REQUIREMENTS FOR THE DEGREE

**Doctor of Philosophy**

APPROVED, THESIS COMMITTEE



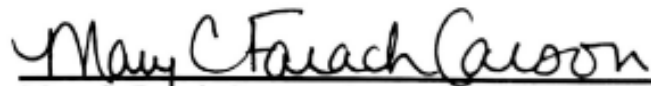
---

K. Jane Grande-Allen, Ph.D., Chair,  
Isabel C. Cameron Professor, Department of  
Bioengineering



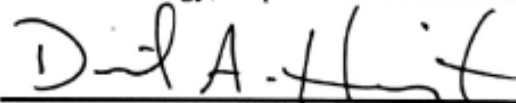
---

Amina A. Qutub, Ph.D.  
Assistant Professor of Bioengineering, Department of  
Bioengineering



---

Mary C. Farach-Carson, Ph.D.  
Ralph and Dorothy Looney Professor of Biochemistry  
and Cell Biology, Department of Biosciences



---

Daniel Harrington, Ph.D.  
Faculty Fellow of Biochemistry and Cell Biology,  
Department of Biosciences

HOUSTON, TEXAS  
December 2015

Copyright

Christopher Alexander Arevalos

2015

RICE UNIVERSITY

**ELUCIDATION OF THE UNIQUE TRANSLATION OF  
ANGIOGENIC SIGNALING BY AORTIC VALVE CELLS**

by

**Christopher Alexander Arevalos**

A THESIS SUBMITTED  
IN PARTIAL FULFILLMENT OF THE  
REQUIREMENTS FOR THE DEGREE

**Doctor of Philosophy**

APPROVED, THESIS COMMITTEE

---

K. Jane Grande-Allen, Ph.D., Chair  
Isabel C. Cameron Professor, Department of  
Bioengineering

---

Amina A. Qutub, Ph.D.  
Assistant Professor of Bioengineering

---

Mary C. Farach-Carson, Ph.D.  
Ralph and Dorothy Looney Professor of  
Biochemistry and Cell Biology, Department of  
Biosciences

---

Daniel Harrington, Ph.D.  
Faculty Fellow of Biochemistry and Cell  
Biology, Department of Biosciences

HOUSTON, TEXAS  
December 2015

# ABSTRACT

## ELUCIDATION OF THE UNIQUE TRANSLATION OF ANGIOGENIC SIGNALING BY AORTIC VALVE CELLS

by

**Christopher Alexander Arevalos**

Angiogenesis is a fundamental biological process but is a critical step in the progression of calcific aortic valve disease (CAVD). However, the process through which native valve cells, valve endothelial cells (VECs) and valve interstitial cells (VICs), form the neovascularization exhibited during CAVD is unclear due to their atypical translation of several angiogenesis related signals. Therefore, the *in vitro* angiogenic capacity of valve endothelial cells was characterized and compared to vascular derived endothelial cells. Their vasculogenic networks were demonstrated to be quantitatively and morphologically different from the networks generated by a vascular endothelial cell line, but the geometry of the VECs' networks could be manipulated with small molecule Rho GTPase inhibitors, similar to previous studies of vascular endothelial cells, thus demonstrating typical and atypical ways in which VECs translate angiogenic signals. Next, the pericyte-like capacity of VICs was demonstrated by tracking fluorescently marked VECs and VICs in a long term *in vitro* angiogenesis co-culture assay. VICs regulated early VEC network organization in a ROCK-dependent manner, wrapping themselves around VEC network edges in a manner similar to a pericyte cell line. Using a novel method to quantify the Lagrangian-corrected chemoattraction of one cell type towards another in a mixed population, we identified and quantified a subpopulation of VICs that demonstrated a pericyte-like chemoattraction towards VECs. Directly comparing valve cell co-cultures to vascular cell co-cultures revealed that unlike vascular control cells, the valve cell cultures ultimately formed invasive spheroids with 3D sprouts. These 3D sprouts were found to have several markers typical of *in vivo* angiogenic root sprouts such as delta-like ligand 4 and  $\beta$ -catenin polarity. VECs co-cultured with VICs displayed significantly more invasion than VECs alone; interestingly, VICs were found leading and wrapping around VEC invasive sprouts demonstrating both tip cell and pericyte behaviors. Angiopoietin1-Tie2 signaling was found to regulate valve cell

organization during VEC/VIC spheroid formation and invasion. Long term co-cultures demonstrated pronounced deviation of several angiogenesis and pericyte markers when measured with qRT-PCR. In the next study, mechanical stimulation is known to be a strong regulator of vascular endothelial cell angiogenic capacity, but its role in regulating VEC angiogenic capacity physiologically or pathologically was unknown. Therefore, experiments were performed to examine the effect of cyclic uni-axial strain on regulating the response of valve endothelial cells to an *in vitro* angiogenesis model. Network analysis revealed a strong pattern that strain decreases the propensity of VECs to form networks. Finally, the factors that govern VEC angiogenesis were investigated from the network scale down using tissue engineering strategies. Vascular networks of varying complexity can be designed within engineered tissues, but the amount of biological complexity necessary for proper biological functionality is unclear, as more complex is not necessarily better or necessary. Since VEC network complexity had been demonstrated to be sensitive to changes in actin regulators, this study used VECs as a framework to examine the fundamental relationship between network structure and endothelial cell biology more specifically it was tested whether the internal signaling biology of endothelial cells could be tuned based upon spatially-defined synthetic networks. Notable differences in several angiogenesis related markers were found as a function of the pattern the cells were seeded on, including several markers for actin activity regulators as well as changes in actin alignment, mimicking changes in signaling previously observed in *in vitro* angiogenesis models with VECs. Overall, this work has contributed to the understanding of the translation of angiogenic signals by valve cells and its potential role in the pathogenesis of valvular disease. Understanding from these studies can be applied to future studies of valve diseases with a similar framework to clarify the role of angiogenic signaling in the pathology of CAVD. This insight will allow development of targeted therapeutic strategies for the treatment of valvular diseases, as well as strategies to assess what level of complexity is sufficient to induce functional angiogenesis in tissue engineered constructs, such as those needed in pediatric aortic valve replacements.



# Acknowledgments

“A person who has become conscious of the absurd is for ever bound to it. A man devoid of hope and conscious of being so has ceased to belong to the future. That is natural. But it is just as natural that he should strive to escape the universe of which he is the creator...I fancy Sisyphus returning toward his rock, when the images of earth cling too tightly to memory, when the call of happiness becomes too insistent, it happens that melancholy arises in man's heart: this is the rock's victory, this is the rock itself.... [However] happiness and the absurd are two sons of the same earth. They are inseparable.... At each of those moments when he leaves the heights and gradually sinks toward the lairs of the gods, he is superior to his fate. He is stronger than his rock...if this myth is tragic, that is because its hero is conscious...All Sisyphus' silent joy is contained therein. His fate belongs to him. His rock is his thing... The struggle itself toward the heights is enough to fill a man's heart. One must imagine Sisyphus happy”

-Albert Camus

I have always felt a great connection with the Greek classics upon learning my name originated from the legend of Iskander. Therefore, I can think of no better way to begin the acknowledgments section of this thesis as I reflect back on my time in graduate school than with the thoughts of Albert Camus on the tale of Sisyphus, because I think there exists no better parable for the journey towards a Ph.D. Although there is much insight in this quote, I find there is an important element missing. That is on this journey we are not alone as we push our rock up the hill each day. I can say from my own experience that at times when the rock was close to victory, it was the support of my friends, lab mates, family, and loved ones that gave me the strength to be stronger than the rock and continue the struggle. Therefore I would like to thank in no specific order Hubert Tseng, Liezl Balaoing, Dena Wiltz, Monica Fahrenholtz, Logan Chih-Wei, Xing Zhu, Dan Pupieri, Jerahme Martinez, Mathew Sapp, Patrick Connel, Reid Wilson, Fergus Wong, future and past Grande-Allen lab mates, my undergraduate assistants of Amada Abrego, Abir Khan, Amy Rupert, Amanda Walborn, Jonathan Berg, Claudia Irinodo, Jacqueline Nyguen, Erika Dankers, Briana Acosta, my family, my mentors, my committee, my Saranas family including my co-founder brother from another family Dr. Mehdi Razavi, and Marianne Beynon who I am unfortunately literarily

incapable of expressing all of which you have meant to me over the years. I would like to acknowledge the AHA, AGEP, and the NSF for their support of this work and of myself. Lastly, I would like to thank Dr. Grande-Allen for accepting me into her lab and her continued support as a paragon of guidance and mentorship and continually encouraging me to explore my moonstruck ideas and ideals.

In this context however, I do not use struggle in a negative context. To me, the purpose of graduate school is the struggle and learning to love the struggle, because the struggle never ends in a career when we continue to explore into the unknown and live to fully examine this world around us be it in biology, physics, or philosophy. Perhaps this is why all Ph.Ds. are all given the same title, because they all share the same inherent journey. So my parting advice to any graduate student who may be reading this in the future, is to not give up, surround yourself with people who will give you strength, and to learn to embrace and to fill your heart with love for the struggle.



# Table of Contents

<b>Acknowledgments</b> .....	<b>v</b>
<b>Table of Contents</b> .....	<b>vii</b>
<b>List of Figures</b> .....	<b>xi</b>
<b>List of Tables</b> .....	<b>xix</b>
<b>List of Abbreviations</b> .....	<b>xx</b>
<b>Introduction</b> .....	<b>23</b>
<b>Background and Significance</b> .....	<b>29</b>
2.1. Gross Heart Valve Anatomy .....	29
2.1.1. Microanatomy .....	30
2.2. Review on Current Understanding of Valve Cells .....	30
2.2.1. Valvular Interstitial Cells (VICs) .....	31
2.2.2. Valvular Endothelial Cells (VECs).....	32
2.3. Valve Disease is Associated with a Very High Prevalence, Morbidity, and Mortality.....	34
2.4. Current Treatment Options Are Inadequate .....	35
2.5. The Role of Inflammation and Angiogenesis in the Progression of Calcific Aortic Valve Disease .....	36
2.5.1. Inflammation.....	36
2.5.2. Pathological Angiogenesis During CAVD .....	37
2.5.2.1. Histological Features of Angiogenesis Found in CAVD .....	37
2.5.3. Previous VEC Angiogenesis Studies.....	39
2.5.4. Current Hypothesis for the Role of Angiogenesis in CAVD .....	41
2.6. Review of Peripheral Vascular Angiogenesis .....	42
2.6.1. The Role of ECM in Modulating Angiogenesis .....	43
2.6.2. Vascular Endothelial Growth Factor .....	45
2.6.3. Potential Links Between EnMT and Angiogenesis .....	47
2.6.4. Cell-Cell Interactions and the Role of Pericytes in Angiogenesis .....	48
2.6.5. Endothelial/Pericyte Signaling Through Angiopoietin-Tie2 Signaling.....	50
2.6.6. Stages of EC Differentiation during Angiogenesis.....	51
2.6.6.1. Tip Cells .....	52
2.6.6.2. Stalk Cell .....	52
2.6.6.3. Phalanx Cells.....	53

2.6.7. Proliferation .....	54
2.6.8. The Role of Actin Remodeling in Angiogenesis .....	54
2.6.9. The Role of Angiogenesis in Atherosclerosis.....	56
2.7. Tissue Engineering Strategies to Better Understand Angiogenesis.....	57
2.7.1. Poly Ethylene Glycol (PEG) Overview .....	58
2.7.2. Biomimetic PEGDA Hydrogel Systems .....	59
2.7.2.1. Induction of Angiogenesis in Tissue Engineered Scaffolds .....	59
2.7.3. Tissue Engineering Heart Valves .....	60
2.8. Summary .....	60
<b>Regulation of Valve Endothelial Cell Vasculogenic Network Architectures with ROCK and Rac Inhibitors<sup>1</sup>.....</b>	<b>62</b>
3.1. Abstract .....	62
3.2. Introduction .....	63
3.3. Materials and Methods.....	65
3.3.1. Isolation, Purification, and Culture of VECs .....	65
3.3.2. Tubule-like Structure (TLS) Vasculogenesis Assay .....	67
3.3.3. Automated Image Analysis for Tubule Characterization .....	68
3.3.4. Immunocytochemistry .....	69
3.3.5. MTT Assay for Cell Number.....	70
3.3.6. Cell Migration Assay .....	71
3.3.7. Statistical Analysis .....	71
3.4. Results .....	72
3.4.1. APAVECs Formed Tubule-Like-Structures (TLS) in an Angiogenic Environment .....	72
3.4.2. ROCK Inhibition Increased Network Complexity in a Dose Dependent Manner .....	72
3.4.3. Rac1 Inhibition Decreased Network Complexity and Inhibits Network Initiation .....	73
3.4.4. ROCK and Rac1 Inhibition Influenced Cell Assemblies.....	75
3.4.5. Rac and ROCK Inhibition Significantly Decreased APAVEC Number .....	77
3.4.6. ROCK Inhibition Significantly Decreased APAVEC Migration .....	78
3.4.7. APAVECs Display Unique Network Formation Compared to Vascular Endothelial Cells .....	79
3.5. Discussion.....	80
3.6. Conclusion .....	84
<b>Valve Interstitial Cells Act in a Pericyte Manner Promoting Angiogenesis and Invasion by Valve Endothelial Cells<sup>1</sup> .....</b>	<b>86</b>

4.1. Abstract .....	86
4.2. Introduction .....	87
4.3. Methods and Materials.....	88
4.3.1. Isolation, Purification, and Culture of Valve Cells and Vascular Cells .....	88
4.3.2. PKH Co-culture Tubule-Like Structure Matrigel Assay .....	89
4.3.3. Immunocytochemistry .....	90
4.3.4. Automated Network Analysis .....	91
4.3.5. Quantification of Post-Network VIC Chemoattractant Behavior .....	91
4.3.6. VEC/VIC Invasive Spheroid (VEVIS) Sprouting and Distribution Analysis.....	93
4.3.7. Investigating the Role of Angiopoietin1-Tie2 signaling on VEVIS Formation.....	94
4.3.8. qRT-PCR.....	94
4.4. Results.....	95
4.4.1. VIC-Driven Collapse of VEC Vasculogenic Networks is ROCK-Dependent .....	95
4.4.2. VEC/VIC Long Term Co-cultures Form 3D Invasive Spheroids .....	97
4.4.3. A Subpopulation of VICs Guide VECs During Network Reorganization.....	101
4.4.4. VICs Promote VEC Invasion and Are Found Throughout VEVIS Sprouts.....	103
4.4.5. VEVIS Sprouts Display Characteristics of Vascular Angiogenesis Sprouts.....	105
4.4.6. Tie2-Angiopoietin Signaling Is Important in Valve Cell Organization.....	107
4.4.7. Long Term Co-Culture in the TLS Assay ± VICs Significantly Increases the Expression of Angiogenesis and Pericyte Related Genes .....	110
4.5. Discussion.....	111
4.6. Conclusion.....	116
<b>Cyclic Strain Inhibits Valve Endothelial Cell Vasculogenic Network Formation Independent of Piezo1.....</b>	<b>117</b>
5.1. Abstract.....	117
5.2. Introduction .....	118
5.3. Materials and Methods.....	121
5.3.1. Cell culture .....	121
5.3.2. Side Specific Isolation of VECs.....	121
5.3.3. Cyclic Straining of Cells.....	121
5.3.4. Matrigel Tube-like Structure Assay .....	122
5.3.5. ICC Imaging.....	122
5.3.6. qRT-PCR.....	123

5.3.7. Piezo1 siRNA Treatment Protocol .....	123
5.4. Results .....	124
5.4.1. Cyclic Strain Inhibits VEC Network Formation as a Bimodal Function .....	124
5.4.2. Cyclic Stretching Alters VEC Expression of Angiogenesis Related Genes.....	125
5.4.3. Cyclic Stretching Alters VEC pAKT Expression and Localization .....	127
5.4.4. VECs Display Side Specific Differences in Network Formation .....	127
5.4.5. VEC Network Formation Due to Cyclic Stretch is Independent of Piezo1 .....	129
5.5. Discussion.....	130
5.6. Conclusion.....	132
<b>Geometry – Dependent Regulation of VEC Angiogenic Phenotype .....</b>	<b>134</b>
6.1. Abstract.....	134
6.2. Introduction .....	135
6.3. Methods and Materials.....	137
6.3.1. PEGDA Synthesis .....	137
6.3.2. PEGylation Reaction .....	137
6.3.3. Creation of Photomask Patterns.....	138
6.3.4. Construction of Synthetic Tubule Like Structures.....	138
6.3.5. Seeding of VECs on syTLS .....	140
6.3.6. Quantification of Actin Alignment .....	141
6.3.7. Immunocytochemistry of syTLS .....	141
6.4. Results .....	142
6.4.1. Two Stage Photolithography Can Reliably and Repeatedly Produce Highly Specific Patterns of Varied Lacunarity.....	142
6.4.2. Altering Lacunarity Alone is Enough to Alter Tubule Actin Alignment .....	146
6.4.3. CD31, aSMA, VEGR2, Perlecan, N-Cadherin, DII4 Display Pattern Independent Expression .....	148
6.4.4. VECs demonstrate active perception of their environment by displaying pattern- specific differences in their expressions of $\beta$ -Catenin, pAKT, pMAPK, and pMLC.....	149
6.5. Discussion.....	151
6.6. Conclusion.....	153
<b>Conclusion .....</b>	<b>155</b>
<b>References.....</b>	<b>161</b>

# List of Figures

Figure 2-1. Images of PAEC and PAVEC under steady fluid flow environments demonstrating one of the major differences between these cell types. The cells are stained for F-actin (red) and cell nuclei (blue) (adapted from <sup>21</sup> ). .....	33
Figure 2-2. Conceptual framework for the role of various angiogenic factors that lead to the formation of angiogenesis in valves. ....	42
Figure 2-3. Basement membrane transitions during angiogenesis. A)Induction B)Provisional matrix production and invasion C) Resolution leading to intact basement membrane production <sup>5</sup> .....	44
Figure 2-4. Diagram displaying the various ontogeny of a perivascular cell. Pericytes can be derived from a variety of sources (adapted from <sup>51</sup> ). CVC's stands for calcifying vascular cells. Additionally, the proposed pathologies in which VICs and VECs could potentially transform into pericyte like cells and how their pathways could fit in to the overall pericyte lineage. Arrows with question marks are pathways that have been proposed but not confirmed.....	50
Figure 2-5. Overview of the major steps of endothelial cell migration and correlating actin cytoskeletal regulators' roles during each step relevant to this thesis(adapted from <sup>91</sup> ). 55	
Figure 3-1. VECs in culture. Note their tight cell-cell junctions and spiral morphology. 67	
Figure 3-2. Representative images of skeletonized networks comparing VECs (A) untreated, or treated with (B) Y-27632 or (C) NSC-23766. ....	69
Figure 3-3. ROCK inhibition increases APAVEC network complexity in vitro. Representative images of the networks formed by APAVECs treated with A) PBS, B) 1 $\mu$ M, C) 10 $\mu$ M, D) 100 $\mu$ M of the ROCK inhibitor. APAVEC form more complex networks and have increased lamellipodia (white arrow) with higher concentrations of the ROCK inhibitor. Scale bars represent 100 $\mu$ m. E) Quantification of dose dependent changes in various network metrics. Results are shown as mean $\pm$ standard error normalized to the control (n=9, ANOVA p < 0.0001 for all but average lacunarity for which p-value< 0.005. *p < 0.05 vs. control, Tukey's HSD,). ....	73
Figure 3-4. Rac inhibition decreases APAVEC network complexity in vitro. Representative images of APAVEC network formation based upon treatment with A) PBS, B) 2 $\mu$ M, C) 20 $\mu$ M, or D) 200 $\mu$ M of the Rac inhibitor. APAVEC form smaller and less dense networks at the highest treatments with the Rac inhibitor. Scale bars represent 100 $\mu$ m. E) Quantification of the changes in various network metrics. Results	

are shown as mean  $\pm$  standard error normalized to the control (n=9, \* p <0.05 vs. all other groups, Tukey's HSD,). Although there were trends in some of the measured network metrics, the lower concentrations of Rac inhibitor resulted in less pronounced effects that did not attain statistical significance. .... 74

Figure 3-5. Representative Z-stack reconstructed confocal fluorescence microscopy images of APAVEC networks treated with A) PBS, B) 50  $\mu$ M of ROCK inhibitor, or C) 100  $\mu$ M of Rac inhibitor taken with a 10x objective. Control APAVECs organized into tightly bound complex linear tubule-like networks, but the ROCK inhibited APAVECs formed flat networks with looser organization and ablated tubule formation. Compared to the control, Rac1 inhibition appeared to affect the initiation of the tubule formation shown by their fewer tubule like structures number between nodes. However, tube-like structures that did form demonstrated tightly clustered cell assemblies and aligned actin structures, similar to the control tubule like structures. Green: CD 31. Red: aSMA. Blue: Dapi. Scale bars represent 100  $\mu$ m.. Green: CD 31. Red: aSMA. Blue: Dapi. Scale bars represent 100  $\mu$ m..... 75

Figure 3-6. Z-stack reconstructed confocal microscopy images of APAVEC networks treated with A) PBS, B) 50  $\mu$ M of ROCK inhibitor, C) or 100  $\mu$ M of Rac inhibitor. Images were taken with a 20x objective. Aligned actin structures and close cell-cell organization typical of tubule-like sprouts (red arrow) were found in the (A) control and (C) Rac-inhibited networks, but neither of these features were displayed in the (B) ROCK inhibited networks (green arrow). In each case, a few aSMA+/CD 31- cells were found binding several CD 31+ VECs (yellow arrow). Scale bars represent 50  $\mu$ m. Green: CD 31. Yellow: aSMA. Red: F-actin. Blue: Dapi..... 76

Figure 3-7. Representative images of APAVEC TLS networks stained with a 1  $\mu$ M of calcein AM (green, Live) and 2  $\mu$ M of ethidium bromide (red, Dead) 7 hours after treatment with A) PBS control, B) 100  $\mu$ M Y-27632, or C) 200  $\mu$ M NSC-23766. Scale bars represent 50  $\mu$ m..... 77

Figure 3-8. Quantification of changes in cell number based upon ROCK or Rac1 inhibition. Results are displayed as the mean absorbance relative to the control at 24 h  $\pm$  standard deviation (n = 6, \* p < 0.05 vs. control). .... 78

Figure 3-9. ROCK and Rac regulated APAVEC migration in a scratch wound healing assay. A) Representative images of APAVEC wounds 24 hours after injury when treated with 50  $\mu$ M ROCK inhibitor or 100  $\mu$ M Rac inhibitor. The black lines represent the size of the initial wound. Scale bar represents 100  $\mu$ m. B) Quantification of wound closure at 24 hours. Results are displayed as the mean percent wound closure normalized to the control  $\pm$  standard error. (n=4-6, \* p < 0.05 vs. control; † p = 0.08 vs. control)..... 79

Figure 3-10. APAVEC network formation was directly compared to MCEC network formation to elucidate differences in their angiogenic signal transduction. A) At 7 hours, both VECs and MCECs displayed branching complex networks, but MCECs displayed

smoother tubule formation as individual cells were more difficult to discern. Scale bars represent 50  $\mu\text{m}$ . B) Quantification of the VEC networks relative to the MCEC networks demonstrated a larger total network size and lower number of end points for VEC-generated networks ( $n=15$ , \*  $p < 0.05$  between cell types). The networks demonstrated no significant difference in lacunarity or junction density, but there was a trend of the VECs having a larger total number of junctions and total vessel percentage area ( $p = 0.07$  and  $0.06$  respectively). Data is displayed as average  $\pm$  standard deviation normalized to the MCEC metrics..... 80

Figure 4-1. Representative image of MCEC differentially stained with 10  $\mu\text{M}$  green or red PKH dyes co-cultured together for 48 hours. Over the time period tested, minimal to no leakage of dye between cells was seen..... 90

Figure 4-2. VICs altered VEC vasculogenic network formation in a ROCK-dependent manner at 7 hours after seeding. A) VECs cultured alone formed complex networks. B) PKH-stained VECs (green) and VICs (red) formed complex vasculogenic networks when co-cultured. VICs were found connected to VEC tubules and in the nodes between tubules. C) Treatment of co-cultures with ROCK inhibitor Y-27632 (3.5  $\mu\text{M}$ ) eliminated macro changes to network architectures, although localization of VICs along VEC tubules and nodes was still found. Scale bars: 100  $\mu\text{m}$  in A-C. D) Quantification of changes to total network lengths and average tubule length in the co-cultures compared to VEC-only controls. Data shown as mean  $\pm$  standard error across 15 independently seeded wells. The p-value for comparison between groups is displayed above the denoted pairs. Immunocytochemistry of E) VEC/VIC co-cultures and F) VEC/VIC co-cultures treated with Y-27632 stained for CD31 (green),  $\alpha\text{SMA}$  (red), and cell nuclei (blue). E) Polymerized  $\alpha\text{SMA}^+$  VICs (yellow arrow) were found wrapped around and in contact with several elongated CD31 $^+$ / $\alpha\text{SMA}^-$  VECs. F) Treatment with the ROCK inhibitor did not affect VIC expression of  $\alpha\text{SMA}$ , but it was present diffusely and not in polymerized stress fibers (green arrow). ROCK inhibition did not eliminate VIC-to-VEC connections, demonstrated by the multiple connections to VECs made by each VIC in panel F. Co-cultures treated with the ROCK inhibitor displayed notably fewer VICs covering VEC network vertexes. Scale bars: 50  $\mu\text{m}$  in E-F..... 96

Figure 4-3: Figure 2. VEC/VIC co-cultures form 3D invasive spheroids during sustained culture in a pro-angiogenic environment. A) MCECs cultured alone form networks that regress after 48 hours. MCEC/ 10T1/2 co-cultures display typical EC/PC dynamics by sustaining MCEC networks after 48 hours of culture. Scale bars: 100  $\mu\text{m}$ . B) Representative images of PKH-stained VEC (green)/VIC (red) co-cultures over long-term culture. Within 24 hours of seeding, VIC/VEC co-cultures formed EC/PC-like vasculogenic networks, spontaneously regressed, and reorganized into spheroid-like structures. After another 24 hours, the VICs begin to invade into the Matrigel, generally acting as tip cells with the VECs acting as the stalk cells. VIC/VEC co-cultures continued to sprout radially for 5 to 7 days. In the 120 hr panel, only the VECs (green) are highlighted to demonstrate their distribution throughout the VEVIS. Scale bars: 100  $\mu\text{m}$ .

Images were taken from 4 independent experiments. 0 and 7 hr panels were taken from the same position in the same well, as were the 24 and 48 hr panels. .... 99

Figure 4-4. In order to compare the longer term co-culture of VICs and VECs to a known endothelial-pericyte co-culture, MCECs and 10T1/2 cells (to serve as pericytes) were co-cultured on matrigel. A) Similar to previous reports of vascular endothelial/pericyte co-cultures<sup>176</sup>, the MCEC (green) and 10T1/2 (red) cells formed interwoven vasculogenic networks. Scale bar represents 100 $\mu$ m. B) Quantification of MCEC/10T1/2 network size over time. MCEC-only cultures formed nascent networks at 7 hours, with a structure similar to VECs alone<sup>175</sup>. By 24 hours, the MCEC networks had consolidated with smooth node-to-tubule transitions. By 48 hours, the MCEC-only network structure had regressed substantially. Co-culturing with the 10T1/2 cells maintained network stability over this time period as demonstrated by the slowed network size decrease over time. \* represents p-value <0.05. .... 100

Figure 4-5. Representative images of valve spheroid formation after 7 days in culture when seeded as VECs alone (left) or co-cultured with VICs (right)..... 101

Figure 4-6: During organization into spheroids, tracking of VEC movement in relation to nearby VICs reveals a subpopulation of VICs that demonstrate chemoattraction. A) Illustration of method to quantify chemotaxis metrics. Confocal microscopy images of differentially stained VECs and VICs were reconstructed into z-stacks at each time point. For each color channel, the PKH staining was assigned a binary threshold, and each cell was tracked by its resultant unique speckle pattern. For each VIC, all nearby VECs were grouped together and a Lagrangian transformation was performed on their movements relative to the VIC of interest. Lagrangian-corrected chemotaxis metrics were then calculated. B) Resultant chemotaxis metrics for a Brownian motion simulation (negative control) and the measured VEC and VIC movements. Compared to the independent-motion negative control simulation, VECs demonstrated a pronounced movement toward VICs in terms of average cosine similarity, directionality, and forward migration index. As defined by a forward migration index > 0.17, 46% of VICs had an overall positive chemotaxis effect on nearby VECs. C) Representative time track of a VIC (red arrow) exhibiting positive chemoattraction on nearby VECs (green arrow) during network contraction and reorganization into spheroids. .... 102

Figure 4-7: VICs display a pericyte-like phenotype promoting and stabilizing VEC invasive angiogenic root formation throughout VEVIS. A) Representative image of quantification of sprouting ratio after 7 days. Scale bar: 100  $\mu$ m. B) Sprouting was significantly greater in VEC/VIC spheroids than in VEC-only spheroids. C) Representative image of the segmentation of a VEVIS into four quartile rings of equal surface area. Scale bar: 100  $\mu$ m. Both VECs and VICs were found throughout the VEVIS. D) A significant relationship was found between cell type and position by two-way ANOVA (  $p < 0.05$ ). The inner quartile ring contained a significantly larger percentage of VECs than VICs, whereas a larger percentage of VICs tended to be located in the third quartile ring. Throughout the VEC/VIC Matrigel co-culture, VICs were



found in diverse locations that included E) wrapping around VEC tubules at 7 hours (red arrow); F) leading (yellow arrow) VEC angiogenic stalk-like cell (white arrow) sprouting from spheroids after 24 hours and co-localized with VEC spheroid nodes; G) wrapping (red arrow) around and stabilizing formed VEC invasive stalks (white arrow); and H) occupying the leading edge (yellow arrow) of VEC sprouts (white arrow) after 5 days in co-culture. Direct VIC-to-VEC contacts could also be found on invasive sprouts. I) 3D reconstruction of panel H demonstrating the 3D nature of VEVIS sprouts. Each arrow in panel I points to the same cell as in panel H. Scale bars represent 25  $\mu\text{m}$  in C and 50  $\mu\text{m}$  in D-F. .... 104

Figure 4-8: VEVIS sprouts display characteristics of vascular angiogenesis sprouts after 7 days in co-culture. A) VECs maintained endothelial phenotype as demonstrated by acetylated LDL uptake (red). Scale bar: 100  $\mu\text{m}$ . B) Most cells throughout the VEVIS, including tip and stalk cells, stained positive for diffusive non-polymerized  $\alpha\text{SMA}$  (red; indicated by blue arrow). Counterstained with phalloidin (green) and DAPI (blue). Scale bar: 200  $\mu\text{m}$ . C) VECs maintained CD31 (red) expression in VEVIS core and sprouts (magenta arrow). Counterstained with phalloidin (green) and DAPI (blue). Scale bar: 200  $\mu\text{m}$ . D) CD31- VIC (green arrow) displayed direct cell-to-cell contact (white arrow) and organized actin on the tip of a stalk of CD31+ (red) VECs (magenta arrow). Counterstained with phalloidin (green) and DAPI (blue). Scale bar: 25  $\mu\text{m}$ . E) DLL4 (green) expression is polarized from tip of the invasive root to the core spheroid (red arrow). In addition, linear and tube-like organized actin structures were recognizable along VEVIS sprouts (white arrow). Cells are counterstained with phalloidin (red) and DAPI (blue). Scale bar: 25  $\mu\text{m}$ . F) pAKT+ (green) expression is localized on the tip cells of VEVIS sprouts (yellow arrow). Counterstained with phalloidin (yellow) and DAPI (blue). Scale bar: 100  $\mu\text{m}$ . .... 106

Figure 4-9: VEVIS demonstrate  $\beta$ -Catenin polarity down angiogenic-like root when visualized at A) 10x and B) 40x. Scale bars represent 25  $\mu\text{m}$ . As shown in panel C), pMLC was present in most cells with no appreciable pattern. Scale represents 200  $\mu\text{m}$ . .... 107

Figure 4-10: Angiopoietin-Tie2 signaling regulates organization of VIC-VEC co-cultures. A) Representative images of the effects of Ang1 and its downstream inhibitors on VEC network formation over 3 days. Scale bars: 100  $\mu\text{m}$ . B) Quantification of the effects of Ang1 and its downstream inhibitors on VEC network formation over time. Results are presented as mean  $\pm$  SE for 12 independently seeded wells.  $p < 0.05$  between groups. C) Representative images of the effects of Ang1 and its downstream inhibitors on VEVIS formation after 7 days in culture. Scale bars: 100  $\mu\text{m}$ . D) Quantification of the effects of Ang1 and its downstream inhibitors on VEC/VIC co-culture after 7 days. Results are presented as mean  $\pm$  SE of the VEVIS of 12 independently seeded wells.  $p < 0.05$  between groups. .... 109

Figure 4-11. VECs and VICs demonstrate several increases in angiogenesis and pericyte related markers after long term culture in the matrigel model. A) Significant

increases in FGFR2 and Tie2 were measured when comparing VECs cultured in the matrigel model after 7 days compared to Day 0 control VECs. Angiopoetin1 did not prime in isolated culture or after 7 days in the matrigel model. No significant change in periostin was measured. B) Significant increases in the angiogenesis and pericyte related markers of FGFR2, Angiopoetin1, Tie2, NG2, and Periostin were measured after 7 days in co-culture in the matrigel model when compared to a control 3:1 mixture of VECs and VICs before co-culture. .... 111

Figure 5-1. VECs demonstrated a complex relationship between network formation and cyclic strain. A) Representative images of VEC vasculogenic network formation after 7 hours in the Matrigel model after static (left) and 0-10% (right) cyclic strain at 0.5 Hz for 24 hours. B) Quantification of the effect of static, 0-5%, and 0-10% strain on total network length and junction number. 0-5% strain demonstrated the largest decrease in total network length and junction number. All treatment groups not connected by the same letter were significantly different from one another in each network metric..... 125

Figure 5-2. Quantification of changes in angiogenesis related genes as a function of degree of cyclic stretch. \* represents a p-value < 0.05 between groups. A) Significant decreases in VEGF and Tie2 expression were seen after 24 hours of 0-5% cyclic strain. B) There were no significant differences in the genes investigated in this study after 24 hours of 0-10% cyclic strain. N = 4 independent biological runs paired for each treatment group..... 126

Figure 5-3. Representative image of pAKT localization without (left) or with (right) 24 hours of cyclic strain. pAKT expression (red) localized to the cytosol as well as the nucleus in the 5% strain condition while pAKT appeared generally just in the nuclei (DAPI, blue) in the control condition. Cells were counter stained with phalloidin (green). ..... 127

Figure 5-4: Quantification of changes in VEC vasculogenic networks as a function of side specificity. VECs harvested from the ventricularis displayed significantly larger networks, but they did not display any significant differences in junction number. .... 128

Figure 5-5. A) Piezo1 expression was measured by RT-qPCR after siRNA treatment. Expression analysis showed a reduction in gene expression by  $90\% \pm 3$ . B) Quantification of the effect of Piezo1 silencing and cyclic stretch on VEC network formation. Treatment with Piezo1 DsiRNAs  $\pm$  stretch were sufficient to reduce network formation to levels comparable to stretched scrambled controls. Groups not connected by the same letter are significantly different from one another (p-value < 0.05). ..... 129

Figure 6-1: Flow diagram demonstrating conversion of an image of VEC network to a repeating vectorized pattern. .... 138

Figure 6-2. A) Diagram of construction of patterned PEGDA hydrogels. B) Diagram of the sterile collimated light source. 1) Fiber optic light source. 2) Fiber optic cable. 3)

Light diffusor. 4) 1.2 numerical amperture plano-convex collimating lens. 5) Light absorbing black flock velvet paper. C) Patterned Acryl-Rhodamine demonstrating pattern specificity. Scale bar represents 200  $\mu\text{m}$ . ..... 140

Figure 6-3. Representative images of the pattern specificity capable with the syTLS method imaged in phase contrast (left) and after staining with ICC (right) for CD 31 (red), vimentin (purple), phalloidin (green), and DAPI. Addition of 1% PEGDA in the secondary solution allows for channel creation appreciable in the phase contrast image on the left which leads to increased pattern specificity. Scale bars represent 200  $\mu\text{m}$ . ..... 143

Figure 6-4. Quantification of syTLS pattern edge thickness as a function of pattern. No significant difference was measured between the thicknesses of 12 randomly chosen VEC tubule segments for each condition. Data is displayed as the mean thickness  $\pm$  the standard deviation. .... 144

Figure 6-5. A) Quantification of varied lacunarity (represented as D) patterns used for patterning of syTLS. B) Representative images of VECs patterned in syTLS imaged with DIC at 1) 4x, 2) 10x, 3) 20x, and 4) 40x images. Scale bars represent 250, 100, 50, and 25  $\mu\text{m}$ . Although some non specific adherence to non-patterned regions can be found in each pattern, VECs demonstrate strong specificity to the patterned areas. The 40x image in panel D shows the rounded appearance of tubule borders at the vertices. ... 145

Figure 6-6. A) Representative images of changes in phalloidin (green) staining as a function of pattern. VECs patterned in the hexagon pattern demonstrated a more rounded phenotype, while vessel-mimicking patterned VECs appeared the most aligned. Scale bars represent 200  $\mu\text{m}$ . B) Representative images of actin fibers as a function of syTLS pattern. Cells seeded on the hexagon patterns appeared rounded whereas the cells seeded on the vessel-mimicking appeared to be the most aligned. Scale bars represent 10  $\mu\text{m}$ . C) Quantification of the distribution of fiber alignment as a function of syTLS pattern demonstrating differences in the fiber alignment as a function of pattern. .... 147

Figure 6-7. All cells demonstrated strong cell-cell staining for CD 31 (Red) and little to no staining for  $\alpha$ SMA (purple) . Scale bars represent 50  $\mu\text{m}$ . .... 148

Figure 6-8. Within 24 hours of seeding, VECs on all patterns begun producing basement membrane proteins as demonstrated by strong staining of perlecan in each condition. Scale bars represent 100  $\mu\text{m}$ . .... 149

Figure 6-9. Representative ICC images for VEC actin regulators as a function of pattern. A)  $\beta$ -Catenin expression was strongest in the triangle pattern with no differences between the hexagon and vessel patterns. B) pAKT staining appeared stronger in the hexagon and triangle patterns compared to the vessel mimicking patterns. C) pMAPK stained strongest in the hexagon pattern, while both the vessel and triangle patterns demonstrated similar levels of pMAPK. D) VEC pMLC expression correlated with

lacunarity of resultant syTLS. Scale bars represent 100  $\mu\text{m}$  in A-C and the middle panel of D. Scale bars represent 50  $\mu\text{m}$  in the remaining panels in D. .... 150

# List of Tables

<b>Table 3-1. Characteristics of tubule-like structures formed by VECs in Matrigel model.....</b>	<b>72</b>
<b>Table 4-1. Primary antibodies for immunocytochemistry.....</b>	<b>90</b>
<b>Table 4-2. Angiogenesis and pericyte related gene expression PCR targets .....</b>	<b>95</b>
<b>Table 5-1. Antibody Targets for FlexCell Study.....</b>	<b>122</b>
<b>Table 5-2. Angiogenesis related genes for RT-qPCR.....</b>	<b>123</b>
<b>Table 5-3: qRT-PCR data comparing expression fold changes of previously identified differentially expressed angiogenic related markers between side specifically harvested populations of VECs. Data is displayed as the ratio between the Fibrosa/Ventricularis delta CT values to the Ubiquitin reference. ....</b>	<b>128</b>
<b>Table 6-1. Angiogenesis markers of interest investigated on the syTLS .....</b>	<b>141</b>
<b>Table 6-2: Compilation of changes in expression of actin and angiogenesis regulators relative to the vessel pattern. ....</b>	<b>151</b>

# List of Abbreviations

alpha-SMA: alpha smooth muscle actin  
Ang: angiotensin  
APAVECs: adult porcine aortic valve endothelial cells  
AV: atrioventricular  
AVA: aortic valve area  
aVICs: activated VICs  
BAD: B-cell lymphoma 2 associated death promoter  
Bcl-2: B-cell lymphoma 2  
BM: basement membrane  
BMPs: bone morphogenic proteins  
BSA: bovine serum albumin  
CAPs: cell adhesive peptides  
CAVD: calcific aortic valve disease  
DCM: dichloromethane  
DLL4: delta like ligand 4  
DsiRNA: dicer-substrate siRNA  
ECM: extracellular matrix  
ECs: endothelial cell  
EMT: epithelial to mesenchymal transdifferentiation  
EnMT: endothelial-to-mesenchymal transdifferentiation  
eNOS: endothelial nitric oxide synthase  
EPCs: endothelial progenitor cells  
Erk: extracellular regulated kinase  
F-actin: filamentous actin  
FAK: focal adhesion kinase  
GAPs: GTPase activating proteins  
GEFs: guanine nucleotide exchange factors  
HDMEC: human dermal microvascular endothelial cells  
HPVEC: human pulmonary valve endothelial cells  
HUVEC: human umbilical vascular endothelial cells  
LaFMI: Lagrangian-transformed Forward Migration Index  
MAPK: mitogen-activated protein kinase  
MCEC: mouse cardiac endothelial cells  
MMP: metalloproteinase  
NICD: Notch intracellular domain  
NVP: 1-vinyl-2-pyrillidinone  
obVICs: osteoblastic VICs  
P/S: Penicillin/Streptomycin  
PAK: p21-activated kinase  
PAVECs: porcine aortic valve endothelial cells  
PBS: phosphate buffered saline  
PCs: pericytes  
PEG: poly(ethylene glycol)  
PKC: protein kinase C  
PMA: phorbol 12-myristate 13-acetate  
pMAPK: p42/44 mitogen-activated protein kinase  
pMLC: phosphorylated myosin light chain

pVICs: progenitor VICs  
qVICs: quiescent VICs  
ROCK: Rho-associated serine-threonine protein kinase  
sFlt: soluble Flt1  
SL: semilunar  
syTLS: synthetic tubule like structure assay  
TEHV: tissue engineered heart valve  
TEOA: triethanolamine  
TGF: transforming growth factor  
TGF-beta1: transforming growth factor beta1  
TIMP: tissue inhibitors of metalloproteinases  
TLS: tubule-like structure assay  
TNF-alpha: tissue necrosis factor alpha  
VECs: valve endothelial cells  
VEGF: vascular endothelial growth factor  
VEGFR1: vascular endothelial growth factor receptor 1  
VEVIS: VEC/VIC invasive spheroid  
VICs: valve interstitial cells  
VSMC: vascular smooth muscle cells  
vWF: von Willebrand Factor





# Chapter 1

## Introduction

Heart valves are essential for guiding the efficient forward flow of blood through the heart. **Valvular heart diseases are among the most prevalent and devastating diseases worldwide affecting both large pediatric and adult populations**, yet there are no non-surgical options for treating these conditions. The lack of fundamental knowledge about heart valve biology limits the development of interventional therapies to halt the progression of the disease. The most common valve disease is calcific aortic valve disease (CAVD). **Understudied in the progression of CAVD is the noted histological change of new blood vessel formation, angiogenesis.**

Angiogenesis is fundamental biological process crucial in development, reproduction, wound repair, and life in general in higher order life forms. It is a highly spatially and temporally regulated process that is required not only for native human physiology, but also for the progression of many pathologies like calcific aortic valve disease (CAVD). Angiogenetic signaling plays an important role not only in valve formation and normal valve function, but also in the pathophysiology of CAVD. Several studies have established the occurrence of neovascularization during CAVD. There has been little investigation, however, into how the cell-mediated mechanisms that underlie vascular angiogenesis play a role in the pathology of CAVD. It has been proposed that a targeted antiangiogenic therapy could stop the progression of valve disease by

preventing neovessel formation generated by the valve cells. In addition, normal pediatric heart valves (unlike normal adult valves) are richly vascularized, which suggests that vascularization is an important factor to consider in the tissue engineering of heart valves for pediatric patients. All in all, there is compelling evidence for further characterization of the translation of angiogenetic signaling behavior by heart valve cells. To achieve this goal, the following specific aims were undertaken to characterize the base angiogenic capacity of valve endothelial cells (VECs), to investigate the pericyte capacity of valve interstitial cells (VICs) on VECs, to quantify the effect of cyclic stretch on VEC angiogenic capacity, and lastly to evaluate the effects of a synthetic tissue engineering inspired angiogenic assay.

*Specific Aim 1: Regulation of Valve Endothelial Cell Vasculogenic Network Architectures with ROCK and Rac Inhibitors*

Aortic valves develop neovascularization during the pathology of CAVD, but the angiogenic capacity of VECs was unclear as only endothelial cells from diseased valves had demonstrated angiogenic capacity. It was not clear if the source of the neovascularization in CAVD was VECs, because the angiogenic potential of VECs was unknown. In addition, in previous non-angiogenic related studies, VECs had previously demonstrated that they atypically regulate several actin regulators crucial for organization during angiogenesis, as well as other factors crucial for vascular angiogenesis. Therefore, a study was performed to characterize the inherent vasculogenic network formation capabilities of valve endothelial cells harvested from healthy aortic valves compared to vascular-derived endothelial cells in an *in vitro* model for angiogenesis. In order to determine if differences in the network formation were due to fundamental differences in their translation of angiogenic signals by their actin regulators, this specific aim tested the ability to tune the complex vasculogenic networks of VECs using small molecule inhibitors of the ROCK and Rac pathways in an *in vitro* angiogenic assay. Applying automated analytical tools for quantifying networks allowed for a novel assessment of the biological response of valve endothelial cells to the vasculogenic environment and to quantify the ability of valve endothelial cells to form complex vasculogenic networks *in vitro*. These networks were demonstrated to be significantly different numerically and morphologically from the networks generated by a vascular endothelial cell line. However, this study additionally demonstrated the ability

to manipulate the geometry of the resulting vascular networks using ROCK and Rac1 inhibitors, as similarly shown by previous studies of peripheral vascular endothelial cells. Therefore, this work suggests that when placed in the right microenvironment, VECs are similar enough to proangiogenic vascular endothelial cells that they have the potential to be the source of the neovascularization during CAVD. With the results of this first specific aim as a starting scaffold, the remaining aims sought to add levels of complexity to improve understanding of the whole picture of the translation of angiogenic signals by valve cells and thus better understand their potential individual role into the contribution of the pathobiology of CAVD.

*Specific Aim 2: Valve Interstitial Cells Act in a Pericyte Manner Promoting Angiogenesis and Invasion by Valve Endothelial Cells*

With the knowledge that VECs could form complex vasculogenic networks similar to vascular endothelial cells and that these networks were manipulable through similar methods, we then studied the capabilities of valve interstitial cells (VICs) to manipulate VEC network spatial arrangement and sustainment in a pericyte manner. Previously, VICs from healthy valves were considered to be an anti-angiogenic cell type despite strong histological evidence for their pericyte capacity *in vivo*. However, VICs had never been demonstrated to act in a pericyte manner. Therefore, in this study VECs and VICs were fluorescently tracked and co-cultured in an *in vitro* angiogenesis assay over long term. VICs regulated early VEC network organization in a ROCK-dependent manner, wrapping themselves around VEC network edges in a pericyte manner similar to a pericyte cell line. Using a novel method to quantify the Lagrangian-corrected chemoattraction of one cell type towards another in a mixed population, we identified and quantified a subpopulation of VICs that demonstrated chemoattraction towards VECs, leading to VEC network contraction. Directly comparing valve cell co-cultures to vascular cell co-cultures revealed that, unlike vascular control cells, the valve cell cultures ultimately formed invasive spheroids with 3D sprouts. These 3D sprouts were found to have several typical markers of *in vivo* angiogenic root sprouts such as delta-like ligand 4 polarity down the root. VECs co-cultured with VICs displayed significantly more invasion than VECs alone, interestingly, VICs were found leading and wrapping around VEC invasive sprouts demonstrating both tip cell and pericyte behaviors. Angiotensin II-Tie2 signaling was found to regulate valve cell organization during

VEC/VIC spheroid formation and invasion. Lastly, long term co-cultures demonstrated significant increases in several angiogenesis and pericyte markers when measured with qRT-PCR, such as Ang1, Tie2, NG2, and the pro-angiogenic ECM protein periostin, which is correlated with increased angiogenesis and worsening of CAVD *in vivo*. The change in phenotype to an invasive sprouting spheroid suggested that both cell types undergo phenotypic changes during long-term culture in the model angiogenic environment to a more proangiogenic phenotype. This study contributed to the growing understanding of valve cell biology and how a sustained pro-angiogenic environment in the aortic valve could lead to an atypical translation of angiogenetic signaling in valve cells enabling angiogenic invasion of the valve through coordinated valve cell behavior. This increase in angiogenic invasion in turn would contribute to the pathology of CAVD through increased inflammatory infiltrates and blood flow to the normally avascular aortic valve.

*Specific Aim 3: Cyclic Strain Inhibits Valve Endothelial Cell Vasculogenic Network Formation Independent of Piezo1*

Although the translation of several factors important to angiogenesis had been elucidated by this work, another key factor, the cyclic stretching of the aortic valve, was unstudied in the context of angiogenesis previously. Mechanical stimulation is known to be strong regulator of vascular endothelial cell angiogenic capacity, but its role in regulating VEC angiogenic capacity and contributing to valve avascularity or how disturbance of the normal mechanical strain contributes to the progression of CAVD was unknown. Therefore, this study examined the effect of cyclic uniaxial strain in regulating the response of valve endothelial cells to an *in vitro* angiogenesis model. In this study, network analysis revealed a strong pattern of strain to decrease the propensity of VECs to form networks. Quantification demonstrated a relationship where in cyclically straining the VECs from 0-5% induced a greater decrease in network junction density and network size than did straining from 0-10% compared to paired unstretched controls. qRT-PCR demonstrated a significant decrease in the gene expression of Tie2 and VEGF in the 0-5% condition while no significant change was measured in the 0-10% compared. Immunohistochemistry demonstrated a change in the localization of pAKT to the cytosol and the nucleus in the 0-5% condition compared to just in the nucleus in the control. Since VECs from different sides of the valve

experience different mechanical stimulation and the presence of calcification during CAVD shows side specificity, a method was developed and verified to harvest VECs specifically from different sides of the valve. In this study, both cell populations formed complex networks in this study, but VECs from the ventricularis formed significantly larger networks than cells from the fibrosa. However, no significant difference in junction density between the 2 side-specific VECs. Lastly, we attempted to identify the mechanotransducer in VECs responsible for mediating the stretch dependent decrease in network formation through the silencing of the mechanically active Ca<sup>+</sup> channel, Piezo1, which had been demonstrated previously to be an important mechanotransducer in endothelial cells. Although Piezo1 gene expression was verified to be silenced by 90% in VECs using DsiRNAs, no significant difference was found between networks as function of cyclic stretch once treated with Piezo1 siRNAs. However, Piezo1 silencing alone was sufficient to inhibit network formation to level that of the 0-5% stretch-induced network inhibition, demonstrating a role for Piezo1 in VEC angiogenic regulation. These results indicate that mechanical stimulation plays a role in maintaining valve avascularity and that a mechanically disrupted valve, such as those stiffened by CAVD, are more prone to worsening disease conditions through increased angiogenesis. Additionally, these results suggest that Piezo1 has a role in regulating angiogenesis signaling in VECs, but this effect was independent of cyclic stretching in this study.

#### *Specific Aim 4: Geometry – Dependent Regulation of Angiogenic Phenotype*

In the last chapter of this work, we began to investigate the factors that govern VEC angiogenesis in the opposite direction - from the network scale down - using tissue engineering strategies. The development of complex engineered tissues is currently limited by the ability to incorporate functional microvasculature to encourage survival and growth. This issue is particularly relevant to pediatric tissue engineered heart valves that must grow over the lifespan of the patient. Vascular networks of varying complexity can be designed within engineered tissues, but the amount of biological complexity necessary for proper biological functionality is unclear as more complex is not necessarily better or necessary. Because VEC network complexity had been demonstrated to be sensitive to changes in actin regulators, this study used VECs as a framework to examine this fundamental relationship between network structure and endothelial cell biology to provide proof-of-principle evidence that the internal signaling

biology of endothelial cells could be tuned based upon the network they were spatially defined into. PEGDA hydrogels were patterned with RGDS into 15  $\mu\text{m}$  deep tubule networks using photolithography. VECs were then seeded on a vessel-mimicking pattern, a higher lacunarity hexagon-based pattern, or a lower lacunarity triangle-based pattern model networks of varying complexity. Notable differences in several angiogenesis-related markers were found as function of the pattern the cells were seeded on including several markers for actin activity regulators as well as significant changes in actin alignment although some notable angiogenesis markers showed no change. Controlling the geometric pattern of VEC networks mimicked changes in signaling previously observed in Specific Aim 1. Preliminarily, these results suggest that more biomimetic vessel pattern stimulates a more biomimetic and potentially functional endothelial response, although more work is required to verify and quantify the changes measured. Addition of further valve-specific elements will enable the creation of structured biomaterial scaffolds for application to pediatric TEHV development as well as models of CAVD.

The subsequent chapters in this dissertation will include a comprehensive background of the aortic valve, CAVD, VEC and VIC biology, and relative factors of peripheral angiogenesis in chapter 2. Investigation into the regulation of valve endothelial cell vasculogenic network architectures with ROCK and Rac inhibitors will be found in Chapter 3. Evaluation of the ability of valve interstitial cells to act in a pericyte manner promoting angiogenesis and invasion by valve endothelial cells will be found in Chapter 4. Evaluation of whether cyclic strain inhibits valve endothelial cell vasculogenic network formation and the role of the mechanosensor Piezo1 in regulating VEC cyclic stretch response will be found in Chapter 5. Proof-of-principle evidence for geometry dependent regulation of angiogenic phenotype in VECs using a synthetic PEGDA hydrogel-based angiogenesis assay will be found in Chapter 6; and a conclusion summarizing the impact of this body of work will be found in Chapter 7.

## Background and Significance

### 2.1. Gross Heart Valve Anatomy

Although the methods in this thesis will focus on cells isolated from the aortic valve, the context in which the cells live in is important to understand how specialized they and their microenvironments are. The basic function of heart valve tissue is to maintain uninterrupted unidirectional blood flow through the heart. In the heart, there are four valves. The aortic and pulmonary semilunar (SL) valves separate the ventricles from the great arteries, whereas the bicuspid (or mitral) and tricuspid atrioventricular (AV) valves separate the atria from ventricle. SL valves are crown-shaped and have cusps (three in each) while AV valves are ring shaped and consist of large, asymmetric leaflets (two in the bicuspid and three in the tricuspid) <sup>1</sup>. Although each valve is structured on a macro scale differently, they each have a similar micro anatomy and layering.

In the aortic valve, the tri-leaflet structure is pushed open by the strong forward flow of blood during systole to allow unobstructed flow. As the blood velocity and pressure behind the valve decrease near the end of systole, the leaflets begin to fold back towards their central axis pushed by blood vortices in the sinuses. Although there is still forward flow, the leaflets offer negligible resistance and become completely closed at the exact moment when forward flow stops. The increased pressure in the aorta over the left ventricle forces the leaflets to remain shut and stretch radially to form a flat surface imperative in preventing backflow<sup>1</sup>. During their relaxed state, the aortic valve leaflets are very soft to allow significant strains to cover the opening. The leaflets maintain this

flat shape during diastole until they are again prompted to open by the forward flow of blood in systole.

### 2.1.1. Microanatomy

As the main focus of this thesis is on the aortic valve, the focus of this review will focus on the aortic valve's microstructure. Although as previously mentioned, all of the valves have a similar microstructure. The aortic valve is an excellent representation of how function follows form. It consists of three thin, membrane-like fibrous layers: 1) the thin *ventricularis* on the inflow surface, 2) the *spongiosa* in the center, and 3) the thick *fibrosa* on the outflow surface as demonstrated by **Error! Reference source not found.** below <sup>2</sup>. The inside of the valve is populated by valvular interstitial cells (VIC) which maintain the ECM composition on the inside of the valve<sup>3</sup>. On the exterior of the valve is an anti-thrombotic layer of valvular endothelial cells (VECs) <sup>4</sup> anchored to a basement membrane consisting of a specific matrix of proteins, glycoproteins, and proteoglycans <sup>5</sup>.

On the whole, healthy adult cardiac valve tissue is sparsely vascularized <sup>2,6</sup>. This is most likely because the leaflets and cusps are sufficiently thin to receive nourishment from blood passing through the heart via diffusion<sup>2</sup>. Curiously, neonatal and young valves are vastly vascularized. This network is potentially necessary for the developing valves as its energy requirements are higher at this stage of its development compared to later when the cell's major role is generally just maintaining its local environment <sup>7</sup>. This pediatric vascularity is important feature to recreate in the design of pediatric tissue engineered heart valves to ensure the valve cells have sufficient nutrients to be able to grow throughout the lifespan of the valve to prevent unnecessary repeat procedures..

## 2.2. Review on Current Understanding of Valve Cells

There are two major cell types found normally in a healthy heart valve: the valvular endothelial cell and the valvular interstitial cell. Although they act similarly to fibroblasts and peripheral vascular endothelial cells respectively, there are several



genetic and physiological differences which are just recently being elucidated that highlight how specialized these cell types are. This specialization provides rationale for why valve specific cells must be utilized when investigating valve specific elements due to their specialization.

### 2.2.1. Valvular Interstitial Cells (VICs)

VICs are the most common cell type found in all three layers of the valve. It is the job of the fibroblast-like VICs to maintain the extracellular matrix (ECM) on the inside of the valve which gives the valve its functional mechanical properties. They maintain the ECM by a combination of synthesizing and excreting new proteins, glycoproteins, proteoglycans, GAGs, the matrix degrading enzymes from the metalloproteinase (MMP) family, and their associated inhibitors, the tissue inhibitors of metalloproteinases (TIMP)<sup>8</sup>.

Throughout the life span of a healthy valve, the majority of the contained VICs are in a quiescent fibroblast-like cell type; however, the population distribution of VICs is always plastic and heterogeneous as they are capable of differentiating towards multiple mesenchymal lineages. The five phenotypes that best represent these various lineages are segmented such as they exhibit specific sets of cellular functions essential in normal valve physiology and what is seen in the pathology of various valvular diseases. The five types are embryonic progenitor endothelial/mesenchymal cells, quiescent VICs (qVICs), activated VICs (aVICs), progenitor VICs (pVICs), and osteoblastic VICs (obVICs)<sup>9</sup>.

During early valvulogenesis during the embryonic stage, the embryonic progenitor endothelial/mesenchymal cells on the exterior of the endocardial valve cushion undergo endothelial-to-mesenchymal transformation (EnMT) that initiates the process of valve formation<sup>1</sup>. The transforming growth factor (TGF) superfamily members, bone morphogenetic proteins (BMPs), Notch, and vascular endothelial growth factor (VEGF) have been shown to regulate EnMT during valvulogenesis via their highly controlled spatial and temporal expression, although it has been shown that mature valve endothelial cells can undergo TGF- $\beta$  mediated and VEGF mediated shielding from EnMT into VICs as well<sup>10</sup>. qVICs are the most commonly found phenotype in the healthy adult valve. It is their job to maintain the physiological structure/function relationship of the valve and they are speculated to inhibit angiogenesis in the valve by the production

of chondromodulin-I<sup>11</sup>. The pVICs are the least defined population and consist of various circulating progenitor cells that enter the valve from the blood stream. These cells are generally CD 34-, CD133-, and/or S100+. Curiously these circulating cell types have been found in both calcified aortic valves and degenerated bioprosthetic valves<sup>12</sup>. The aVICs are the cells that are the main culprits in the pathobiological overreaction to various disease and injury stimuli. aVICs are generally alpha smooth muscle actin ( $\alpha$ -SMA) and vimentin positive with marked increases in proliferation, migration, and matrix remodeling compared to qVICs. qVICs differentiate towards aVICs in response to various pathological conditions such as high matrix stiffness, abnormal hemodynamic forces, and various other stimuli<sup>13</sup>.

Lastly, the obVICs are the end stage of the pathology towards CAVD phenotype that lead to chondrogenesis and osteogenesis of the valve. These cells are considered the source of cartilaginous and hard bone nodules seen in calcific aortic valves, and they are generally associated with an increased expression of the osteogenic proteins osteopontin, bone sialoprotein, alkaline phosphatase, and BMPs 2 and 4<sup>14,15</sup>.

### 2.2.2. Valvular Endothelial Cells (VECs)

Although VICs are relatively understudied compared to similar cell types, VECs are particularly understudied compared to similar vascular derived endothelial cell types such as human umbilical vascular endothelial cells (HUVEC)<sup>16</sup>. VECs, like other endothelial cell types in the circulation, form a monolayer on the exterior of valve leaflets creating a barrier separating the circulation from the underlying interstitium. VECs have several roles in maintaining the homeostasis of its underlying tissue, while their dysfunction contributes to various pathologies. The major roles of VECs are to act as an anti-thrombotic barrier, to regulate permeability, to modulate inflammation, and to control various VIC functions via angiocrine signaling similar to how endothelial cells control vascular smooth muscles cells (VSMC)<sup>17,18</sup>. Curiously, it has been shown the VECs display side specific differences in gene expression of various factors that mediate inflammation, permeability, and angiocrine signaling.<sup>19,20</sup> Additionally, VECs have been shown to have very distinct gene and protein expression patterns from that of other vascular endothelial cell types, further demonstrating their uniqueness<sup>4,21</sup>. A study by Butcher et al. eloquently demonstrated one of these major differences by demonstrating

that porcine aortic valve endothelial cells (PAVECs) align perpendicular to a steady flow environment, while porcine aortic endothelial cells aligned themselves parallel to flow.

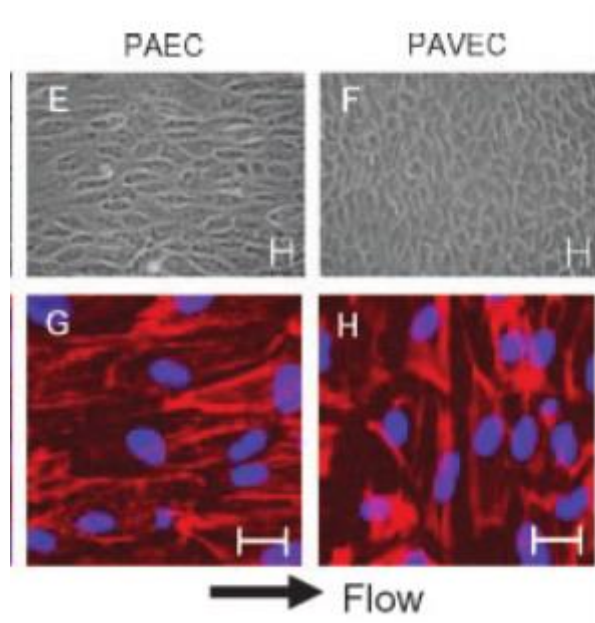


**Figure 2-1. Images of PAEC and PAVEC under steady fluid flow environments demonstrating one of the major differences between these cell types. The cells are stained for F-actin (red) and cell nuclei (blue) (adapted from<sup>21</sup>).**

VECs are generally positive for CD 31, CD 34, CD 146, vascular endothelial growth factor receptor 1 (VEGFR-1), VEGF-R2, vascular endothelial cadherin, and von Willebrand Factor (vWF) while they are generally  $\alpha$ -SMA negative in culture<sup>21-23</sup>. In culture, VECs are generally identified by their tight swirling cobblestone morphology and staining positive for CD 31 and negative for fibrous  $\alpha$ -SMA<sup>16</sup>; however, it is known that VECs can exhibit differential amounts of  $\alpha$ -SMA while they are transdifferentiating towards a VIC like phenotype creating a combined VEC/VIC phenotype in which the cell is positive for both markers<sup>10</sup>. As valvular endothelial cell biology is still in its infancy, there is still much to be elucidated about this cell type to truly understand the role of its dysfunction in the pathology of valvular diseases. The prevalence, morbidity, and mortality associated with these diseases are discussed further below.

### 2.3. Valve Disease is Associated with a Very High Prevalence, Morbidity, and Mortality

Valve diseases are some of the most prevalent and devastating diseases worldwide. They currently account for approximately 21,800 deaths and 92,000 hospitalizations a year in the US alone. Aortic valve disease alone has an annual mortality rate of approximately 14,300, which makes it the most lethal of the valvular diseases. The current prevalence of aortic valve disease in patients age 70 to 80 years is estimated to be about 2%<sup>24</sup>. Similar to other cardiovascular diseases like vascular atherosclerotic disease, this incidence risk towards calcification was associated with increased age, male sex, body mass index, and smoking. Among men and women of 65 years of age or older in a study, the aortic valve was found to be sclerotic in 29% of patients and stenotic in 2% of patients. This aortic sclerosis was found to be associated with a 50% increase in the risk of death and myocardial infarction in this sample group and greatly associated with the risk factors for atherosclerotic disease<sup>24</sup>. It has been estimated that the annual actual direct cost for valvular diseases is actually around 1 billion dollars<sup>25</sup>. Valve disease generally manifests clinically in several forms such as a stenosis, obstruction, or regurgitation. Clinically, valve diseases are generally diagnosed using echocardiography. With echocardiography, the severity of the disease can be determined by calculating the mean and peak aortic valve gradients, aortic valve area (AVA), and aortic valve velocity. Since these measurements are not always precise, cardiac catheterization is the concluding method used to verify the electrocardiogram diagnosis. During cardiac catheterization, a catheter is inserted into the blood stream and directed to the heart. In contrast to echocardiography, cardiac catheterization can directly measure the aortic valve gradient and cardiac output, and it can accurately calculate the AVA<sup>26</sup>. Severe AS is defined as an AVA of less than 1 cm<sup>2</sup>, a mean pressure gradient greater than 40 mmHg, and a peak flow velocity greater than 4 m/s. Using these measurements and guidelines, an accurate depiction of the severity of AS can be established<sup>27</sup>.

Sadly, one of the larger groups of valvular disease patients are patients born with congenital heart defects. Currently, congenital heart valve defects appear in approximately 2% of live births, while it is estimated that number could be higher as

many cases may be asymptomatic and go undiagnosed<sup>1,28</sup>. There is growing evidence that these congenital defects have various genetic bases that manifest during development. For example in a perlecan/HSPG2-deficient mouse model, 73% of animals showed complete transposition of the great arteries, and 27% of animals showed defects in the aorta and pulmonary valve<sup>29</sup>.

A major issue with degenerative valvular diseases are that the symptoms typically are not present until the late stages of the disease when it becomes life threatening. Common symptoms include chest pain, weakness, fatigue, and breathlessness. However, few patients experience notable symptoms, so the diagnosis of more stenotic valves is heavily dependent on imaging modalities and patient examinations. Furthermore, an accurate judgment of the severity of the disease is critical for effective management of the disease. Patients who have more severe stenosis may immediately need an aortic valve replacement<sup>26</sup>. A current major failing in the treatment options for valvular diseases is that there are currently no interventional treatments for the disease, leaving only a few imperfect solutions which will be described in further detail below.

## **2.4. Current Treatment Options Are Inadequate**

Once it has been determined that a valve is too diseased to function properly, the only treatment options are surgical. The most common heart valve treatment performed is the aortic valve replacement. There are nearly 100,000 valve replacements performed annually in the United States alone with a large portion of them being aortic valve replacements<sup>24</sup>. The two major types of clinically available replacements are either mechanical prosthetic valves or bioprosthetic valve. Bioprosthetic valves include porcine aortic valve or bovine pericardial xenografts, an allograft from a cadaver, or using the pulmonary valve in the place of the aortic valve which is called the Ross procedure<sup>30</sup>. Both of these alternatives have major failings associated with them. Although mechanical valves can remain structurally functional for years, they require aggressive anticoagulation to prevent any thromboembolism formation that can lead to the closure of the valve or the formation of clots, which can cause downstream strokes or myocardial infarctions. Although bioprosthetic valves do not require long term drug

treatment, they regularly become calcified and stenotic requiring their relatively frequent replacement<sup>31</sup>.

Strongly lacking in the treatment of any valvular disease is the presence of any interventional medical treatments that are non surgical in nature. The lack of the fundamental knowledge about the cellular and biochemical nature of the pathology of these diseases has stalled the discovery of these highly needed drugs. What is currently known about the pathology of calcific aortic valve disease will be discussed in further detail below.

## **2.5. The Role of Inflammation and Angiogenesis in the Progression of Calcific Aortic Valve Disease**

Calcification of the aortic valve is the third leading cause of heart disease in adults<sup>32</sup>. Despite the frequency, the mechanisms of valve calcification are not known. Until recently, the concept was generally accepted that calcific aortic valve disease is a degenerative and unmodifiable process, basically induced by long-lasting mechanical stress<sup>25</sup>. CAVD is now recognized as an active disease process with several pathological molecular and histological markers. CAVD is characterized by calcification, loss of layering and distribution of the ECM leading to fibrotic thickening, inflammation, neoangiogenesis, and the presence of other ectopic mesenchymal tissues, which will be discussed in further detail below.

### **2.5.1. Inflammation**

Inflammation is a hallmark of the pathology of atherosclerosis and CAVD. Atherosclerotic risk factors, such as increased low-density lipoprotein cholesterol, increased lipoprotein(a), male gender, cigarette smoking, hypertension, elevated body mass index, and diabetes, increase the incidence of atherosclerosis and aortic stenosis and likely contribute to valve endothelial dysfunction, as they do with atherosclerosis<sup>18,33-35</sup>. The dysfunctional, activated VEC in early valve disease have increased permeability to inflammatory infiltrates and upregulated leukocyte adhesion molecules like ICAM-1, VCAM-1, and E-selectin compared to healthy valves<sup>36</sup>. Histologically it has been shown that monocytes and T-lymphocytes attach to adhesion molecules, migrate into the

subendothelial space of the valve, and differentiate into macrophages where they release various inflammatory cytokines that induce the release of various proangiogenic molecules by VICs<sup>37,38</sup>.

Curiously, these same inflammatory signals are widely present in a controlled spatio-temporal manner during valvulogenesis, furthering the hypothesis that the pathology of CAVD mimics a disorganized valvulogenesis suggesting that similar pathways are involved in both processes<sup>39</sup>.

### 2.5.2. Pathological Angiogenesis During CAVD

Physiological angiogenesis is governed by a complex and integrated circuit which is necessary for maintaining homeostasis, wound healing, and growth; however, its loss of control leads to several pathologies. As will be reviewed in greater detail below, angiogenesis is controlled by a combination of pro and antiangiogenic molecules, cytokines, and the ECM in basement membrane and the underlying interstitium. Heart valves, like cartilage and eyes, are very avascular via a highly conserved anti-angiogenic microenvironment. During the progression of CAVD and other diseases like cancer however, angiogenesis is deregulated allowing it grow out of control. The true role of angiogenesis in the pathology of CAVD, whether it is causative or merely symptomatic, in the pathology of CAVD is still greatly understudied. The great majority of studies investigating angiogenesis in CAVD are histological in nature and therefore only descriptive. The lack of controlled *in vitro* studies inhibits the ability to explore cause and effect relationships<sup>40,41</sup>. The relevant studies describing angiogenesis as a histological feature of CAVD will be reviewed below.

#### 2.5.2.1. Histological Features of Angiogenesis Found in CAVD

Angiogenesis is a widely recognized histological characteristic of calcific aortic disease<sup>10,14,23,37,38,40–45</sup>. In one study, vessel formation was found to stain most intensely in moderate to medium levels of stenosis. Vascular density was shown to be correlated with various angiogenic markers such as VEGF, VEGFR-2, eNos, and nNOS. In addition, vascular density was associated with increasing levels of inflammation. Curiously, neovessel localization with calcification was shown not to be statistically significant<sup>41</sup>.

Another study showed that the density of organized arterioles correlated strongly with the degree of valvular calcification and the patient's prognosis. Additionally, this study found VEGF secreting myofibroblast differentiated VICs and inflammatory mast cells highly colocalized near neovessel formation. This study suggested that these two cell types work together in a positive feedback mechanism to increase neovascularization via three mechanisms. First, mast cells secrete VEGF to encourage neovessel formation. Secondly, the mast cells secrete inflammatory cytokines like tissue necrosis factor alpha (TNF- $\alpha$ ), which invoked further VEGF secretion by VICs in perivascular manner. Thirdly, the mast cells release various proteases to accelerate up the neovessel formation<sup>37</sup>. It had been shown previously that mast cells in stenotic aortic valves secrete tryptase, chymase, and cathepsin G, which are necessary to create channels for angiogenesis and thus provided supporting evidence for the role of these mechanisms<sup>46</sup>.

VICs harvested from these valves showed significant increase in VEGF secretion when treated with mast cell treated media, TNF- $\alpha$ , hypoxia, or tobacco extract. Interestingly, osteogenic media decreased VEGF secretion by these VICs. Additionally, the VIC conditioned media was able to stimulate VEGF production by the cultured mast cells providing evidence for the positive feedback mechanism<sup>37</sup>.

Another study by Hakuno et al. again showed that calcified valves contained activated mast cells co-localized around vWF positive neovessel formation. Additionally, they showed neovessel formation was co-localized with a loss of Chm-I and an increase in periostin. This study also found  $\alpha$ -SMA and vimentin positive cells wrapped around the neovessel formations acting in an apparent pericyte-like manner as in previously mentioned studies<sup>45</sup>.

Another study by Mazzone et al. supplied more evidence for the inflammation mediated angiogenesis formation in CAVD model showing increased vessel formation with increased inflammatory infiltrates and expression of inflammatory adhesion molecules<sup>38</sup>.

A histological study by Chalajour et al. showed patterns of vessel formation in accordance with previously mentioned studies. CD 34, Tie 2, and CEACAM-1 were



shown to stain neovessel formation additionally in this study. Interestingly, only neovessel formation in stenotic valves were shown to be positive for CEACAM-1<sup>44</sup>.

In another study by Chalajour et al, aSMA, VEGFR-2, and Tie2 were found to be co-upregulated. This upregulation was found strongly in the VECs on the leaflet exterior and in the cells on the interior of the valve. It is unclear however, if the cells staining on the interior of the valve are VICs or invading VECs as the exterior VECs stained just as strongly as the interior cells.

In conclusion, several studies have shown an increase in markers relating to angiogenesis and pericyte signaling in valve cells during the progression of CAVD. Most notably VEGF-VEGR2 and Angiopoietin-Tie2 are commonly found upregulated by both valve endothelial cells and valve interstitial cells which is a common finding when investigating peripheral vascular pathological angiogenesis. This group of studies' results make a strong case for the presence of increase angiogenetic signaling during CAVD which the valve cells are actively participating in and presumably the source of the neovascularization and the pericyte cells stabilizing the blood vessels. Although the source of the endothelial cells in the neovascularization has not been casually determined, this is in part due to that most of the studies to date investigating angiogenesis in the pathology of CAVD have been histological in nature as it is the standard of evaluating heart valve composition and microstructure. The problem with these studies is they are only able to perform meta analysis making cause and effect difficult to establish. To get around this limitation various studies have utilized *in vitro* assays to answer various angiogenesis related questions. However due to gaps in the previous research, this thesis is highly motivated to help bridge this gap of causality by providing controlled *in vitro* studies to better understand the unique behavior of valve cells to respond to this increased angiogenetic signaling environment to better predict how the cells are experiencing and responding to their changing microenvironment. Prior valve specific angiogenesis related work will be reviewed in further detail below.

### 2.5.3. Previous VEC Angiogenesis Studies

There have been a few studies investigating the angiogenic potential of VECs published in recent years. In one study by Chalajour et al. <sup>44</sup>, an aortic valve assay similar to the traditional aortic ring assay was performed. In the traditional study, a

freshly excised aortic ring is placed in a collagen gel and the capillary sprouts that grow from it are quantified using various angiogenesis metrics such as vessel length and branching points<sup>47</sup>. In this study, human calcific and control aortic valves were implanted into collagen gels to induce vessel formation. In this study, Chalajour et al. found capillary like channels emanating out of the calcific valves into the collagen matrix; meanwhile, they found very few of these sprouts in the non-stenotic valves. These capillary sprouts from both control and calcific valves showed positive staining for the angiogenesis/endothelial cell markers CD 31, CD 34, and vWF, although the staining was weaker in the control valve sprouts. Both the early capillary formation marker CEACAM1<sup>48</sup> and the basement membrane derived anti-angiogenic molecule endostatin were found only in vessels from the calcific valves<sup>44</sup>.

The study established that the valve endothelial cells from stenotic aortic valves are predisposed to forming angiogenic sprouts. While the non stenotic valves formed sparse vessels, morphologically the vessels they showed did not look like they would become functional vessels *in vivo*. Immunohistochemical staining on these various vessels suggested that these vessels originated from the valvular endothelium, were polarized, and began to lay their own basement membrane proteins. This data supplies evidence that the VECs are the cells that are actively undergoing angiogenesis in the pathology of CAVD. Ultimately this study lead the authors to hypothesize that a valve specific targeted anti-angiogenic therapy may preserve the integrity of the valvular endothelium and halt the progression of CAVD before any clinical signs would occur<sup>44</sup>. Although this study was able to demonstrate the angiogenic activation of cells from the calcific aortic valves, this model is suboptimal, because it is unable to determine the major factors that predispose a healthy VEC to undergo angiogenesis.

In a study by Paruchuri et al., human pulmonary valve endothelial cells (HPVEC) were clonally expanded to investigate the competing roles of VEGF and TGF-B on mediating endothelial to mesenchymal transdifferentiation (EnMT). A tubule like structure vasculogenesis matrigel assay<sup>49</sup> was performed with the HPVEC to establish they had an endothelial phenotype based on their tubule formation in the assay. Since the focus of the paper was on EnMT, the authors merely stopped there claiming that the vessel formation indicated they were endothelial cells. This is a common issue in the currently published *in vitro* angiogenesis related studies. Either the authors test

angiogenic factors they have seen histologically in the stenotic valve on non valvular endothelial cells<sup>11,45</sup> which have been shown to behave very differently from normal vascular endothelial cells<sup>4</sup> or the process of angiogenesis is merely glanced over as it is not the main focus of the paper<sup>50</sup>.

As angiogenesis has been implicated in the progression of CAVD for over 20 years now, several models have been proposed to its mechanistic role in the progression of CAVD.

#### 2.5.4. **Current Hypothesis for the Role of Angiogenesis in CAVD**

Like in human atherosclerotic lesions, neovascularization in the thickened aortic valves could both suppress and provoke disease progression. By providing oxygen and nutrients to the deeper parts of a hypertrophied valve leaflet, neovascularization could act to prevent cellular necrosis and the formation of necrotic core areas. On the other hand, by facilitating the transport of inflammatory cells and lipids into the leaflets, neovascularization could accelerate valvular thickening and calcification. Neovascular endothelium secretes angiogenic mediators, including VEGF, which may exert effects on osteogenic cells, and thereby induce ectopic calcification. Moreover, neovascular pericytes may act as osteogenic progenitors, thus contributing to the calcification<sup>51</sup>.

A proposed conceptual framework for this model of angiogenesis mediated calcification of the aortic valve is shown below. The conceptual framework centers on the competing roles of various pro and anti-angiogenic factors in the progression of atherosclerotic and rheumatic valvular disease. The circulating CD14-positive inflammatory cells (and possibly fibrocytes) that express periostin initially infiltrate the zona ventricularis of the SL valve. Thereafter, periostin secreted from these cells not only promotes angiogenesis by induction of endothelial cells (EC) migration and inhibition of EC apoptosis, but also stimulates the production of MMP-2, MMP-9, and MMP-13 by ECs, VICs, and engrafted macrophages, which advance cardiac valve degeneration. Valve degeneration in turn facilitates the infiltration of circulating periostin-expressing cells, thereby creating a vicious circle. The origin of the engrafted ECs is unknown; it is possible that periostin enhances the recruitment of circulating endothelial progenitor cells into the valves or promotes the penetration of microvessels from the annulus region or roots into the leaflets. In contrast, Chm-I blocks angiogenesis through

inhibition of EC migration and induction of EC apoptosis, although other angiogenic factors are involved during the earlier stages of valve degeneration. Therefore, the equilibrium between periostin and Chm-I I (as well as other angiogenic factors) defines the progression of atherosclerotic and rheumatic cardiac valve degeneration by controlling angiogenesis and MMP production.

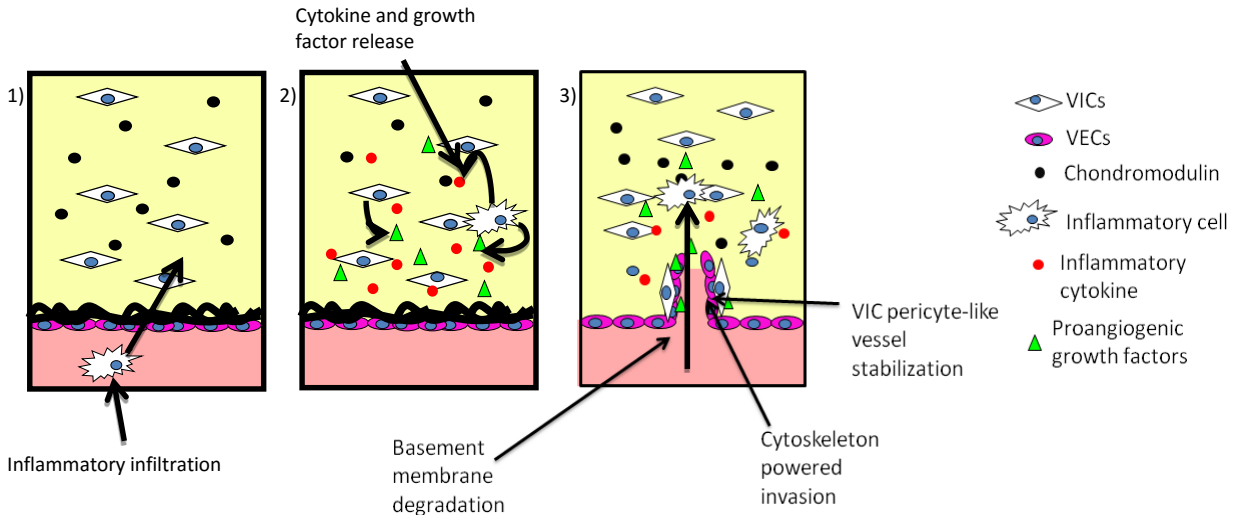


**Figure 2-2. Conceptual framework for the role of various angiogenic factors that lead to the formation of angiogenesis in valves.**

## 2.6. Review of Peripheral Vascular Angiogenesis

Angiogenesis is an important biological process, not only under physiological conditions, but in a variety of diseases including cancer, diabetic retinopathy and rheumatoid arthritis<sup>52</sup>. It is an essential process for forming new blood vessels and is fundamental for development, reproduction, wound repair, and life in general in higher order life forms. It is generally a highly regulated process that is only turned on for brief periods of time and then immediately shut off. The switch being left on is the source of many diseases.

The process of angiogenesis depends on a balance of a myriad of various signals released by the endothelial cells, the vessel wrapping pericytes, the

proangiogenic source, the surrounding ECM, and the local biomechanical environment.

<sup>53</sup> Upon activation, angiogenesis consists of a series of steps that involve separation from the host vasculature and pericytes, degradation and migration across the basement membrane, followed by coordinated migration and proliferation towards the source of the angiogenic signal in a series of differentiation steps that involve tip, stalk, and phalanx cell production as the neovessel grows to its new home. The many factors that modulate and drive this process include soluble growth factors and inflammatory cytokines, membrane bound proteins, cell-matrix interactions, cell-cell interactions from surrounding cells and fellow endothelial cells, and several internal interacting signals which will be covered in greater detail below <sup>52</sup>.

#### 2.6.1. The Role of ECM in Modulating Angiogenesis

It is recognized that these growth factors play an important role in modulating and driving angiogenesis, but a crucial factor that is often overlooked is the role of the ECM in modulating angiogenesis. The ECM is the fundamental component in the microenvironment in every organ in a biological system. The ECM provides a dynamic and bioactive structure that controls cellular behavior through chemical and mechanical signals. This fact holds true for endothelial cells as well. The ECM controls EC through a variety of mechanisms including cell anchorage, ECM-integrin mediated intracellular signaling, sequestration and release of the growth factors mentioned in the previous section, and alterations in the suprastructure of the ECM which physically impedes the movement of the ECs during angiogenesis<sup>54</sup>.

As reviewed earlier, endothelial and epithelial cells are anchored in place to the basement membrane (BM) which plays a major role in maintaining endothelial cell quiescence and maintaining proper hemodynamics. Angiogenesis, however, requires the degradation of the BM and the surrounding ECM using matrix-metalloproteases, serine proteases, and cysteine proteases <sup>54</sup>. After the BM is degraded, it transitions to a provisional matrix comprised of newly laid fibronectin, fragments of the previous BM, and the secreted beginnings of the new BM. Upon degradation, various growth factors such as VEGF, FGF, and others are released to encourage the sprouting through the new hole in the BM. As EC invade during angiogenesis, they begin to produce a new BM around the new sprout which matures as the EC and pericytes secrete the appropriate

new matrix molecules<sup>5</sup>. Figure 2-3 diagrams this transition from a loose unorganized provisional matrix to a mature pericyte covered new blood vessel.

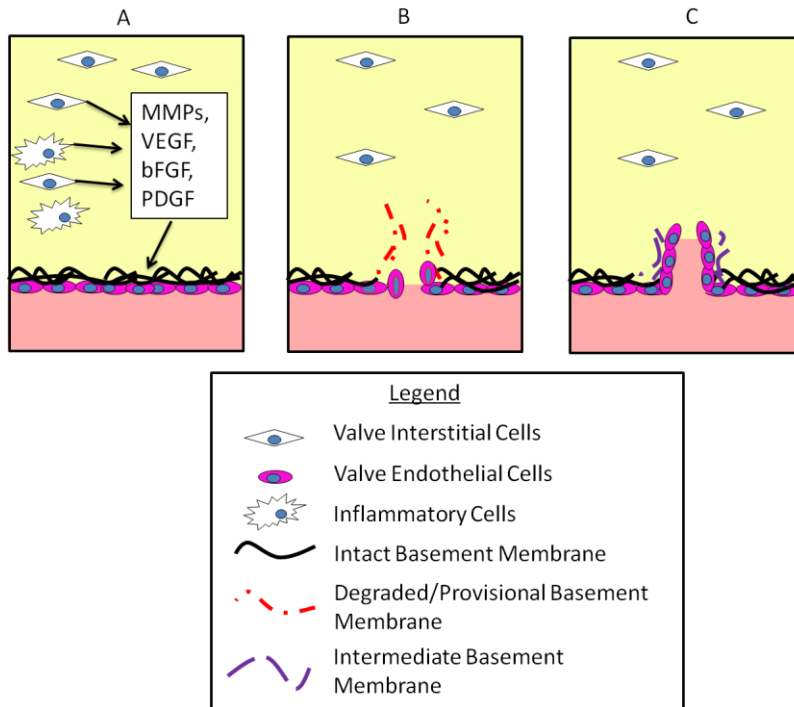


**Figure 2-3. Basement membrane transitions during angiogenesis. A) Induction B) Provisional matrix production and invasion C) Resolution leading to intact basement membrane production<sup>5</sup>.**

Most of the endothelial cell–matrix biomechanical force transduction and resultant internal cell signaling transduction occurs through the integrins. Integrins have a cell type–specific and context-dependent expression. There are at least eight members of the integrin family currently identified, which include the collagen-binding integrins ( $\alpha1\beta1$ ,  $\alpha2\beta1$ ), the laminin-binding integrins ( $\alpha3\beta1$ ,  $\alpha6\beta1$ ,  $\alpha6\beta4$ ), and the fibronectin based RGD-binding integrins ( $\alpha5\beta1$ ,  $\alpha\nu\beta3$ ,  $\alpha\nu\beta5$ )<sup>55</sup>. Additionally, the  $\alpha\nu\beta3$  as well as  $\alpha\nu\beta5$  integrins have been shown to be the most upregulated integrins on endothelial cells during angiogenesis compared to their low quiescent expression<sup>56</sup>. Upon binding to the ECM, these integrins facilitate more than just anchorage to their substrate. Upon their binding and following dimerization, numerous internal cellular cytoplasmic proteins become activated and can organize nearby cytoskeletal structures or cause changes in expression of various downstream genes.

It has been shown that many angiogenic responses require working through specific integrin-matrix interactions, and some work better than others <sup>57,58</sup>. For example, the integrins  $\alpha\text{v}\beta 3$  and  $\alpha\text{v}\beta 5$  along with focal adhesion kinase (FAK) are all three necessary for the activation of the Ras-ERK pathway which induces cell survival during angiogenesis in FGF downstream signaling <sup>59</sup>. These and other studies have shown the importance of collaboration between integrin and growth factor mediated signaling as angiogenesis cannot proceed without both of them working together and activating parallel pathways. Collectively, these studies provided evidence for the importance of the integrin-growth factor crosstalk in endothelial cells and for the bidirectional flow of information between the extracellular and intracellular compartments.

Matricellular signaling is an important role of the ECM. In angiogenesis, several regulating growth factors such as FGF, VEGF and transforming growth factor- $\beta 1$  (TGF- $\beta 1$ ) or their activity-modifying molecules bind to various ECM components limiting or increasing their bioactivity. In particular, the heparan sulfates on heparan sulfated proteoglycans like perlecan have been identified as growth factor binding sites<sup>60</sup>. Growth factor-ECM interactions can significantly control tissue homeostasis and the underlying EC and interstitial cell function, because these molecules are instrumental in establishing the gradients of these angiogenic molecules. These gradients are necessary for any functional vascular network formation as they guide where the new vessels form as demonstrated by several knockout mouse models <sup>61</sup>. Additionally, these gradients are essential for designating the leading edge of a new sprout and the role of each EC in the new sprout. This mechanism will be detailed in greater detail later section when discussing the various differentiation stages of ECs during angiogenesis.

### 2.6.2. Vascular Endothelial Growth Factor

Perhaps the most studied of these factors is the effects of soluble growth factors and the downstream signaling of their affected receptors. By understanding the role of these proteins in physiological angiogenesis, insight can be gained into which of these factors are important to study in further detail in the context of valve cell angiogenesis and CAVD.

The VEGF family of growth factors is the best characterized and most studied growth factor that affects angiogenesis. It has several versions each with different isoforms. The most important and most widely studied of the versions is VEGF-A<sup>52</sup>. It is a secreted cytokine that is important in physiological and pathological angiogenesis<sup>62</sup>. The VEGF exon is differentially spliced to yield several mature forms (VEGF 121, VEGF 145, VEGF 165, VEGF 183, VEGF 189, and VEGF 206)<sup>63,64</sup>. VEGF165 is widely considered to be the predominantly expressed and to have the highest bioactivity<sup>65</sup>.

VEGF exerts its biological effects through the VEGF family of receptors. These receptors are transmembrane tyrosine kinase receptors that include VEGF Receptor-1 (VEGFR-1), VEGFR-2, and VEGFR-3 which are selectively expressed in endothelial cells. VEGF also binds the neuropilin receptors NP-1 and NP-2 which are expressed on neurons and endothelial cells<sup>66</sup>. Once VEGF has bound its extracellular domain, it causes a dimerization and autophosphorylation of the intracellular receptor tyrosine kinase. VEGFR-1 (or Flt-1) is a 180-kDa with a high affinity for VEGF (Kd 10pM). VEGFR-1 role is to sequester excess VEGF and to prevent its binding to other VEGF receptors thus acting as a competing inhibitor to pro-angiogenic VEGF signaling. This mechanism is demonstrated by a study that found that deletion of the intracellular domain of VEGFR-1 showed no signs of abnormal vascular development demonstrating that its activity is merely extracellular<sup>67</sup>.

VEGFR-2 (also known as KDR or Flk-1) is a 200 kDa high affinity receptor for VEGF (Kd of 75-125 pM). VEGFR-2 is considered to be the major mediator of several physiological and pathological effects of VEGF-A on endothelial cells. These include proliferation, survival, migration, and permeability<sup>68</sup>.

VEGFR-2 induces proliferation through activation of the classical extracellular regulated kinase (Erk) pathway p42/44 mitogen-activated protein kinase (pMAPK). VEGFR-2 activates Raf directly via protein kinase C (PKC) in a Ras-independent manner and dependent manner through PKC and sphingosine kinase<sup>69-71</sup>. VEGFR-2 also activates PI3K, which results in an increase in the lipid phosphatidylinositol (3, 4, 5)P<sub>3</sub> and activation of several important intracellular molecules such as Akt and the small GTP-binding protein Rac which plays an important role in actin cytoskeletal remodeling and regulating vascular permeability. The Akt/PKB pathway regulates cellular survival by



inhibiting pro-apoptotic pathways such as B-cell lymphoma 2 (Bcl-2)-associated death promoter homologue (BAD) and Caspase 9<sup>72</sup>. The Akt/PKB pathway also activates endothelial nitric oxide synthase (eNOS) generating NO, which is implicated in the increase in vascular permeability and cellular migration observed with VEGF-A. Other components implicated in VEGFR-2-dependent cytoskeletal regulation and cell migration include p38 mitogen-activated protein kinase (MAPK) and focal adhesion kinase (FAK) and its substrate paxillin<sup>52</sup>.

### 2.6.3. Potential Links Between EnMT and Angiogenesis

The TGF- $\beta$  family of cytokines stimulate type II and type I transmembrane serine-threonine kinase receptors. In response to TGF binding to the type II receptor, it phosphorylates the type I receptors which activate the downstream signaling transcription factors from the Smad family<sup>73</sup>. TGF signaling has been described as an angiogenic switch with both pro- and antiangiogenic properties. At low doses, TGF- $\beta$ 1 contributes to the angiogenic switch by upregulating angiogenic factors and proteinases of other cell types, whereas at high doses, TGF- $\beta$  inhibits EC growth, promotes basement membrane reformation and stimulates smooth muscle cells differentiation and recruitment<sup>74</sup>.

Another important signaling aspect of TGF is its role in epithelial to mesenchymal transdifferentiation (EMT) which has an important role in development and the development of several pathologies like CAVD and various cancers. EMT involves the loss of their major characteristics of epithelial cells including the dissolution of tight junctions, adherens junctions, and desmosomes, and additionally a loss of their apical polarity followed by acquiring a mesenchymal phenotype which involve actin reorganization, stress fiber formation, and migration into the underlying interstitium<sup>75</sup>.

Curiously, VECs have been demonstrated to undergo EMT towards a VIC phenotype in response to TGF. Human pulmonary valves endothelial cells were shown to undergo endothelial to mesenchymal transdifferentiation (EnMT) in response to TGF- $\beta$ 2 specifically. The increase in EMT markers was correlated with an increased migration and invasion capacity and a loss of various EC phenotypes. These included the loss of the ability to form tube-like structures on matrigel, the ability to adhere to leukocytes in response to inflammatory signals, of tight cell to cell junctions, of

cobblestone morphology, and of CD 31 and VE-cadherin. Interestingly, VEGF was able to inhibit this loss of EC phenotype, and it was able to reverse it partly restoring the expression of CD 31<sup>50</sup>. These studies provided *in vitro* causal evidence for angiogenesis related signaling to keep VECs in a partial transdifferentiating state while maintaining their endothelial phenotype. As it has been shown that only VECs from calcified valves are proangiogenic and there is suspected to be greater EnMT by VECs during the CAVD, these results and along with the histology studies previously reviewed beg the question if there is a link between partial VEC EnMT and the VEC angiogenic potential. These results led us to hypothesize that VEC angiogenesis begins as an EnMT process as in normal VEC physiology and valvulogenesis, but the increased angiogenic environment from the normal anti-angiogenic environment forces the VECs to sustain their endothelial phenotype and become proangiogenic. This link between partial EnMT and angiogenesis has been proposed in vascular endothelial cells and has been detailed in a recent review.<sup>76</sup>

#### 2.6.4. Cell-Cell Interactions and the Role of Pericytes in Angiogenesis

Endothelial cells alone cannot form functional and mature sprouts though. Angiogenesis requires communication with perivascular cells through direct cell-cell interactions or indirectly through other pericyte-EC specific soluble factors. These perivascular cells are just as important in regulating vascular destabilization, remodeling, formation, stabilization, and final functionality of the neovessel. Whether VICs can act in a pericyte manner and promote angiogenesis remains to be elucidated.

In the mature vascular system, the endothelium is supported by mural cells that express characteristics specific to their localization. The larger vessels are surrounded by single or multiple layers of vascular smooth muscle cells (vSMC), whereas the smallest capillaries are partially covered by solitary cells referred to as pericytes. Intermediate-size vessels, arterioles and venules, have mural cells with properties intermediate between those of typical vSMC and pericytes. Based on the morphological similarities and the heterogeneity of the expression of various markers like  $\alpha$ -SMA and desmin, it is hypothesized that pericytes and vSMC represent phenotypic variants of the same cell lineage whose phenotype depends upon where they lie and their

corresponding external stimuli along the vasculature and exist in heterogeneity along the length of the vasculature<sup>77</sup>.

Interestingly, it has been suggested that pericytes can detach from their vessel wall and differentiate into an ECM fibroblast-like cell that can contribute to inflammatory mediated fibrosis in a similar manner as VICs<sup>78</sup>.

The vSMCs provide structural support to the large vessels and regulate blood flow due to their contractile behavior. They are not in direct cell-cell contact with the endothelial cells, but they are separated from the endothelium by an intact basement membrane. Pericytes, on the other hand, share basement membrane with the endothelial cells and directly contact ECs through holes in the basement membrane. These heterologous peg-and-socket contacts have been reported to contain tight and gap junctions, to have high levels of fibronectin, to be comprised of adherens junctions, and to transmit biomechanical forces from the pericytes to the EC and back<sup>79-82</sup>.

There have been several markers for pericytes identified to date, but due to the heterogeneity of their phenotype there exists no one definitive pericyte marker. The currently recognized markers are  $\alpha$ -SMA, desmin, high molecular weight melanoma antigen (NG2), PDGFR, aminopeptidase N, and G-protein signaling<sup>77</sup>. Making the identification of these cells more difficult is the fact that their expression is dynamic based upon the species, tissue, or phase in angiogenesis that is being studied.<sup>78</sup>

Complicated by their previously mentioned heterogeneity, the true origin of pericytes is hard to establish. They have been shown to originate from the neural crest and mesoderm during development. Additionally, they have been demonstrated to differentiate from progenitor cells when treated with PDGF-BB<sup>51</sup>.

Interestingly, it has been suggested that pericytes may also be derived from smooth muscle cells, fibroblasts, endothelial cells, and the bone marrow, although the factors that stimulate the differentiation of these cells into pericytes and the relative contributions of these cells to the generation of pericytes in adult and embryonic tissues is not clear. As well as being derived from multiple cell types, it is now apparent that pericytes are capable of differentiating and dedifferentiating into a variety of different cell types as shown by Figure 2-4<sup>51</sup>.

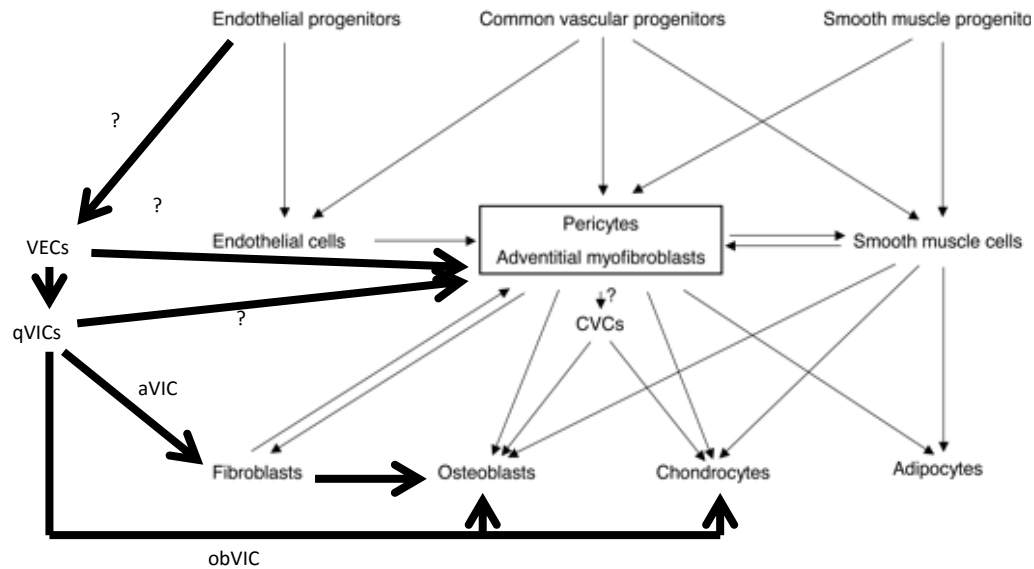


**Figure 2-4. Diagram displaying the various ontogeny of a perivascular cell. Pericytes can be derived from a variety of sources (adapted from<sup>51</sup>). CVC's stands for calcifying vascular cells. Additionally, the proposed pathologies in which VICs and VECs could potentially transform into pericyte like cells and how their pathways could fit in to the overall pericyte lineage. Arrows with question marks are pathways that have been proposed but not confirmed.**

With all of the many possible sources for pericytes, there is the question of whether VICs can act in a perivascular manner or whether the VECs are differentiating towards the perivascular phenotype in situ. Histologically, it appears there is an  $\alpha$ -SMA positive cell wrapping itself around neovessels in CAVD, but its source is still not clear. In my preliminary data, I will present evidence that suggests that VICs differentiated from VECs can indeed wrap themselves in a perivascular manner around neovessels formed by VECs. Whether VICs can act in a pericyte manner was the fundamental hypothesis of the second specific aim of the thesis.

#### 2.6.5. Endothelial/Pericyte Signaling Through Angiopoietin-Tie2 Signaling

As reviewed earlier, the effect of VEGF stimulus on valve cells has received some interest of late. However, in the context of valve cells, an important angiogenesis signaling method which has not received any investigation *in vitro* and has been highly implicated to have a role in CAVD progression through histological examination is the Angiopoietin (Ang) - Tie2 pathway. Understanding the role of this pathway in vascular

pericyte/EC communication can give insights into its potential role in valve cell interactions. The Angiopoietins (Ang1 and Ang2) and their corresponding receptor Tie2 are another important signal in angiogenesis that is involved in vessel maintenance, growth, and stabilization.<sup>74</sup> Many studies have established that this pathway is involved in reciprocal communication between endothelial and pericyte cells.<sup>78</sup> The Tie2 receptor was originally considered to be endothelial cell specific with its agonistic ligand expressed mainly by perivascular and mural cells; however, recent studies have suggested that it is expressed in both cell types to act as a communicatory feedback mechanism. Ang1/Tie2 signaling is required for vessel stabilization. Signals originating from binding of pericyte-derived Ang1 to Tie2 lead to stabilization of endothelial cells. Genetic knockout studies have demonstrated that this pathway stimulation is required for vascular stabilization and recruitment of pericytes to blood vessel. These studies suggest a role for Ang1/Tie2 signaling in both recruitment and stabilization<sup>78</sup>. This interaction is studied for valve cells in Specific Aim2. In addition, Ang2 is known to act as an antagonist to Ang1/Tie2 signaling in endothelial cells, leading to vessel destabilization. Ang2 upregulation in endothelial cells marks the beginning of angiogenic sprouting and correlates negatively with pericyte coverage. These findings reinforce the concept of autocrine Ang2 antagonism of Ang1/Tie2 signaling leading to endothelial-endothelial cell destabilization through loss of pericyte-endothelial signaling. Interestingly, Ang2 was found to be rapidly released from endothelial cells from Wiebel-Palade bodies upon excitation with phorbol 12-myristate 13-acetate (PMA), thrombin, or histamine suggesting a role for inflammation to initiate autocrine Tie2 antagonism.

#### 2.6.6. **Stages of EC Differentiation during Angiogenesis**

Once the endothelial cells are activated by the previously reviewed factors, they differentiate in a specific manner to produce a specific organization. Based on their current local environment of growth factors, ECM, and surrounding EC, the EC either stay in the same stage of differentiation, or they differentiate into a tip, stalk, or phalanx endothelial cell type. Each stage has a positive feedback loop to maintain its phenotype until it receives the proper signal to change. These signals can be sensing high/medium/ low concentrations of specific pro-angiogenic molecules, specific cell-cell contacts from its neighbors, or cell-ECM interactions. It is important to be able to recognize these various stages because they offer insight in to how the VECs respond to

their environment's signals in the studies of this thesis.<sup>83</sup> These three differentiations make up the core of the neovessel and are covered in more detail below.

#### 2.6.6.1. Tip Cells

Genetic studies utilizing the mouse retina have shown that a VEGF gradient is necessary to induce the tip cell phenotype. Upon binding to VEGFR2 at a high concentration, VEGF's downstream signaling cascades designate a cell to become a tip cell while lateral inhibition by the now designated tip cell prevents other cells from becoming a tip cell forcing them to become a stalk cell<sup>83</sup>. This lateral inhibition relies on tip-to-stalk cell communication via Dll4/Notch signaling<sup>84</sup>. ECs express various Notch receptors (Notch1, 3, 4) and ligands (Dll1, Dll4, Jagged1, Jagged2). After ligand binding, Notch is cleaved intracellularly, generating the Notch intracellular domain (NICD) that acts as a transcriptional regulator. Tip cells are exposed to the highest levels of VEGF, which induces the expression of Dll4 in these cells. Dll4 binds to Notch on neighboring (future stalk) ECs and down regulates VEGFR2 signaling; this dampens the VEGF-induced expression of Dll4 in these cells, thereby establishing a self-reinforcing feedback that allows the leading cell to gain and retain its tip position, while preventing the follower neighbors from leaving their position in the stalk<sup>85</sup>.

Sprouting angiogenesis is an invasive process that requires proteolytic degradation of the ECM. Tip ECs express MMPs, and their expression is regulated by the composition of the surrounding ECM they have to invade. At the leading edge of invading tip cells, membrane type-1 MMP is indispensable for ECs to form invading channels<sup>86</sup>. Meanwhile, these MMPs are downregulated via EC-pericyte interactions during vessel stabilization preventing excessive branching and inconsistencies in the vessel<sup>87</sup>.

#### 2.6.6.2. Stalk Cell

As mentioned previously, the second subphenotype in a neo vessel is the stalk cell. The purpose of the stalk cell is to proliferate, elongate the stalk, form a lumen via pinocytosis, begin producing a new BM, and open the new vessel to the existing circulation<sup>85</sup>. The lateral inhibition via Dll4/Notch signaling from tip cells dampens the stalk cell's response to VEGF by lowering the expression of VEGFR2, VEGFR3, NRP1,

and CXCR4. Therefore, even though the stalk cell may be in a high VEGF local environment compared to previously in the neovessel formation, the stalk cell senses a much lower concentration of VEGF and acts accordingly. Stalk cells are instead encouraged to push the stalk forward via proliferation<sup>84</sup>. In order to help push the stalk forward while the tip cells pull it forward, the stalk cells must divide while maintaining contact with the tip cell and each other. During this coordinated migration, each EC must rapidly reorganize its cell-cell junctions to the leading edge and its connecting cytoskeletal components to allow for fluid movement of the whole stalk in a forward movement<sup>87</sup>. Additionally, Wnt and FGF have been demonstrated to have important roles in improving and tightening these intracellular junctions<sup>88,89</sup>.

Curiously, Notch has been implicated to have a role in TGF- $\beta$  mediated EMT of VECs from the post natal valve endothelium<sup>90</sup> while Jagged1 expression was unaffected by TGF- $\beta$  treatment<sup>50</sup>.

#### 2.6.6.3. Phalanx Cells

Unlike tip cells, phalanx cells extend few filopodia and migrate poorly in response to VEGF, but they form tighter intercellular barriers. They resemble stalk cells by depositing a basement membrane and establishing junctions, but differ from these cells by their increased quiescence and reduced mitogenic response to VEGF. However, it is known that a basal level of VEGF and other factors are required to maintain survival. Additionally, increased levels of VE-Cadherin and soluble Flt-1 work together to maintain the phalanx cell phenotype<sup>83</sup>.

This phenotype is interesting because VECs are physiologically in this state under normal conditions displaying the characteristic phalanx morphology. Interestingly, VECs appear to orient themselves perpendicular to flow compared to the parallel orientation of traditional endothelial cell types. The morphological response to shear stress appeared to be both calpain and Rho-kinase dependent in VECs, but they were PI3K independent unlike endothelial cells from the aorta<sup>21</sup>.

### 2.6.7. Proliferation

One of the more dramatic effects of angiogenesis is a sudden and rapid increase in proliferation. EC's turnover time is usually in the hundreds of days, but during angiogenesis, they can proliferate as rapidly as bone-marrow cells. This fact is why proliferation is such an important marker of angiogenesis <sup>5</sup>.

### 2.6.8. The Role of Actin Remodeling in Angiogenesis

In order for endothelial cells to respond to form new angiogenic sprouts, they require a highly coordinated reorganization of their actin skeleton in response to the various signals they receive from their microenvironment.

In response to a proangiogenic gradient, ECs become polarized, so that their leading front extends towards the source. In tip cells, this leads to the formation of filopodia while the rear maintains contact with trailing stalk cells to avoid branch disintegration. There are several small GTPase molecular switches in the Rho family that control each element of the actin cytoskeletal rearrangement and work together to produce the organized movement of each EC that sums up to be angiogenesis.

The key job of endothelial tip cells during neovessel formation is to navigate along proangiogenic gradients which relies on correctly probing the microenvironment for cues, and translating these cues into a dynamic process of adhesion (at the front) and release (at the rear), which translates to cellular movement [156]. In order to produce this movement, the tip cell must form lamellipodia and filopodia to reach out into the transitional ECM to form new focal adhesions at the leading edge. Lamellipodia are short veil-like structures in close proximity to the plasma membrane that contain a highly branched actin network. Filopodia, on the other hand, consist of long spiky plasma membrane protrusions containing tight parallel bundles of filamentous actin (F-actin), which usually extend from lamellipodia. However to produce movement, the EC uses contracting stress fibers to pull its rear forward as it simultaneously recycles focal adhesions from the rear to the leading edge. Each of these processes is regulated by a different member of the Rho family<sup>83,91</sup>.

The main regulators of filopodia and lamellipodia formation are RhoA, Rac1, and Cdc42 are discussed below<sup>92</sup>. These molecules are activated by binding of GTP



nucleotides, supplied by Guanine nucleotide Exchange Factors (GEFs). Inactivation occurs via their intrinsic GTPase activity, which converts GTP into GDP; this process is stimulated by GTPase Activating Proteins (GAPs). RhoA, Rac1, and Cdc42 are activated in response to stimulation of many membrane receptors, including receptor tyrosine kinases and G protein–coupled receptors.<sup>92</sup> Cdc42 and Rac1 regulate filopodia and lamellipodia formation, respectively, through activation of p21-activated kinase (PAK); RhoA is involved in adhesion and forward movement through regulation of stress fiber formation and contraction via the Rho-associated serine-threonine protein kinase (ROCK) that leads to the phosphorylation of myosin light chain (pMLC);<sup>92–94</sup> PAK and ROCK activate LIM-kinase, which, through inhibition of Cofilin, blocks F-actin depolymerization. Activated Cdc42 and Rac1 also interact with the WASP:ARP2/3 complex, thereby inducing F-actin branching. Filopodia extension is also regulated by targeting Ena/Vasp proteins to the membrane at the leading edge of migrating cells<sup>92,93</sup>. Once extended, filopodia make contact with ECM components such as laminin, fibronectin, and collagen through integrins on their surface that initiate the formation of focal contact points<sup>94</sup>. An important regulator of this process is the focal adhesion kinase (FAK)<sup>95</sup>. Hence, signals from integrins and growth factor receptors are transduced to the cytoskeleton in these filopodia.

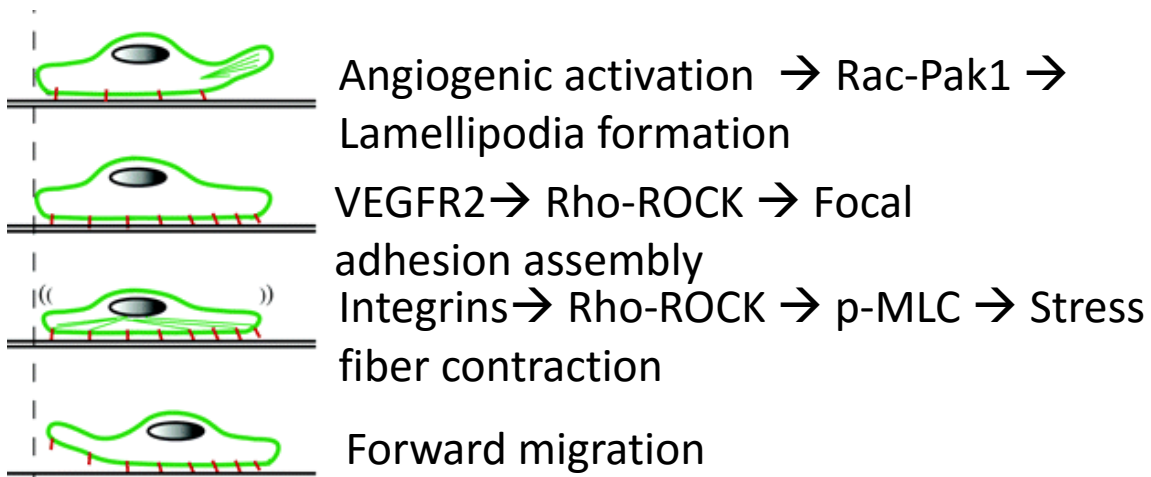


**Figure 2-5. Overview of the major steps of endothelial cell migration and correlating actin cytoskeletal regulators' roles during each step relevant to this thesis(adapted from <sup>91</sup>).**

### 2.6.9. The Role of Angiogenesis in Atherosclerosis

A central motivation of the work in this thesis is to provide insight into how the translation of angiogenesis signaling by valve cells plays a role in the pathology of CAVD. To better understand how to address this research topic, one can look at more studied disease pathways that are similar in their nature to CAVD.

For example, both atherosclerosis and CAVD are slowly progressing diseases that develop slowly over time. Both diseases have precursor lesions that remain asymptomatic during early stages of the pathology. They show similar risk factors of hypertension, elevated low-density lipoprotein, male gender, smoking, and diabetes <sup>18</sup>.

Both atherosclerosis and CAVD show inflammatory induced fibrosis with variable lipid composition. The diseased valves show chronic inflammatory cells, lipoproteins, lipid, extracellular bone matrix proteins, and bone mineral, similar to atherosclerotic lesions. However, atherosclerotic plaques have a unique feature in that there is a reasonably well demarcated central area of necrosis which is separated from the bloodstream by a fibrous cap. When this fibrous cap ruptures, it can lead to acute luminal thrombosis of the coronary artery and myocardial infarction. CAVD does not show a similar necrotic core and fibrous cap, and calcification tends to be more prominent, forming calcified nodules. Calcified nodules have been seen in atherosclerotic plaques as well; however, they are not as prominent <sup>96</sup>.

Curiously, both atherosclerosis and CAVD are characterized by a pathological ectopic angiogenesis although there are some marked differences. In atherosclerosis, as the plaque forms and develops, the hypercholesterolemic, inflammatory, and hypoxic conditions in the thickened vessel wall trigger the onset of angiogenesis<sup>97</sup>. These neovessels contribute to the enlargement of the plaque and the necrotic core extending from the vasa vasorum to the intima <sup>98</sup>. The neovessels are generally poorly developed, have thin walls, and have incomplete endothelial junctions giving red blood cells a route into the middle of the plaque where they release cholesterol which is taken up by macrophages creating foam cells and enlargement on the plaque <sup>96</sup>. Furthermore, the neovessels provide a route for greater inflammatory cell infiltration, which promotes further angiogenesis but also disrupts the fragile vessels and destabilizes the plaque,

leading to intraplaque hemorrhage and possible plaque rupture<sup>97</sup>. Interestingly, it does not appear that plaque stability is an issue in CAVD<sup>96</sup>.

The full role of angiogenesis in the pathology of CAVD has not been described however. As mentioned previously, the neovessel formed during CAVD could act as channels facilitating the increase of inflammatory infiltrates and other sources of calcification. The work in this thesis sought to model this phenomenon by investigating the effects of inflammatory cytokines found in both CAVD and atherosclerosis which are known to be proangiogenic on valve endothelial and interstitial cells in the context of angiogenesis. Curiously, it is not fully understood which cell type is the major contributor to the neovessels' walls as it has been hypothesized to be VECs, VICs, and/or circulating progenitor cells<sup>18</sup>. Until CAVD is as nearly understood as atherosclerosis, it will be difficult to repeat the same successes from interventional treatments for atherosclerosis that have come from increased knowledge of the cellular based pathology of the disease. Recently there have been several advances in synthetic tissue engineered strategies that may aid in finding this needed knowledge.

## **2.7. Tissue Engineering Strategies to Better Understand Angiogenesis**

Tissue engineering in general is defined as applying methods and techniques from engineering combined with the life sciences to create artificial constructs to evoke a specific biological response. This response can range from regeneration, replacement of the function of a tissue, or simply recapitulation of a native response to better understand it<sup>99,100</sup>. The work in this thesis will expose valve cells to customized microenvironments inspired by physiological features of angiogenesis to better understand the roles of these features in initiating VEC angiogenesis.

Although there are many approaches that have been used for tissue engineering strategies, hydrogels are the most relevant for this thesis. Hydrogels are water-swollen, three dimensional polymer matrices that allow diffusion of nutrients and waste from their mesh. They have been used as platforms for a variety of tissues such as for cartilage, bone, and blood vessels<sup>101-103</sup>. Hydrogels generally fall into two categories: natural and synthetic. Natural hydrogels, as their name implies, are derived from natural polymer-

based materials such as collagens, various polysaccharides like hyaluronic acid, and other materials found in nature. Synthetic polymers are made from such materials as poly(acrylic acid), polyacrylamide, and poly(ethylene glycol) (PEG).

Although natural scaffolds inherently have many beneficial properties for tissue engineering applications such as biocompatibility, inherent cell adhesiveness, and biodegradation. However due to their sourcing, these scaffolds are generally met with immunogenic and infectious responses *in vivo* in addition to their poor mechanical properties<sup>104</sup>. Meanwhile, synthetic scaffolds have become a popular choice in medium lately due to their customizability in shape, mechanical properties, chemical composition, diffusive properties, and biofunctionality<sup>105</sup>.

### 2.7.1. Poly Ethylene Glycol (PEG) Overview

PEG is a hydrophilic polymer that has been used in various biomedical applications such as surface modification of other materials to increase their biocompatibility, bioconjugation, drug delivery to lower the immunogenic response, and many tissue engineering applications. PEG is becoming the synthetic polymer of choice for several applications due to its good biocompatibility, low protein adsorption, non-immunogenicity, ability to be photopolymerized at physiological temperatures and pH, and its ability to be specifically modified with various biological agents in a spatio-temporal manner using various photocrosslinking strategies<sup>99</sup>. In order to better design these hydrogels to increase their cellular adhesiveness, biodegradability, and to better recreate the local biochemical/mechanical microenvironment, researchers have looked towards various natural ECM components as inspiration in designing their bioactive scaffolds. This modification to promote bioactivity often involves binding various growth factors and cell adhesive domains derived from various ECM proteins.

The ECM protein derived cell adhesive peptides (CAPs) have been important targets for cell-adhesive modification of PEG hydrogels to overcome their lack of protein adsorption and thus poor innate cell adhesion. They are mainly derived from four ECM proteins, including fibronectin, (e.g., RGD, KQAGDV, REDV and PHSRN), laminin (e.g., YIGSR, LGTIPG, IKVAV, PDGSR LRE, LRGDN and IKLLI), collagen (e.g., DGEA and GFOGER) and elastin (e.g., VAPG)<sup>106,107</sup>.

In order to covalently attach CAPs and growth factors to create biomimetic scaffolds, there have been several strategies developed to chemically modify these proteins allowing them to be attached to the PEGDA utilizing thiols, acrylates, and/or other chemical groups. The most prominent method which will be used in this thesis has been utilized by West et al. in recent years to develop a copolymerization method for covalently tethering acrylated growth factors to PEG networks. The growth factors that they have incorporated into their PEGDA gels have included bFGF, EGF, VEGF, PDGF-BB, Ephrin-1, TGF $\beta$ , and others.<sup>108-112</sup> These studies demonstrated that it was possible to covalently tether growth factors to hydrogels while maintaining their proangiogenic bioactivity in a spatio-temporal manner.

### 2.7.2. Biomimetic PEGDA Hydrogel Systems

In recent years, various groups have displayed the versatility of these hydrogel systems for probing for the inner workings of cells. These systems have helped investigators to understand how to control cell behavior and to screen for various drug targets.

#### 2.7.2.1. Induction of Angiogenesis in Tissue Engineered Scaffolds

Another major enduring problem of tissue engineered scaffolds is their need to be vascularized to allow for proper nutrient flux. This fact has led investigators to design scaffolds to probe what is necessary for cells to produce neovessel formation *in vitro* and *in vivo* in their tissue engineered tissues. Whereas before using natural scaffolds prevented scientists from controlling how specific ECM and growth factor cues are presented to endothelial cells to induce angiogenesis, they can now covalently bind these cues to scaffolds of specific stiffness, porosity, and physical shape in an unprecedented spatio-temporal manner<sup>113-122</sup>. In order to better understand what induces VECs to undergo angiogenesis, similar tissue engineering strategies would be greatly beneficial to understanding which valve specific cues are causative and which are merely effects of angiogenesis. When it is understood what is primarily responsible for valvular angiogenesis, efforts to control this process, thus prevent the progression of CAVD, will be very promising.

### 2.7.3. Tissue Engineering Heart Valves

As mentioned previously, the current options for heart valve replacements each have their own drawbacks and limitations. Tissue engineered heart valves (TEHV) have the potential advantages of combining proper hemodynamics, nonthrombogenicity, infection resistance, and cellular viability. Where these valves are most needed, however, is in the pediatric population. Many children with congenital heart defects require valve replacements as part of their treatment plan. Because of their age, they are generally implanted with mechanical valves that require heavy anticoagulation. This surgical option is non-ideal for children due to the nature of their lifestyles. Because the valves cannot grow with their host, they must be replaced often throughout their life span requiring many risky reoperations. A TEHV would have the ability to grow, repair itself, and remodel as the child grows eliminating the need for the repetitive surgeries greatly increasing their overall quality of life and long term prognosis <sup>2</sup>.

However, as in any tissue engineered material, achieving rapid host integration is an important step. Near the annulus and cusps of the valve, the tissue would require rapid neovascularization to encourage incorporation and to increase the viability of those cells. Additionally, it is hypothesized that too much angiogenesis leads to various heart valve pathologies such as CAVD. Therefore, any optimal TEHV would require spatio-temporally controlled angiogenesis as it is controlled in the native valve. This would likely involve patterning proangiogenic environments near the annulus and anti-angiogenic agents such as chondromodulin near the free edge. Over time, the encapsulated VICs would produce their own native anti-angiogenic compounds which would switch off the angiogenesis where it would be no longer necessary. Better understanding of how valve cells translate and respond to these angiogenesis signaling such that they could be utilized in the design of a TEHV is a guiding principle of this thesis.

## 2.8. Summary

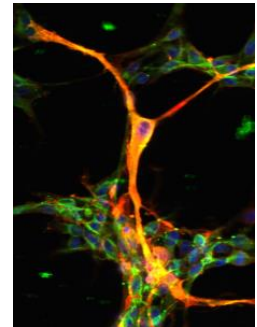
Valvular diseases are one of the largest health problems not only in the United States but also in the entire world. Until recently, these diseases were considered natural degeneration that was a merely a product of mechanical strain over time. Now

we know that these are active disease processes with a cellular basis that must be better understood in order to develop new treatments for these diseases. By looking towards diseases with similar pathologies, we can begin to hypothesize what factors may play an important role in the valvular diseases of interest. As the study of valve physiology and microstructure was born from histology and pathology, most of the studies investigating the contributing factors towards valve diseases are histological in nature. Although these studies are successful in identifying major changes that present themselves during the pathology, it is difficult to establish any causality from these observations. Identifying the causative versus symptomatic elements of these pathological changes will be instrumental in guiding investigators towards new, effective treatments for valvular disease. More studies on what factors cause these valvular cells to enter into a diseased state are greatly needed.

A major histological aspect of CAVD that needs more study is angiogenesis. Angiogenesis is known to play an integral role in many similar pathologies but is not widely investigated with respect to CAVD on a cellular level. Many important questions remain about the role of angiogenesis in the pathology of CAVD. For one, do valvular endothelial cells truly have the ability to form functional neovessels in the valve? Additionally, controversy remains as to the source of the endothelial cells lining the neovessels seen in stenotic valves: whether they are VECs, VICs, or circulating endothelial progenitor cells (EPCs). Secondly, can the VICs function as pericytes on the inside of the valve to support these neovessels, or are the VECs merely differentiating towards a pericyte phenotype as needed? Can VICs support this neovessel formation with the necessary cell-cell contacts and signaling. Thirdly, which of the proangiogenic histological features that have been documented are truly important in driving angiogenesis and which are merely symptomatic of the neovessel formation? Lastly, can we harness this knowledge of valve specific pathological angiogenesis to build better TEHV with the necessary physiological level of angiogenesis to encourage their host integration and viability? This thesis aims to provide insights into these questions.

The ultimate question, however, is what the role of angiogenesis is in CAVD and whether we can harness it to stop this debilitating disease that affects patients worldwide.

## Regulation of Valve Endothelial Cell Vasculogenic Network Architectures with ROCK and Rac Inhibitors<sup>1</sup>



### 3.1. Abstract

**Objective:** The age- and disease-dependent presence of microvessels within heart valves is an understudied characteristic of these tissues. Neovascularization involves endothelial cell (EC) migration and cytoskeletal reorientation, which are heavily regulated by the Rho family of GTPases. Given that valve ECs demonstrate unique mesenchymal transdifferentiation and cytoskeletal mechanoresponsiveness, compared to vascular ECs, this study quantified the effect of inhibiting two members of the Rho family on vasculogenic network formation by valve ECs.

**Approach and Results:** A tubule-like structure vasculogenesis assay (assessing lacunarity, junction density, and vessel density) was performed with porcine aortic valve ECs treated with small molecule inhibitors of Rho-associated serine-threonine protein kinase (ROCK), Y-27632, or the Rac1 inhibitor, NSC-23766. Actin coordination, cell number, and cell migration were assessed through immunocytochemistry, MTT assay, and scratch wound healing assay. ROCK inhibition reduced network lacunarity and interrupted proper cell-cell adhesion and actin coordination. Rac1 inhibition increased lacunarity and delayed actin-mediated network

1. This work was published as: Arevalos, C. A., A. T. Walborn, A. A. Rupert, J. M. Berg, E. L. Godfrey, J. M. V. Nguyen, and K. J. Grande-Allen. Regulation of valve endothelial cell vasculogenic network architectures with ROCK and Rac inhibitors. *Microvasc. Res.* 98C:108–118, 2015.



formation. ROCK inhibition alone significantly inhibited migration, whereas both ROCK and Rac1 inhibition significantly reduced cell number over time compared to controls. Compared to a vascular EC line, the valve ECs generated a network with larger total vessel length, but a less smooth appearance.

**Conclusions:** Both ROCK and Rac1 inhibition interfered with key processes in vascular network formation by valve ECs. This is the first report of manipulation of valve EC vasculogenic organization in response to small molecule inhibitors. Further study is warranted to comprehend this facet of valvular cell biology and pathology and how it differs from vascular biology.

### 3.2. Introduction

Calcific aortic valve disease (CAVD) has a prevalence of about 3% in patients older than 75 and leads to ~ 50,000 heart valve replacements each year <sup>123</sup>. Neovascularization (the formation of new blood vessels) is a well-recognized histological characteristic of CAVD <sup>10,23,37,38,40–42,44,45,124,125</sup>. Angiogenesis, the process in which new vessels and capillaries sprout from existing ones, is also known to promote mineralization within diverse tissues, thereby contributing to the progressive hardening and resultant lack of function in pathologies such as atherosclerosis or ectopic bone formation <sup>126</sup>. The cell-mediated mechanisms of angiogenesis have not been widely investigated in CAVD, with some notable exceptions. The glycoprotein chondromodulin, which is anti-angiogenic, was demonstrated to be abundant in normal adult heart valves but present in lower amounts in regions of diseased heart valves marked by neovascularization <sup>127</sup>.

It has been proposed that a targeted antiangiogenic therapy could stop the progression of valve disease by preventing the entrance of excess nutrients and inflammatory infiltrates through neovessels generated by the valve endothelial cells (VECs) <sup>45</sup>. Statin-based, lipid-lowering therapies used in the treatment of atherosclerosis progression do not appear to reduce CAVD progression <sup>128</sup>. Studies showing that CAVD involves endochondral bone formation <sup>18</sup> – a process that, in normal bone, requires neovascularization <sup>129</sup> – also supports investigating the inhibition of functional neovessel formation as a treatment for CAVD. Interestingly, normal pediatric heart valves (unlike normal adult valves) are richly vascularized <sup>7</sup>, which suggests that vascularization may

be an important factor to consider in the tissue engineering of heart valves for pediatric patients. All in all, there is compelling evidence for further characterization of vasculogenic behavior by heart valve cells.

During angiogenesis, the Rho family of GTPases transduces proangiogenic signals into organized cytoskeletal movements. These GTPases, RhoA, Rac1, and Cdc42, are activated by downstream signaling cascades of the membrane receptors of several angiogenic molecules<sup>92</sup>. Rac1 regulates lamellipodia formation through activation of p21-activated kinase (PAK), whereas RhoA is involved in cell adhesion and forward movement through regulation of stress fiber formation and contraction via the Rho-associated serine-threonine protein kinase (ROCK), which leads to the phosphorylation of myosin light chain (pMLC)<sup>92-94</sup>. Therefore, these proteins transduce angiogenic stimuli into coordinated cellular motility and network formation. Several studies have demonstrated the unique attributes of valve endothelial cells (VECs) compared to vascular-derived endothelial cells (ECs) including their transduction of angiogenic stimuli. Additional sources of differences include the valve cells' physiological predisposition towards endothelial to mesenchymal transdifferentiation during valvulogenesis and their distinct mechanical environment<sup>1,4,18,42,130,131</sup>. Further, key differences between ECs and VECs arise in the expression of genes and proteins that regulate blood vessel development, angiogenesis, adhesion, migration, and cell fate in *in vitro* comparisons<sup>4,21</sup>.

Compared to ECs, however, the Rho family of GTPases has had limited study in the context of heart valves. ROCK inhibition was previously shown to block calcific nodule formation by valvular interstitial cells (VICs)<sup>132</sup> and to inhibit mesenchymal invasion by cultured atrioventricular endocardial cells, which are embryonic precursors to VECs<sup>133</sup>. It was also reported that flow-dependent VEC orientation was independent of PI3K, a downstream effector of Rac1, despite its known role in regulating vascular endothelial cell organization in response to flow and during angiogenesis<sup>21,68</sup>. Given the importance of ROCK and Rac1 in regulating endothelial cell motility and organization during angiogenesis<sup>134</sup>, as well as the atypical nature of VEC responses to various angiogenic stimuli<sup>130,131</sup>, and the potential impact of a VEC-specific anti-angiogenic therapy for the treatment of CAVD<sup>45</sup>, there is compelling motivation for further study of the effects of ROCK and Rac1 inhibition on vasculogenic network formation by heart valve cells.

This study investigated the ability to tune the complex vasculogenic networks using small molecule inhibitors of the ROCK (Y-27632) and Rac (NSC-23766) pathways of adult porcine aortic valve endothelial cells (APAVECs) on Matrigel, a reconstituted basement membrane substrate that has been widely used previously to invoke a vasculogenic response from endothelial cells<sup>49</sup>. Several basement membrane components such as SPARC<sup>124</sup>, laminin<sup>135</sup>, and collagen type 4<sup>135</sup>, as well as transforming growth factor  $\beta$ <sup>136</sup> have been found to be increased in fibro-calcific valves compared to normal valves. Thus, Matrigel was used to mimic the transition from an anti-angiogenic to a pro-angiogenic environment that the aortic valve cells experience during the progression of CAVD. The geometry of the resulting vasculogenic networks was controlled using small molecule inhibitors for the ROCK (Y-27632) and Rac1 (NSC-23766) pathways. Since cell migration and proliferation play crucial roles in angiogenesis, the effect of the inhibitors on these outcomes was also assessed. Furthermore, the cells in these networks were immunostained for actin, CD31, and  $\alpha$ -smooth muscle actin ( $\alpha$ -SMA) to demonstrate how cell phenotypes were affected by ROCK and Rac1 inhibition.

### 3.3. Materials and Methods

#### 3.3.1. Isolation, Purification, and Culture of VECs

Adult porcine aortic valve endothelial cells (APAVECs) were used to model physiologically healthy adult human valve cells due to the established similarities between human and porcine valve physiology<sup>137</sup>. Previous studies with human cells have demonstrated that VECs from diseased valves are more angiogenic than those harvested from control tissues<sup>44</sup>. This study aimed to induce previously healthy, quiescent VECs to enter into the proangiogenic phenotype that is associated with CAVD, and to control this phenotype using small molecule inhibitors. Therefore, all APAVECs were harvested from aortic valve leaflets removed from healthy 6-month old pig hearts received from a local abattoir (Fisher Ham and Meats, Houston, TX).

Aortic heart valve leaflets were harvested from fresh adult (3-6 months old) porcine hearts procured from a local abattoir (Fisher Ham and Meats, Spring TX). Within 24 hours of porcine slaughter, the hearts will be dissected with sterile surgical

tools. Briefly, the procedure for aortic valves harvest is performed by: 1) removing the apex and left auricle of the heart, 2) cutting posteriorly through the left atria so that the mitral valve is easily visible, 3) trim the mitral valve and chordae for easy access to the bottom of the aortic root through the left ventricle, 4) dissect anteriorly from under the aortic root, between the leaflets, along the axis of the aorta, 5) excise each leaflet carefully from the sinuses of Valsalva along the commissures into sterile phosphate buffered saline (PBS), pH 7.4.

VECs were harvested immediately after aortic valve harvest. The VEC harvest protocol is modified from techniques described previously<sup>16,21</sup>. After dissection, each valve leaflet was briefly rinsed in sterile PBS with 5% (v/v) Penicillin/Streptomycin (P/S). Next, the leaflets were soaked in an enzyme digestion composed of 2U/mL of dispase and 60U/mL of collagenase type II in a rocking incubator at 37°C for 1 hour. This enzyme digestion caused the degradation of basal lamina and the VECs to loosen from the underlying matrix, but was mild enough to prevent additional ECM degradation and VIC release. After the enzyme digestion, the leaflets were removed and placed in sterile PBS. Then, using sterile forceps and cotton swabs, the VECs were gently wiped off of the leaflet surface by gently rolling a swab tip across both sides of the leaflet surface. The cells were then rinsed off the cotton swab with multiple washes of EGM-2 media supplemented with 2% P/S and a growth factor bullet kit containing hEGF, hydrocortisone, gentamicin, fetal bovine serum, VEGF, hFGF-B, R3-IGF-1, ascorbic acid, and heparan (Lonza). This process was repeated for each leaflet, with one swab per leaflet. Once cells had been harvested from the leaflets, the cell-media suspension was centrifuged at 750xg for 5 minutes at room temperature to concentrate the cells. After centrifugation, the supernatant of the solution was aspirated to remove any residual enzyme solution, and the cells were resuspended with EGM-2 media. The cell solution was plated onto sterile 2.5% gelatin coated T-75 tissue culture flasks and cultured in an incubator (37°, 5% CO<sub>2</sub>) until they reached confluence. The culture media was changed every 2-3 days.

Once a primary (P0) cells T-75 flask was at least 90% confluent, the cells were magnetically sorted to ensure VEC purity. Before sorting, the primary cells were trypsinized, centrifuged, and resuspended in 1mL of serum free DMEM media. Pan mouse IgG coated magnetic beads (Invitrogen, Carlsbad CA) were coated with 0.1-0.5µg of mouse anti-CD31 antibodies. 25µL of the antibody coated magnetic beads were

added to the 1mL cell suspension, and allowed to mix for 20 minutes at 2-8°C. Then the cell-bead suspension was magnetized using a bead sorting rack and the supernatant containing non-CD31 expressing cells were removed. The CD31 positive VECs were released from the magnetic beads by resuspending the bead mixture in 200µL of preheated RPMI media and 4µL of DNase I release buffer for 15 minutes at RT. After the release, the cells in the solution were plated onto a sterile 2.5% gelatin coated T-75 tissue culture flasks and cultured in an incubator until they were ready for downstream studies. VECs were cultured till passage 6 and in full bullet kit supplemented EGM-2 media. This media has been shown in our lab to maintain VEC quiescence and prevent EnMT towards a VIC phenotype.

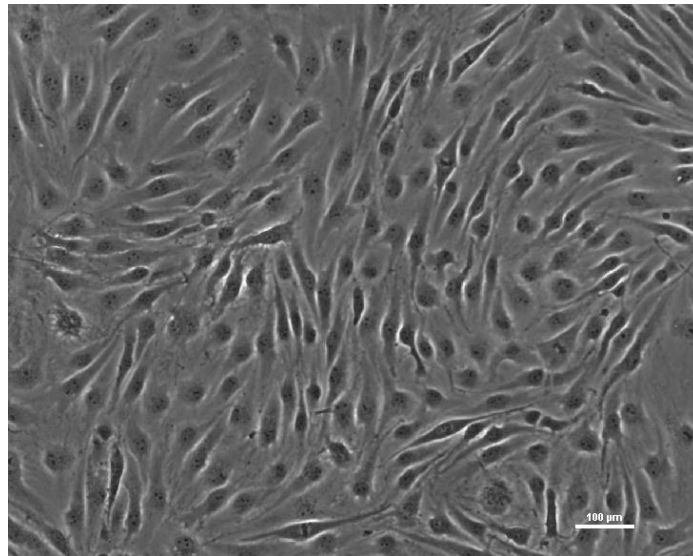


**Figure 3-1. VECs in culture. Note their tight cell-cell junctions and spiral morphology.**

### 3.3.2. Tubule-like Structure (TLS) Vasculogenesis Assay

The TLS assay is widely used to study vasculogenesis in cultured cells <sup>49</sup>. This study investigated the extent to which APAVECs cultured from healthy aortic valves could form complex vasculogenic networks on Matrigel, a reconstituted basement membrane substrate that has been widely used previously to invoke a vasculogenic response from endothelial cells <sup>49</sup>. The geometry of the resulting networks was altered using small molecule inhibitors for ROCK and Rac1.

Prior to the start of each study, phenol red free Matrigel (BD Biosciences, San Jose, CA) was thawed overnight on ice. On day 1, 50  $\mu$ l volumes of cold Matrigel were added to the wells of a 96-well plate and then placed in the incubator at 37°C for 1 hour to allow for gelation. APAVECs in EGM-2 (100  $\mu$ l) were then plated on top of the Matrigel at a concentration of 24,000 cells per well. In each assay in this study, controls and treatment groups were pipetted from the same source of mixed cells to ensure the same number of cells was seeded each time. Upon seeding, the cells were treated with the ROCK inhibitor Y-27632 (Sigma-Aldrich Research Biochemicals Inc., St. Louis, MO) or the Rac1 inhibitor NSC-23766 (Tocris Bioscience, Bristol, UK) at the concentrations noted below. Controls were treated with PBS. Plates were then returned to the incubator. After 7 hours, the resultant tubule-like network structures were imaged in the middle of each well using phase contrast microscopy with a 10X objective. Each condition was applied to at least triplicate wells, and the assay was repeated three separate times.

For a comparison of baseline vasculogenic network formation between the valvular and vascular cells, the MCECs were cultured under the same TLS assay conditions, but were not subjected to ROCK or Rac1 inhibition.

### 3.3.3. Automated Image Analysis for Tubule Characterization

Phase contrast microscopy can be utilized to image vessel formation in a high throughput manner without interrupting the vessel formation, but this approach suffers from a lack of contrast when imaging cells grown on gels. To circumvent this limitation and allow for downstream analysis, a custom automated script written for ImageJ (Bethesda, MA) was used to convert the phase contrast images to a binary mask using an edge detection algorithm that ignores small and circular objects, allowing it to only detect elongated tubule networks. All images obtained during the TLS experiments were processed using this script prior to quantification of network parameters.

Quantitative analysis of vascular networks is not standardized across labs or fields. Most commonly this work proceeds in a non-automated fashion that is a labor intensive process and prone to human error and biases. The free, open source software Angiotool<sup>138</sup> offers an automated mechanism to quantify several angiogenesis network metrics in a high throughput and repeatable manner. In brief, the binary images generated from the ImageJ script were convolved with a fast reclusive Gaussian kernel,

and the tube-like structures were then computed based on the combination of the eigenvalues of the 2D Hessian matrix. The vessel response was computed for a set of scales that denotes the standard width of the Gaussian filter, and was then in turn interpreted as vessel diameter in the graphical user interface. These features were then skeletonized and analyzed for several angiogenesis metrics: number of junctions, junction density, vessel length, number of endpoints, and average lacunarity. Lacunarity is a parameter that describes the distribution of the sizes of gaps surrounding an object within an image. Greater lacunarity reflects a greater size distribution of these gaps and lower lacunarity reflects a more uniform size distribution. Lacunarity can be used to distinguish objects with similar fractal dimensions, and can be used in general for describing the spatial pattern in which neovascularization occurs <sup>139</sup>. Figure 3-2 shows representative images of skeletonized networks treated with Y-27632 and NSC-23766.

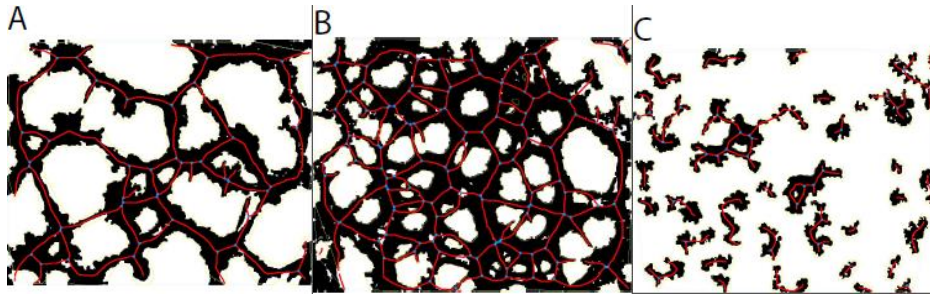


**Figure 3-2. Representative images of skeletonized networks comparing VECs (A) untreated, or treated with (B) Y-27632 or (C) NSC-23766.**

#### 3.3.4. Immunocytochemistry

In order to image the tubule-like network structures to assess the coordination of cell-cell interactions and actin throughout the networks, the TLS assay was repeated in an 8-well #1 glass chamber slides (Thermo Fisher, Waltham, MA) and immunocytochemistry was performed on the resultant networks to elucidate the localization of CD31, alpha smooth muscle actin (αSMA), and F-actin after 7 hours. A volume of 218 μl of Matrigel was added to each well of an 8-well #1 glass chamber slides (Thermo Fisher, Waltham, MA) and allowed to harden as previously described for the TLS assay. In order to maintain the same seeding density of cells as in previous studies, 52,000 APAVECs in 218 μl of EGM-2 media were added to each well and

incubated with either the ROCK inhibitor (50  $\mu$ M) or the Rac1 inhibitor (100  $\mu$ M) for 7 hours at 37°C. PBS was added in the control condition. The resultant tubule-like structure networks were fixed using 4% paraformaldehyde for 30 minutes at room temperature. The cells were then washed with PBS followed by treatment with 0.1% Triton X-100 for 5 minutes to permeabilize the cell membranes. A blocking solution of 10% donkey serum (Jackson ImmunoResearch, West Grove, PA) and 2% bovine serum albumin (Sigma-Aldrich, St. Louis, MO) was then applied for 1 hour at room temperature. Cells were washed again with PBS prior to an overnight incubation with primary antibodies for CD31 (ab28364, 1:100, Abcam, Cambridge, UK) and  $\alpha$ SMA (ab7817, 1:100, Abcam) diluted in the blocking solution at 4°C. Following exposure to primary antibodies, cells were washed with PBS and incubated with the fluorescent secondary antibodies AlexaFluor 555 (A-31572, 1:200, Invitrogen) and AlexaFluor 633 (A-21052, 1:200, Invitrogen) in the same blocking agent overnight at 4°C. The cells were then stained with phalloidin 488 (A12379, 1:200, Invitrogen) for 20 minutes. After a final wash with PBS, fluoromount containing Dapi (to demonstrate the cell nuclei) was applied to each well. The networks were then imaged using a confocal fluorescence microscope (Zeiss LSM Live 5, Oberkochen, Germany) using 10x and 20x objectives. The images were evaluated to assess the APAVECS' expression of CD31 to confirm their endothelial phenotype, their expression of  $\alpha$ SMA to ascertain whether transdifferentiation had occurred, and their overall cell-cell and actin cytoskeleton organization using phalloidin 488. Live-Dead staining was performed by adding 1  $\mu$ M of calcein-AM (Sigma-Aldrich Research Biochemicals Inc.) and 2  $\mu$ M of ethidium bromide (Sigma-Aldrich Research Biochemicals Inc.) to the Matrigel-seeded cells 7 hours after treatment with ROCK or Rac inhibitors. Thirty minutes later, cells were then washed with PBS and imaged using confocal fluorescence microscopy.

### 3.3.5. MTT Assay for Cell Number

An assay for MTT (3-(4,5-dimethylthiazol-2-yl)-2,5-diphenyltetrazolium bromide; Sigma-Aldrich, St. Louis, MO, USA) was performed to quantify relative changes in number of APAVECs due to ROCK and Rac1 inhibition<sup>140</sup>. In brief, 120,000 APAVECs were seeded on a gelatin-coated 24-well plate and incubated at 37°C for 24 hours with



the ROCK inhibitor Y-27632 (10, 50, or 100  $\mu$ M) or the Rac1 inhibitor NSC-23766 (20, 100, or 200  $\mu$ M). The final concentrations of these inhibitors were selected to range from 5-fold below the EC50 to 2-fold above the EC50<sup>141,142</sup>; this range captured the upper range of the concentrations used for the TLS assay. The control group received only PBS. The media was then replaced with 500  $\mu$ l of 1% BGS and 100  $\mu$ l of MTT reagent (5 mg/ml sterile MTT in PBS) for 4 hours at 37°C. 1 ml of MTT solvent (DMSO) was then added to each well and triturated thoroughly. The resultant absorbance was read (570 nm - 670 nm) using a spectrophotometer (SpectraMax M2; Molecular Devices, Sunnyvale, CA, USA). Six independent wells were tested per treatment group.

### 3.3.6. Cell Migration Assay

To observe the migratory behaviors of cells in the presence on ROCK and Rac1 inhibitors, APAVECs were first seeded on gelatin-coated 48-well plates and allowed to grow to confluence in a volume of 200  $\mu$ l of medium. A cross-shaped wound was then made in the cell layer of each well using a vertical and horizontal scratch from a sterile 200  $\mu$ l pipette tip. The media was changed and a 3  $\mu$ l aliquot of the ROCK inhibitor Y-27632 or the Rac1 inhibitor NSC-23766 was added to achieve the same range of concentrations as described above for the MTT assay. In the control group, cells received a treatment of only PBS. In a negative control group, media was instead replaced with EGM2 containing neither serum nor bullet kit. An image was taken at the intersection of the vertical and horizontal scratches using a 10x objective with phase contrast microscopy at hour 0. After 24 hours, another image was taken at the same location in each well. Percent wound healing was quantified as previously reported<sup>143</sup> and reported normalized to the control treated with PBS. This study was performed with a total n=4-6 for each condition.

### 3.3.7. Statistical Analysis

A one-way ANOVA was performed followed by a Tukey HSD for post hoc analysis to analyze for differences between groups in all assays. Statistical significance was accepted for  $p < 0.05$ .

### 3.4. Results

#### 3.4.1. APAVECs Formed Tubule-Like-Structures (TLS) in an Angiogenic Environment

Since the source of the cells responsible for the neovascularization in the aortic valves during CAVD has not been definitively determined <sup>22</sup>, we sought to establish the ability of CD31-positive APAVECs to form vasculogenic networks and to quantify the complexity of any networks formed. After 7 hours, the CD31+ APAVECs formed a pronounced vascular network structure with readily quantifiable vessel density, junction density, total number of junctions, total number of end points, total vessel length, and lacunarity (**Error! Reference source not found.**).

**Table 3-1. Characteristics of tubule-like structures formed by VECs in Matrigel model.**

<b>Vascular Network Metric</b>	<b>Value</b>
<b>Vessel Density (%)</b>	45 ± 1.6
<b>Junction Density (%)</b>	36 ± 2
<b>Total Number of Junctions</b>	38 ± 2.3
<b>Total Number of End Points</b>	25 ± 1.4
<b>Total Vessel Length (mm)</b>	8.2 ± 0.38
<b>Lacunarity</b>	0.22 ± 0.02

\* Values are reported as the average ± the standard error (n=14)

#### 3.4.2. ROCK Inhibition Increased Network Complexity in a Dose Dependent Manner

As ROCK is an important mediator of angiogenesis, APAVECs were treated with a logarithmic range of concentrations of the ROCK inhibitor Y-27632. At 1, 10, and 100 µM of Y-27632, the resulting APAVEC networks displayed significantly increased vessel density, junction density, and total network length compared to the untreated control networks ( $p < 0.0001$ , Figure 3-3). At these same concentrations, the number of junctions, vessel percentage area, and total number of end points were increased (193, 260, and 290%; 130, 144, and 144%; and 93, 134, and 158%, respectively; data not shown).

There was also a significant decrease in lacunarity of the network structures with increased concentrations of Y-27632 ( $p < 0.005$ , Figure 3-3).

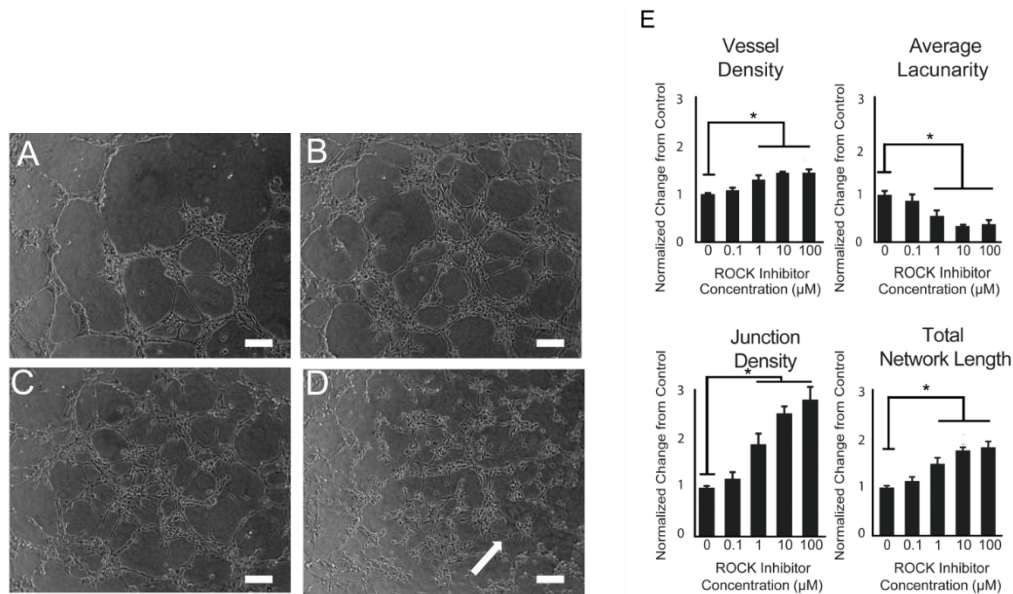


**Figure 3-3. ROCK inhibition increases APAVEC network complexity in vitro.** Representative images of the networks formed by APAVECs treated with A) PBS, B) 1 μM, C) 10 μM, D) 100 μM of the ROCK inhibitor. APAVECs form more complex networks and have increased lamellipodia (white arrow) with higher concentrations of the ROCK inhibitor. Scale bars represent 100 μm. E) Quantification of dose dependent changes in various network metrics. Results are shown as mean ± standard error normalized to the control (n=9, ANOVA  $p < 0.0001$  for all but average lacunarity for which  $p$ -value  $< 0.005$ . \* $p < 0.05$  vs. control, Tukey's HSD,).

#### 3.4.3. Rac1 Inhibition Decreased Network Complexity and Inhibits Network Initiation

As shown in Figure 2, APAVECs treated with the highest dose of 200 μM of the Rac1 inhibitor NSC-23766 displayed significantly decreased total numbers of junctions ( $p < 0.01$ ) and vessel percentage area ( $p < 0.01$ ), and the treatment increased lacunarity ( $p < 0.05$ ) compared to the control. Whereas ROCK inhibition dose-dependently changed the geometry of the vasculogenic networks as indicated by the average lacunarity and junction density, the highest concentration of Rac1 inhibition actually blocked the formation of vasculogenic networks. Although Rac1 inhibition (at 200 μM) decreased the

total number of junctions, it did not decrease the overall degree of branching, since there was no change in junction density (data not shown). Furthermore, the network metrics in the groups treated with Rac1 inhibitor did not display dose dependency to the same extent as the ROCK inhibitor. Although differences in the network morphology could be observed at Rac1 inhibitor concentrations of 2 and 20  $\mu\text{M}$  as shown by Figure 3-4A-C, these differences were not statistically significant. The dramatic changes in the network metrics at the higher concentration, however, could be attributed in part to the inability of the software to quantify the lack of a network.

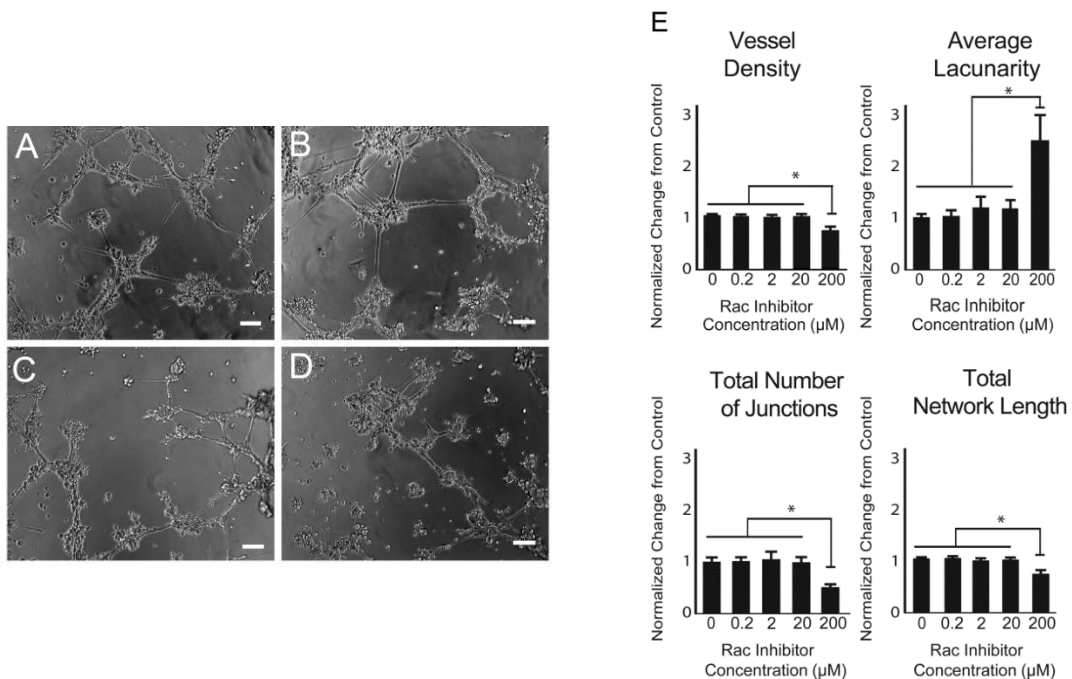


**Figure 3-4. Rac inhibition decreases APAVEC network complexity in vitro.** Representative images of APAVEC network formation based upon treatment with A) PBS, B) 2  $\mu\text{M}$ , C) 20  $\mu\text{M}$ , or D) 200  $\mu\text{M}$  of the Rac inhibitor. APAVEC form smaller and less dense networks at the highest treatments with the Rac inhibitor. Scale bars represent 100  $\mu\text{m}$ . E) Quantification of the changes in various network metrics. Results are shown as mean  $\pm$  standard error normalized to the control ( $n=9$ , \*  $p < 0.05$  vs. all other groups, Tukey's HSD,). Although there were trends in some of the measured network metrics, the lower concentrations of Rac inhibitor resulted in less pronounced effects that did not attain statistical significance.

#### 3.4.4. ROCK and Rac1 Inhibition Influenced Cell Assemblies

Immunostaining analysis of the APAVEC vasculogenic networks demonstrated that the cells maintained their endothelial phenotype in each condition as demonstrated by positive staining for CD31 (Figure 3-5, green). Since alpha smooth muscle actin ( $\alpha$ SMA) positive cells that co-express endothelial markers have been shown to sprout from calcific aortic valves <sup>40</sup>,  $\alpha$ SMA expression in APAVEC vasculogenic network formation was also assessed. In each sample, a small number of  $\alpha$ SMA+/CD31- cells were found along the exterior borders of the tubule structures as shown in Figure 3-6A. As demonstrated by the actin stain and CD31 localization, the control samples demonstrated tightly assembled, multicellular, linear tubule-like structures as shown in Figure 3-5 and Figure 3-6. Structures formed in the presence of Rac1 inhibitor displayed a similar multicellular tube-like morphology, but overall these tube-like structures were fewer in number compared to the control (Figure 3-5C). As shown in Figure 3-5B, the ROCK-inhibited cells formed multicellular networks, but displayed more flattened junctions and extensions, as opposed to the tube-like morphology characteristics of the control.

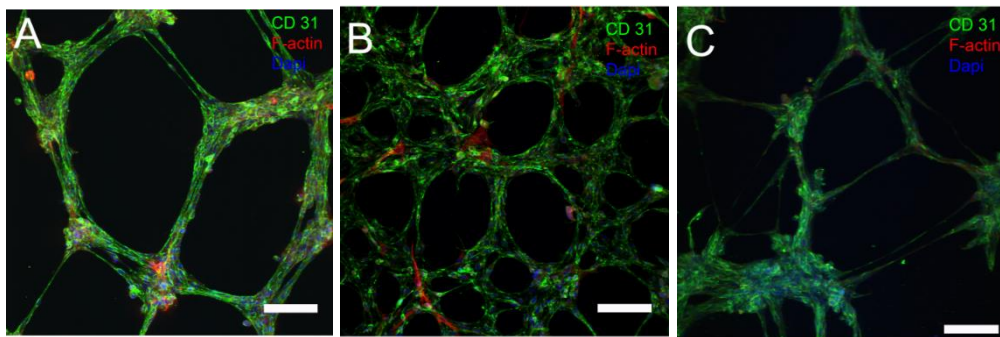


**Figure 3-5. Representative Z-stack reconstructed confocal fluorescence microscopy images of APAVEC networks treated with A) PBS, B) 50  $\mu$ M of ROCK inhibitor, or C) 100  $\mu$ M of Rac inhibitor taken with a 10x objective. Control APAVECs organized into tightly bound complex linear tubule-like networks, but the ROCK inhibited APAVECs formed flat networks with looser organization and ablated tubule formation. Compared to the control, Rac1 inhibition appeared to affect the initiation of the tubule formation shown by their fewer tubule like structures number between nodes. However, tube-like structures that did form demonstrated tightly clustered cell assemblies and aligned actin structures, similar to the control tubule like structures. Green: CD 31. Red:  $\alpha$ SMA. Blue: Dapi.**

Scale bars represent 100  $\mu\text{m}$ .. Green: CD 31. Red:  $\alpha\text{SMA}$ . Blue: Dapi. Scale bars represent 100  $\mu\text{m}$ .

The higher magnification images allowed for improved visualization of cell-cell organization through the localization of the homologous cell-cell binding protein CD31. Both the control and Rac1-inhibited multicellular structures displayed tightly organized cell assemblies, whereas ROCK inhibition appeared to interrupt this organization during vasculogenic network formation, resulting in a looser cell assembly (Figure 3-6B). A small number of  $\alpha\text{SMA}^+$  VECs were apparent in each condition as shown by Figure 3-6A. In each of these cases, these cells appeared to be co-localizing and binding several CD31+/ $\alpha\text{SMA}^-$  VECs at the same time.

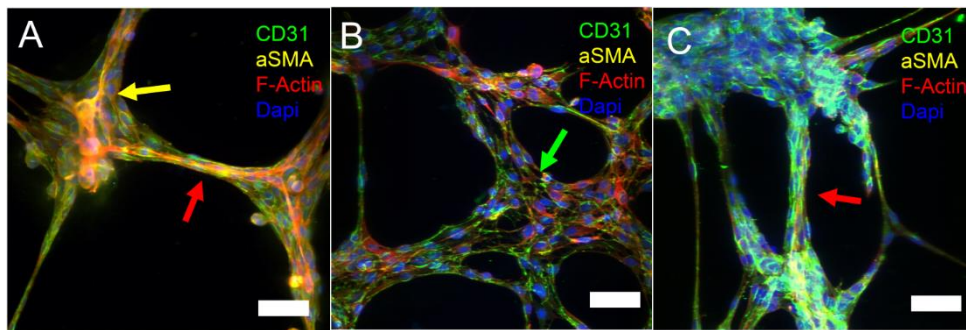


**Figure 3-6. Z-stack reconstructed confocal microscopy images of APAVEC networks treated with A) PBS, B) 50  $\mu\text{M}$  of ROCK inhibitor, C) or 100  $\mu\text{M}$  of Rac inhibitor. Images were taken with a 20x objective. Aligned actin structures and close cell-cell organization typical of tubule-like sprouts (red arrow) were found in the (A) control and (C) Rac-inhibited networks, but neither of these features were displayed in the (B) ROCK inhibited networks (green arrow). In each case, a few  $\alpha\text{SMA}^+/\text{CD 31}^-$  cells were found binding several CD 31+ VECs (yellow arrow). Scale bars represent 50  $\mu\text{m}$ . Green: CD 31. Yellow:  $\alpha\text{SMA}$ . Red: F-actin. Blue: Dapi.**

Changes in the network assemblies were not due to cell death, as demonstrated by the lack of ethidium bromide staining and ubiquitous presence of positive calcein AM staining in the Live/Dead assay as shown in Figure 3-7, and by the dynamic motion of the cells as shown in Supplemental Movie 1 .

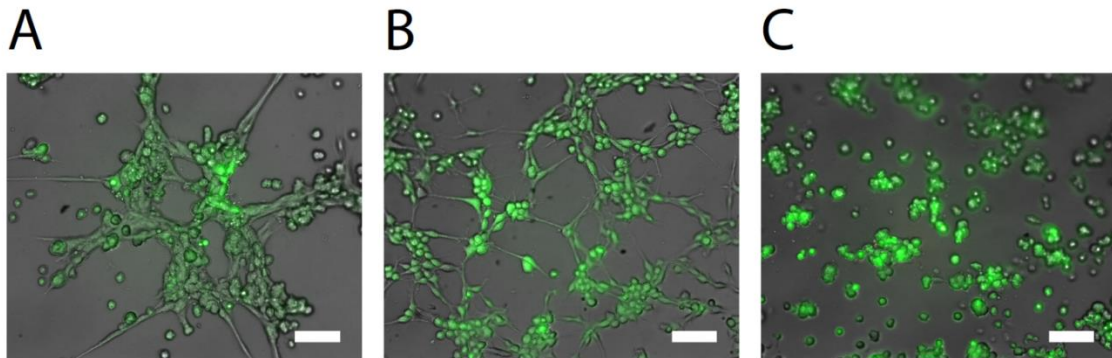


**Figure 3-7. Representative images of APAVEC TLS networks stained with a 1  $\mu$ M of calcein AM (green, Live) and 2  $\mu$ M of ethidium bromide (red, Dead) 7 hours after treatment with A) PBS control, B) 100  $\mu$ M Y-27632, or C) 200  $\mu$ M NSC-23766. Scale bars represent 50  $\mu$ m.**

#### 3.4.5. Rac and ROCK Inhibition Significantly Decreased APAVEC Number

One of the more dramatic events of angiogenesis is a sudden and rapid increase in endothelial cell proliferation<sup>5</sup>. The resulting normalized change in MTT absorbance, as a measure of cell number, is shown in Figure 3-8. The number of APAVECs was significantly reduced by both Rac (reduced by 25% at 100  $\mu$ M and 42% at 200  $\mu$ M) and ROCK (reduced by 23% at 50  $\mu$ M and 20% at 100  $\mu$ M) compared to untreated controls, although Rac1 displayed a greater dose dependency in its effect. No significant effect was found at the lowest doses for either Rac1 or ROCK inhibition.

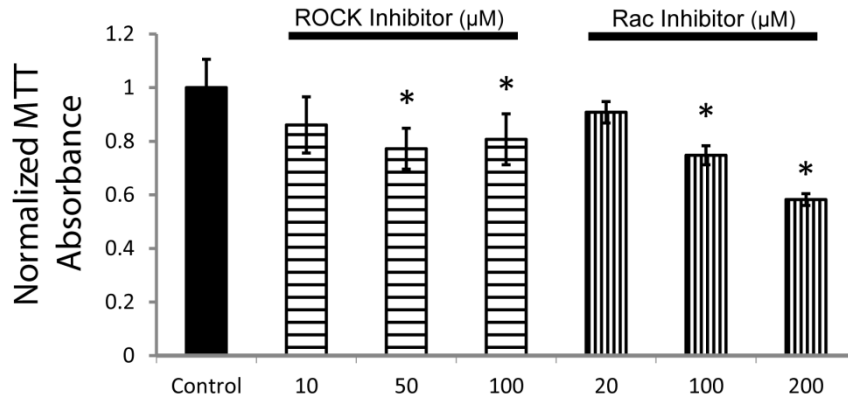


**Figure 3-8. Quantification of changes in cell number based upon ROCK or Rac1 inhibition. Results are displayed as the mean absorbance relative to the control at 24 h  $\pm$  standard deviation (n = 6, \* p < 0.05 vs. control).**

#### 3.4.6. ROCK Inhibition Significantly Decreased APAVEC Migration

Since cell migration is an important process in angiogenesis and valvulogenesis, the effects of ROCK and Rac1 inhibition on APAVEC migration were investigated using a scratch wound healing assay. A comparison of the average wound closure given treatment with the ROCK or Rac inhibitor is shown in Figure 3-9. Inhibition of the ROCK pathway with Y-27632 significantly inhibited migration (by 18-19% at the two highest inhibitor concentrations), a finding that is consistent with prior studies that inhibited ROCK in VECs from embryonic aortic valve explants<sup>133</sup>. Inhibition of the Rac pathway with NSC-23766 showed a trend of reducing APAVEC migration at 200  $\mu$ M (by 26%), but this result was not quite statistically significant ( $p = 0.08$ ). No significant effect was found at the lower inhibitor concentrations.



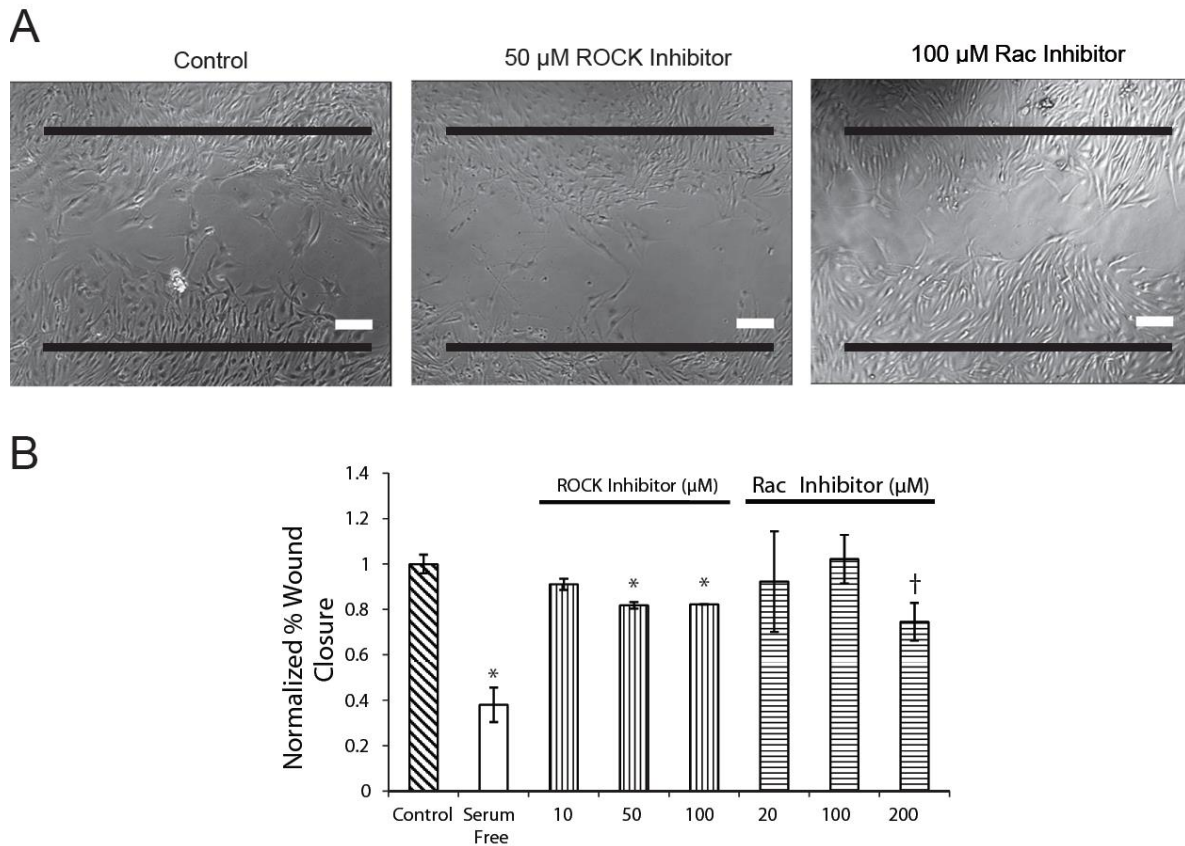


**Figure 3-9. ROCK and Rac regulated APAVEC migration in a scratch wound healing assay. A) Representative images of APAVEC wounds 24 hours after injury when treated with 50  $\mu\text{M}$  ROCK inhibitor or 100  $\mu\text{M}$  Rac inhibitor. The black lines represent the size of the initial wound. Scale bar represents 100  $\mu\text{m}$ . B) Quantification of wound closure at 24 hours. Results are displayed as the mean percent wound closure normalized to the control  $\pm$  standard error. (n=4-6, \* p < 0.05 vs. control; † p = 0.08 vs. control).**

### 3.4.7. APAVECs Display Unique Network Formation Compared to Vascular Endothelial Cells

MCECs were directly compared to APAVECs to elucidate differences in the vasculogenic networks formed by each cell type under baseline conditions. At 7 hours, both VECs and MCECs displayed complex branching networks, but the MCEC networks displayed smoother tubule formation as individual cells were more difficult to discern (Figure 3-10A). Quantification of the MCEC networks relative to the APAVEC networks

demonstrated a 27% larger total network size and 22% lower number of end points for the APAVECs (Figure 3-10B). The networks demonstrated no significant difference in lacunarity or junction density between the vascular and valvular cells, but there was a strong trend of the APAVECs having a 15% larger vessel percentage area ( $p=0.07$ ) and 36% greater total number of junctions ( $p=0.06$ ).

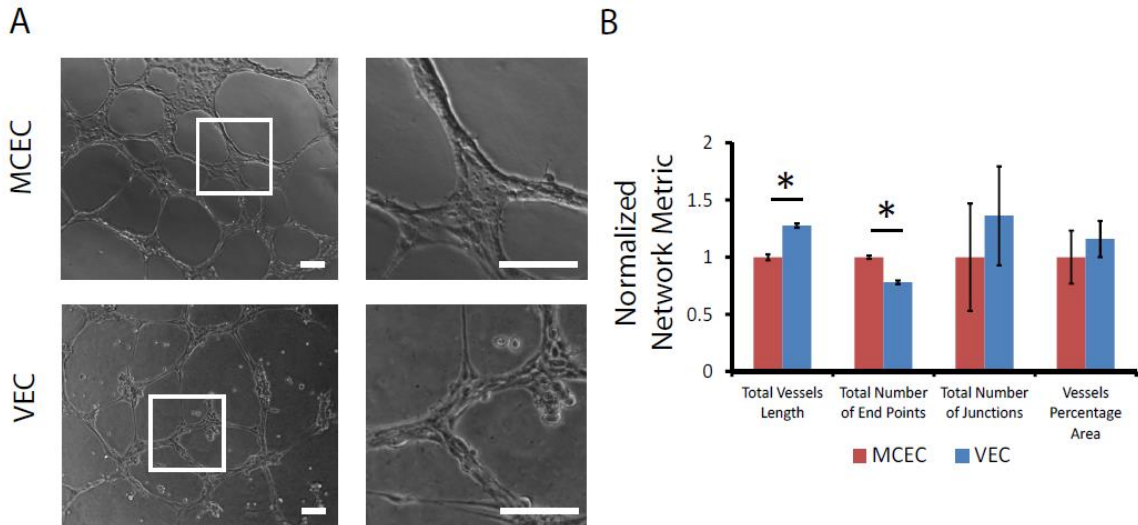


**Figure 3-10. APAVEC network formation was directly compared to MCEC network formation to elucidate differences in their angiogenic signal transduction. A) At 7 hours, both VECs and MCECs displayed branching complex networks, but MCECs displayed smoother tubule formation as individual cells were more difficult to discern. Scale bars represent 50  $\mu\text{m}$ . B) Quantification of the VEC networks relative to the MCEC networks demonstrated a larger total network size and lower number of end points for VEC-generated networks ( $n=15$ , \*  $p < 0.05$  between cell types). The networks demonstrated no significant difference in lacunarity or junction density, but there was a trend of the VECs having a larger total number of junctions and total vessel percentage area ( $p = 0.07$  and  $0.06$  respectively). Data is displayed as average  $\pm$  standard deviation normalized to the MCEC metrics.**

### 3.5. Discussion

The Rho family of GTPases are important mediators of vascular endothelial cell-cell and actin reorganization during angiogenesis<sup>134</sup>. This study investigated the effects

of ROCK and Rac1 inhibition on APAVEC reorganization. ROCK was shown to have a role in APAVEC migration and network organization, whereas Rac1 influenced APAVEC proliferation and network initiation. This data provides motivation for further investigation into the targeting of Rho family GTPases for the treatment of CAVD by preventing valve cell reorganization into a vasculogenic network. In addition, it elucidated differences between vascular and valvular endothelial networks.

These ROCK inhibition findings confirmed previously reported effects on VEC migration, and provided new information about the effects of ROCK on vascular network formation by VECs. There has been only limited study regarding the ROCK inhibition of VECs despite its important role in cellular organization<sup>134</sup>. Previously, ROCK inhibition was shown to prevent transwell migration by transdifferentiating VECs<sup>133</sup>, as reported here for CD31+ APAVECs using the scratch wound healing assay. As a complement to the migration data, quantifying the changes in the complexity of network formation offers a novel assessment of APAVEC responses to vasculogenic stimuli. These results demonstrated that ROCK inhibition can be utilized to control the geometry of the vascular networks formed by APAVECs. Although ROCK inhibition dose-dependently increased the number of junctions, the resulting quality of the overall network after ROCK inhibition appeared poor as shown by the flattened nature of the tube-like structures and loosely connected nature of the cell assemblies (arrow in Fig. 4B). This observation is consistent with previous reports demonstrating the role of Rho signaling in pinocytosis-mediated lumen formation, which requires tight cell-cell connections, a tube-like morphology<sup>144</sup> and overall vascular endothelial cell organization during angiogenesis<sup>134</sup>. The poor network formation found in this TLS assay may be due in part to the ability of the ROCK inhibitor to block cell migration. Rho-ROCK machinery is normally engaged to arrange the cells into tubule structures<sup>145</sup>, but when the ROCK pathway is inhibited, the cells are less able to pull themselves to a new location<sup>91</sup>. The resulting cell phenotype resembles that of tip cells, which have spiny, elongated lamellipodia reaching out to their next location<sup>83</sup>. Due to the density of the seeded cells, the APAVECs appeared to extend out to one another and form a flattened network with a low average lacunarity with ablated tubule formation.

In contrast to ROCK, the effect of Rac1 inhibition on network formation by APAVECs was less pronounced, except at the highest concentrations, at which few

network structures formed. Rac1 is understudied in the field of heart valves, despite its well-known role in the initiation of cellular extensions and lamellipodia, which is a critical step in migration and thus important for angiogenesis<sup>54</sup>. The findings of decreased number of junctions, decreased vessel percentage area, and increased lacunarity in APAVECs treated with Rac1 inhibitor are similar to previous reports of decreased network connections in human umbilical vein endothelial cells treated with drugs that inhibit Rac and Cdc42<sup>146</sup>. The smaller APAVEC networks might also be explained by the dose-dependent reduction in cell number for APAVECs treated with NSC-23766, given that cell proliferation is an important facet of tubule elongation during angiogenesis<sup>83</sup>. Live/Dead staining of the resultant APAVEC networks at the higher concentration of NSC-23766 displayed no signs of cell death during the timeframe of these experiments (Supplemental Figure 2), therefore the ablated network formation cannot be attributed to cell death but is instead due to an inability of the cells to respond to the Matrigel environment. Rac1 inhibition appeared to affect the initiation of the tubule-like structures, however, the tube-like structures that did form demonstrated tightly clustered assemblies of cells and aligned actin structures, similar to the control tubule-like structures.

Further understanding of the differences between vascular and valvular biology will be crucial to developing targeted valve therapies that minimize systemic side effects. Several studies have demonstrated the unique attributes of VECs compared to vascular-derived endothelial cells<sup>1,4,18,21,42,130,131</sup> and this study identified a new set of functional differences between the two. Both cell types formed complex networks, but in this work the VECs formed networks that were visibly and measurably different, and appeared to branch more. Since VEC networks were also demonstrated to be tunable by regulating ROCK and Rac, the regulation of the Rho family of GTPases may play a significant role in the functional differences between vascular and valvular endothelial cells. Furthermore, modification to that regulation could influence their switch to a more angiogenic phenotype, such as occurs during CAVD.

Taken together, these data, showing that APAVECs can form vasculogenic structures *in vitro* in a manner that can be regulated by inhibition of ROCK and Rac1, provide compelling motivation for future research investigating this inhibition as an interventional treatment for CAVD. Based upon the network macrostructures from

Figure 1 and 2, the microstructure changes displayed in Figure 3 and 4, and the effects of ROCK and Rac inhibition demonstrated previously *in vivo*<sup>145,147,148</sup>, it is hypothesized that ROCK or Rac inhibition would prevent the functional formation of VEC angiogenic structures *in vivo*. By manipulating these aspects of cell behavior to block the vascular network architecture, the presumed function of these vessels – delivery of inflammatory infiltrates to VICs and enabling mineralization – could be inhibited to prevent progression to CAVD and stenosis. As angiogenesis is reported to occur more in early to mid-stage calcification<sup>41</sup>, this treatment could be applied as soon as CAVD is detected using echocardiography. In general, translation of many of the currently investigated pathways<sup>149–154</sup> toward interventional treatments for CAVD will likely require the delineation of key characteristics of valvular cells in order to target the valve properly; this body of information, however, is continually expanding<sup>155</sup>. For example, there is growing interest in how the VECs interact with VICs<sup>127,156–160</sup>, which could reveal whether the VICs play a role in vasculogenic behavior by the VECs. Furthermore, there are a myriad of biomaterial platforms that have been developed to investigate valvular cell biology and pathology<sup>161–168</sup>; the use of more complex biomimetic *in vitro* models and *in vivo* models should facilitate discovery of the conditions that regulate vasculogenesis within heart valves.

As a better understanding of angiogenesis within heart valves is developed, there is also the potential to apply this research to produce improved pediatric tissue engineered heart valves<sup>169</sup> and gain further insight into valve developmental pathways. Heart valves in the young normally have a rich microvasculature<sup>7</sup>. It may be that in young tissue engineered valves, spatio-temporal control of angiogenesis would encourage rapid host integration allowing the tissue to grow with the patient. It has also been proposed that certain aspects of valve disease progression involve triggering dormant developmental pathways<sup>155</sup>, thus a greater understanding of the many angiogenic mechanisms occurring during valvulogenesis would provide new avenues for the investigation of angiogenesis in CAVD.

There were some limitations to this study. First, although both Y-27632 and NSC-23766 are widely characterized specific inhibitors of the ROCK and Rac1 pathways, the degree of inhibition of these pathways was not quantified by a Rho GTP activation assay. Rather, the range of concentrations of the inhibitors used in this study was based

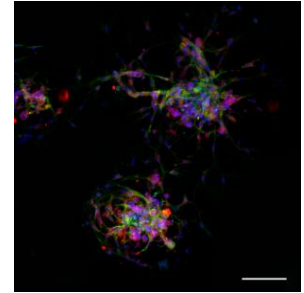
on prior reports and encompassed the IC 50 of both inhibitors<sup>141,142</sup>. Differences between the effective concentration ranges of the ROCK and Rac1 inhibitors could be attributed to the availability of their respective targets and their individual strengths, which was not investigated in this study. Second, there are limitations associated with the use of Matrigel. Matrigel is a widely used model for vasculogenesis and angiogenesis, although it may not represent the exact pathological microenvironment experienced by valve cells during the progression of CAVD. Nonetheless, the use of Matrigel is consistent with the reports of increased abundance of selected basement membrane constituents in valve leaflets from CAVD<sup>124,135</sup>. Thus, the Matrigel was meant to serve as a pro-vasculogenic environment in comparison to the more quiescent gelatin coated environment on which the cells were originally cultured. This change from an anti- to pro-angiogenic environment within diseased heart valves has been well-assessed histologically<sup>10,23,37,38,40–42,44,45,124,125</sup>. Third, it is possible that the aSMA+ cells in the TLS assay could have arisen from spontaneous transdifferentiation from normal culture conditions. However, there was no immunostaining or morphological evidence for the presence of aSMA+ cells prior to performing the TLS assay.

### 3.6. Conclusion

In this study, we demonstrated the ability of valve endothelial cells to form vasculogenic networks *in vitro*, which were significantly different from the networks generated by a vascular endothelial cell line, and showed the ability to manipulate the geometry of the resulting vascular networks using ROCK and Rac1 inhibitors. Applying analytical tools for quantifying networks allowed for a novel assessment of the biological response of valve endothelial cells to the vasculogenic environment of Matrigel and the Rho GTPase family inhibitors. The results provide motivation for future research to manipulate this pathway and regulate vasculogenesis within heart valves as needed, either to prevent pathologic mineralization, to promote the formation of a vascular network within pediatric tissue engineered heart valves, or to improve understanding of this fundamental aspect of valvular biology.



## Valve Interstitial Cells Act in a Pericyte Manner Promoting Angiogenesis and Invasion by Valve Endothelial Cells<sup>1</sup>



### 4.1. Abstract

**Introduction:** Neovascularization remains an understudied aspect of calcific aortic valve disease (CAVD). Within diseased valves, cells along the neovessels' periphery stain for pericyte markers, but it is unclear whether valvular interstitial cells (VICs) can demonstrate a pericyte-like phenotype. This specific aim examined the perivascular potential of VICs to regulate valve endothelial cell (VEC) organization and explored the role of Angiopoietin1-Tie2 signaling in this process.

**Approach and Results:** VECs and VICs were fluorescently tracked and co-cultured in Matrigel over 7 days. VICs regulated early VEC network organization in a ROCK-dependent manner, then guided later VEC network contraction through chemoattraction. Unlike vascular control cells, the valve cell cultures ultimately formed invasive spheroids with 3D angiogenic-like sprouts. VECs co-cultured with VICs displayed significantly more invasion than VECs alone; with VICs generally leading and wrapping around VEC invasive sprouts. Lastly, Angiopoietin1-Tie2 signaling was found to regulate valve cell organization during VEC/VIC spheroid formation and invasion. VICs demonstrated pericyte-like behaviors toward VECs throughout sustained co-culture. The change from a vasculogenic network to an invasive sprouting spheroid

---

1. This work is under review as: **C. Alexander Arevalos**, Jonathan M. Berg, Jaqueline M. V. Nyguen, Elizabeth L. Godfrey, Claudia Iriando, K. Jane Grande-Allen, : Valve Interstitial Cells Act in a Pericyte Manner Promoting Angiogenesis and Invasion by Valve Endothelial Cells, In review: ABME (2015)



suggests that both cell types undergo phenotypic changes during long-term culture in the model angiogenic environment. Valve cells organizing into spheroids and undergoing 3D invasion of Matrigel demonstrated several typical angiogenic-like phenotypes dependent on basal levels of Angiopoietin1-Tie2 signaling and ROCK activation.

**Conclusion:** These results suggest that the ectopic sustained angiogenic environment during the early stages of valve disease promotes organized activity by both VECs and VICs, presumably contributing to neovessel formation and the progression of CAVD.

## 4.2. Introduction

Angiogenetic signaling plays an important role not only in valve formation and normal valve function, but also in the pathophysiology of calcific aortic valve disease (CAVD).<sup>170,171</sup> Several studies have established the occurrence of neovascularization during CAVD.<sup>37,38,45</sup> There has been little investigation, however, into how the cell-mediated mechanisms that underlie vascular angiogenesis play a role in the pathology of CAVD. During valve development and normal endothelial-to-mesenchymal transformation (EndMT), valve endothelial cells (VECs) undergo a physiological transdifferentiation that shares several characteristics with the process of vascular angiogenic root formation.<sup>76</sup> Due to the increased abundance of factors important for angiogenic signaling within calcified valves, and the predisposition of VECs to undergo EndMT, we hypothesized that VECs cultured long-term in a model environment rich in pro-angiogenic signaling factors would maintain their endothelial phenotype while also gaining invasive mesenchymal characteristics, ultimately leading to an intermediate phenotype. The presence of alpha smooth muscle actin (aSMA) – the marker for activated valve interstitial cells (VICs) – was demonstrated surrounding neovessels in CAVD,<sup>172</sup> and it is also reported that a subpopulation of VICs demonstrate the pericyte marker NG2<sup>157</sup> and respond to pericyte-related signaling molecules.<sup>173</sup> However, it has also been shown that VICs can be anti-angiogenic in basal conditions.<sup>127</sup> Therefore, it is unclear whether myofibroblast-like VICs can serve as pericytes during neoangiogenesis.

Studying how VEC and VIC signaling guides their phenotypes is an important step toward understanding the cell-mediated pathobiology of CAVD. The Angiopoietin1

(Ang1)-Tie2 pathway is an important pathway in vascular angiogenesis influencing endothelial cell growth, migration, vessel maintenance and destabilization, and maturation,<sup>52</sup> but the role of this pathway is understudied in the context of valve cell biology. There is some evidence for activation of this pathway during CAVD,<sup>44</sup> but its significance in VEC/VIC interactions or CAVD histopathology has not been established. Prior studies of VECs and VICs have investigated the importance of endothelial nitric oxide synthase (eNOS) and Rho-associated protein kinase (ROCK) in VEC/VIC signaling behavior;<sup>160</sup> the Ang-Tie2 pathway is upstream of both of these mechanisms. Ang-Tie2 is also important in NF- $\kappa$ B activation and leukocyte recruitment, which are speculated to have significant roles in CAVD.<sup>174</sup> Moreover, previous co-culture investigations of VICs and VECs have demonstrated communication between these two cell types,<sup>158–160</sup> but have not examined the pericyte-like potential of VICs to influence VEC angiogenic behavior.

The purpose of this study was to investigate how direct contact co-culture with VICs affected short-term and long-term (7 days) VEC network formation in a Matrigel model in comparison to a co-culture of vascular-derived cells, to quantify their spatial-temporal relationships, and to identify the role of Ang-Tie2 and its downstream signaling pathways in VEC/VIC dynamics. Clarification of these valve cell relationships would provide fundamental insights into this transformative stage of CAVD pathology.

### **4.3. Methods and Materials**

#### **4.3.1. Isolation, Purification, and Culture of Valve Cells and Vascular Cells**

Valve cells were harvested from healthy 6-month-old adult porcine hearts from a local commercial abattoir (Fisher Ham and Meats, Spring, TX) or Animal Technologies (Tyler, TX). VECs were harvested and cultured from the aortic valves as previously described in this work<sup>158,175</sup>, and used between passages 2-4.

Since VICs are found encapsulated in the middle of the aortic valve, a more powerful enzymatic digestion is necessary to isolate them from the ECM. After the harvest of the VECs, the leaflets were minced sterilely and placed in a second digest of 1x DMEM with 2mg/ml collagenase II, .1 mg/ml of hyaluronidase, 2 mg/ml of neutral

protease, 2.5% of HEPES, and 2.5% ABAM for 4 hours to further break down the ECM to allow the VICs to be freed. The leaflets will then be sifted using a cell filter and the resulting cells were pelleted. The cells were then plated on tissue culture flasks in VIC media ( F12 45% v/v, BGS 10% v/v, ABAM 1% v/v, DMEM with 25 mM HEPES 45% v/v). Cells were then separated out from VECs via CD 31- bead sorting. VIC media were changed every 2-3 days and used between passage 0 to 6. In all subsequent studies, VICs and VECs used were matched by their common lineage.

Immortalized mouse cardiac endothelial cells (MCECs) (CELLutions Biosystems Inc, Toronto, Canada) were purchased and cultured in the same manner as VECs.

10T1/2 fibroblast cells (American Type Culture Collection, Manassas, VA) were cultured in DMEM supplemented with 10% w/v fetal bovine serum (Lonza) and 2 mM L-glutamine, 1000 U/mL penicillin, and 100 mg/L streptomycin (Sigma, St. Louis, MO).

#### 4.3.2. PKH Co-culture Tubule-Like Structure Matrigel Assay

The Tubule-Like Structure (TLS) Matrigel Assay was used to investigate valve and vascular endothelial cell (EC)-PC dynamics in a model pro-angiogenic environment as previously described<sup>49</sup>. In order to track relative EC-PC dynamics, cells were differentially stained with PKH26 (red) or PKH67 (green) fluorescent dyes (10  $\mu$ M, Invitrogen) following the manufacturer's guidelines. The EC and PC cells were then seeded on phenol red-free Matrigel (BD Biosciences, San Jose, CA) in a 3 EC:1 PC ratio at 240,000 cells/ml in order to recreate culture conditions from previous vascular EC/PC Matrigel studies.<sup>176</sup> Intermittently throughout the culture period, live cell movement was tracked for 4-6 hours using a Nikon A1-Rsi confocal fluorescence microscope (Tokyo, Japan).

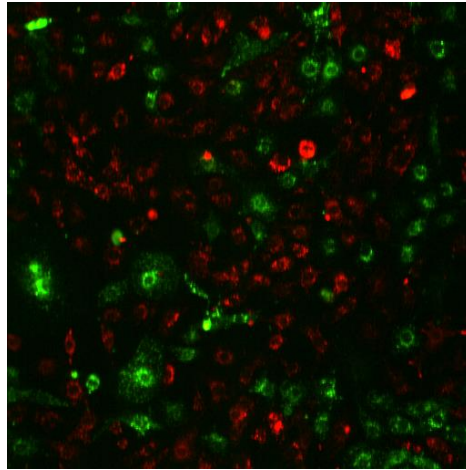


**Figure 4-1. Representative image of MVEC differentially stained with 10  $\mu$ M green or red PKH dyes co-cultured together for 48 hours. Over the time period tested, minimal to no leakage of dye between cells was seen.**

To investigate the role of ROCK signaling on VEC/VIC network organization, once seeded the co-cultures were treated with the small molecule ROCK inhibitor Y-27632 (Calbiochem, San Diego, CA)<sup>175</sup>.

#### 4.3.3. Immunocytochemistry

Immunocytochemistry was performed as described previously<sup>175</sup> to demonstrate the cells' phenotypic characteristics (Table 1). In order to confirm that VECs retained their endothelial cell phenotype, co-cultures were stained with Dil-Ac-LDL (Invitrogen) at 10  $\mu$ g/ml for 4 hours before washing with PBS.

**Table 4-1. Primary antibodies for immunocytochemistry**

Antibody Target	Function
CD31 <sup>a</sup>	VEC Marker
Alpha smooth muscle actin <sup>a</sup> ( $\alpha$ SMA) <sup>a</sup>	VIC Marker
Delta-like ligand 4 (DLL4) <sup>a</sup>	Angiogenic Tip Cell Marker
Phosphorylated Akt1 <sup>b</sup>	AKT Activation Marker
B-Catenin <sup>a</sup>	Wnt Signaling Marker
pMLC <sup>a</sup>	ROCK Activation Marker

<sup>a</sup>Abcam, Cambridge UK

<sup>b</sup>Cell Signaling Technology, Danvers, MA

#### 4.3.4. Automated Network Analysis

Networks were analyzed using the automated image analysis toolset Angiogenesis Analyzer in ImageJ (Bethesda, MA) on 10X phase contrast microscopy images from the middle of each well as used previously.<sup>175</sup> The total network length and number of tubule like structures were analyzed, and the resultant average tubule length was calculated using equation (1):

$$\textit{Average Tubule Length} = \frac{\textit{Total Network Length}}{\textit{Number of Tubules}} \quad \text{Equation 1}$$

Groups were statistically compared using one-way ANOVA with post-hoc Tukey tests.

#### 4.3.5. Quantification of Post-Network VIC Chemoattractant Behavior

In the Nikon AR automated tracking module, each cell could be identified uniquely due to the PKH fluorescent staining, cell size, and cell morphology. VECs and VICs could be distinguished by the different color PKH dyes.

VIC chemoattractant towards VECs was quantified during the period of network regression and spheroid formation. The null hypothesis was that the motion of each VEC was independent of the influence of nearby VICs, so that no net chemoattraction existed between the two cell types. For each VIC, a subset of VECs ( $VEC_{sub}$ ) was identified as cells whose average Euclidian distance was less than 50  $\mu m$  from the current VIC of interest ( $VIC_i$ ). In order to quantify the movement of each VEC in the  $VEC_{sub}$  in relation to the  $VIC_i$ , their X/Y/time positions underwent a Lagrangian transformation in relation to the X/Y/time movements of the  $VIC_i$ . At each time point, for each set pairing of  $VIC_i$  and  $VEC_{sub}$  cells, the cosine similarity was calculated using equation (2):

$$\Theta_{u,v} = atan2^{-1} \left( \frac{\det(u,v)}{u \cdot v} \right) \quad \text{Equation 2}$$

where  $u$  represents the Lagrangian-corrected vector of the displacement that the currently paired VEC in the  $VEC_{sub}$  underwent during the current time step,  $v$  represents the vector if it was perfectly directed at the  $VIC_i$  which is by definition set to the new

origin, and  $\det(u, v)$  represented the determinant of  $(u, v)$ . In this definition, an angle of 0 degrees represented a VEC that is perfectly converging towards the  $VIC_i$  at that time, and an angle of 180 degrees represented a cell moving perfectly away from the  $VIC_i$ . The cosine similarity of each pairing over time was averaged, and the average  $VEC_{sub}$  time-averaged cosine similarity was then calculated for each  $VIC_i$ . This metric quantified the directional tendency of the  $VEC_{sub}$  in relation to the  $VIC_i$ .

The radial distribution of these angles was compared with an even radial distribution using a Rayleigh's test for nonuniformity, with  $p < 0.05$  indicating a statistically different radial directionality. The average directionality of this migration of VECs toward  $VICs$  was calculated using equation (3):

$$\text{Average Lagrangian Directionality} = \frac{1}{n} \sum_{k=1}^n \frac{\text{Lagrangian Corrected Displacement}_k}{\sum_{t=1}^{tf} |u|_{k,t}}$$

### Equation 3

where  $k$  represents the current VEC out of  $VEC_{sub}$ ,  $n$  represents the number of cells in  $VEC_{sub}$ ,  $t$  represents the current time step, and  $tf$  represents the final time step of the  $VEC_{sub}$  track. This metric represents the directional persistence of migration of  $VEC_{sub}$  in relation to the motion of the  $VIC_i$  with the maximal amount 1 representing a perfectly straight line of movement<sup>177</sup>.

Finally, the Lagrangian-transformed Forward Migration Index (LaFMI) was calculated using equation (4) adapted from Martins et al.<sup>178</sup>:

$$\text{LaFMI} = \frac{1}{n} \sum_{k=1}^n \frac{\sum_{t=1}^{tf} \cos \Theta_{u_{t,k} v_{t,k}} \cdot |u|_{t,k}}{\sum_{t=1}^{tf} |u|_{t,k}} \quad \text{Equation 4}$$

In this context, the LaFMI quantifies the percent of the total distance that the movement of a  $VEC_{sub}$  was directed towards the  $VIC_i$ , with the maximum value of 1 representing a  $VEC_{sub}$  moving perfectly towards the  $VIC_i$  at each step as the  $VIC_i$  moved. In this equation,  $k$ ,  $t$ ,  $u$ ,  $t$ ,  $tf$ , and  $n$  were defined as in equations (2) and (3), and  $\Theta$  was

defined as the cosine similarity between the  $u$  and  $v$  vectors as defined above at time  $t$  for  $VEC_k$ .

In order to benchmark the measured metrics to random independent motion, a Gaussian-based Brownian motion simulator was implemented to simulate the random movements of both the VECs and VICs from their starting positions, and each chemoattractant metric was calculated in parallel. A total of 732 VICs and corresponding 2196 VECs from three independent cultures were tracked and used in the analysis. A t-test assuming unequal variances was used to compare the directionality and LaFMI distributions between the measured and random motions, with  $p < 0.05$  indicating a significant difference.

#### 4.3.6. VEC/VIC Invasive Spheroid (VEVIS) Sprouting and Distribution Analysis

As the VECs and VICs co-cultured for 7 days on Matrigel formed spheroids and then formed angiogenic sprouts into the Matrigel, additional methods were developed to quantify this behavior. To quantify the amount of Matrigel penetration by the VEVIS angiogenic sprouts, the spheroid core and outer perimeter of penetration were manually traced using Nikon AR software, and then the invasion ratio was calculated as the penetration perimeter divided by the core perimeter. Randomly chosen spheroids were selected in each of 9 independently-seeded VEC-only and VEC/VIC cultures after 7 days. Differences between VEC-only and VEC/VIC co-cultures were analyzed using a t-test assuming equal variance.

In order to quantify the distribution of VECs and VICs within the VEVISs, VEVISs with differentially PKH-tracked cells were imaged after 7 days of culture using confocal fluorescence microscopy ( $n=17$  different VEVIS samples). Images were analyzed using a binary filter that assigned an X-Y position to each cell, and determined the area of that cell. Each VEVIS image was then divided into 4 concentric quartile rings with equal surface area, and each cell was allocated into one of the quartile rings based upon its Euclidean distance from the middle of each VEVIS. For each cell type (VIC or VEC), the total cell area per quartile ring was calculated and then normalized to the total cell area overall. The proportions of VICs and VECs in the quartile rings were compared using a two-way ANOVA with a Tukey's post hoc analysis comparing across cell type and quartile.

#### 4.3.7. Investigating the Role of Angiopoietin1-Tie2 signaling on VEVIS Formation

To quantify the effect of Angiopoietin1 and its downstream effectors on VEC network formation, VECs were cultured alone in the TLS assay. Upon seeding, VECs were treated with Angiopoietin1 (Ang1) (R&D Systems, Minneapolis) at a final concentration of 14  $\mu$ M, with Ang1 and the Tie2 Kinase Inhibitor (Calbiochem) at a final concentration of 3.5  $\mu$ M, or with the Ang1 and the pAKT inhibitor LY 294002 (Cell Signaling Technology) at a final concentration of 14  $\mu$ M. Treatment reagents were delivered in 2  $\mu$ l of PBS or DMSO.

Since Angiopoietin1-Tie2 signaling is an important pathway in endothelial cell-pericyte communication, the effect of Angiopoietin1 and its downstream effectors were also quantified during VEVIS formation. VECs and VICs were co-cultured as described above for 7 days and treated with Angiopoietin1, the Tie2 Kinase Inhibitor, and the p-Akt inhibitor. Co-cultures were additionally treated with the Tie2 Kinase Inhibitor alone to investigate the role of basal Angiopoietin signaling. After 7 days, the sizes of at least 6 randomly selected spheroids from 6 independent wells from 2 independent experiments were quantified using ImageJ.

#### 4.3.8. qRT-PCR

After 7 days in culture, mRNA was harvested using a Quick-RNA Micro Prep (Zymo Research). 100 ng of RNA was then converted to cDNA using a PrimeScript™ 1st strand cDNA Synthesis Kit (Clontech). RT-qPCR was then run at a 1:100 dilution using the SYBR® Advantage® qPCR Premix for the targets in Table 4-2. Ubiquitin was used as the housekeeping gene in each run. Fold change was then calculated between 7 day VEVIS cocultures and a 3 to 1 VEC to VIC control mixture of cells before they were seeded into the matrigel model in order to compare expression changes in the system before and after coculture in the Matrigel model.  $\Delta$ Ct was averaged between runs of the same condition. This averaged  $\Delta$ Ct was then used to calculate the fold increase between the reference condition and the target by taking the ratio of (Efficiency of amplification)<sup>avg $\Delta$ Ct</sup> for the target and the Ubiquitin reference. The error is represented by the square root of the average of the variances of the reference condition and the target.



**Table 4-2. Angiogenesis and pericyte related gene expression PCR targets**

<b>Gene</b>	<b>Primer</b>
<b>Ubiquitin FWD</b>	TGA CCA GCA GCG TCT GAT T
<b>Ubiquitin REV</b>	TCT TGT CGC AGT TGT ATT TCT GAG
<b>NG2 FWD</b>	CAT CTT GCC TCT GCT CTT CTA C
<b>NG2 REV</b>	TGT CCC TCC CTT CTC TTT CT
<b>Periostin FWD</b>	ACC TGG AGA TTG GAC CTT ATT T
<b>Periostin REV</b>	CTG CTG GGT AGA GGA GTT TAT C
<b>Ang1 FWD</b>	TTT CCA GAG AGG TTG GAA AGA A
<b>Ang1 REV</b>	GTA CTG CCT CTG ACT GGT TAT G
<b>Ang2 FWD</b>	CCG TCA ACT GCA TCA CTT AAA C
<b>Ang2 REV</b>	TTA TCT TCC CAC AGG CTT TCT C
<b>VEGF FWD</b>	TAT GCG GAT CAA ACC TCA CC
<b>VEGF REV</b>	CTT GCC TCG CTC TAT CTT TCT T
<b>Tie2 FWD</b>	TGG AAC CTC GAA CAG AAT ATG AG
<b>Tie2 REV</b>	GGA GGA GGA AGA CCG ATA GAA
<b>FGFR2 FWD</b>	AAC GAT TAC GGG TCC ATC AA
<b>FGFR2 REV</b>	CCG TTC TTT TCC ACG TGT TT

## 4.4. Results

### 4.4.1. VIC-Driven Collapse of VEC Vasculogenic Networks is ROCK-Dependent

To test the role of VICs in VEC vascular networks, we grew VECs and VICs in direct co-culture in a 3:1 (VEC:VIC) ratio in the model pro-angiogenic environment of Matrigel. After 7 hours of co-culture, VECs cultured alone were organized (Figure 1A) as previously reported.<sup>175</sup> PKH labeling of VECs (green) and VICs (red) in co-culture demonstrated that they organized together in well-defined networks with VICs scattered among the nodes and along the length of the tubule-like structures (Figure 1B). This arrangement was similar to previous reports of PKH-tracked vascular ECs and pericytes (PCs).<sup>176</sup> Automated network analysis showed that co-culturing with VICs reduced total network length while increasing average tubule length between nodes compared to VECs cultured alone (Figure 1D).

ROCK inhibition (3.5  $\mu$ M Y-27632) largely prevented the VIC-mediated network formation, while maintaining multicellular clusters of VECs and VICs in direct contact (Figure 4-2C), and brought the total network length and average tubule length metrics

closer to the scale of the VEC-only cultures (Figure 4-2D). Immunocytochemistry of the co-cultures demonstrated networks consisting of CD31+ (green) and aSMA- VECs with polymerized aSMA+ (yellow) VICs covering VEC tubules (Figure 4-2E, yellow arrow). Treatment with the ROCK inhibitor did not affect VIC expression of aSMA, but it was present more diffusely within VICs (green arrow) as opposed to presenting as stress fibers. ROCK inhibition did not ablate VIC-VEC connections, given the multiple VIC-to-VEC connections observed (Figure 4-2F). Co-cultures treated with the ROCK inhibitor displayed notably fewer VICs covering around VEC tubules.

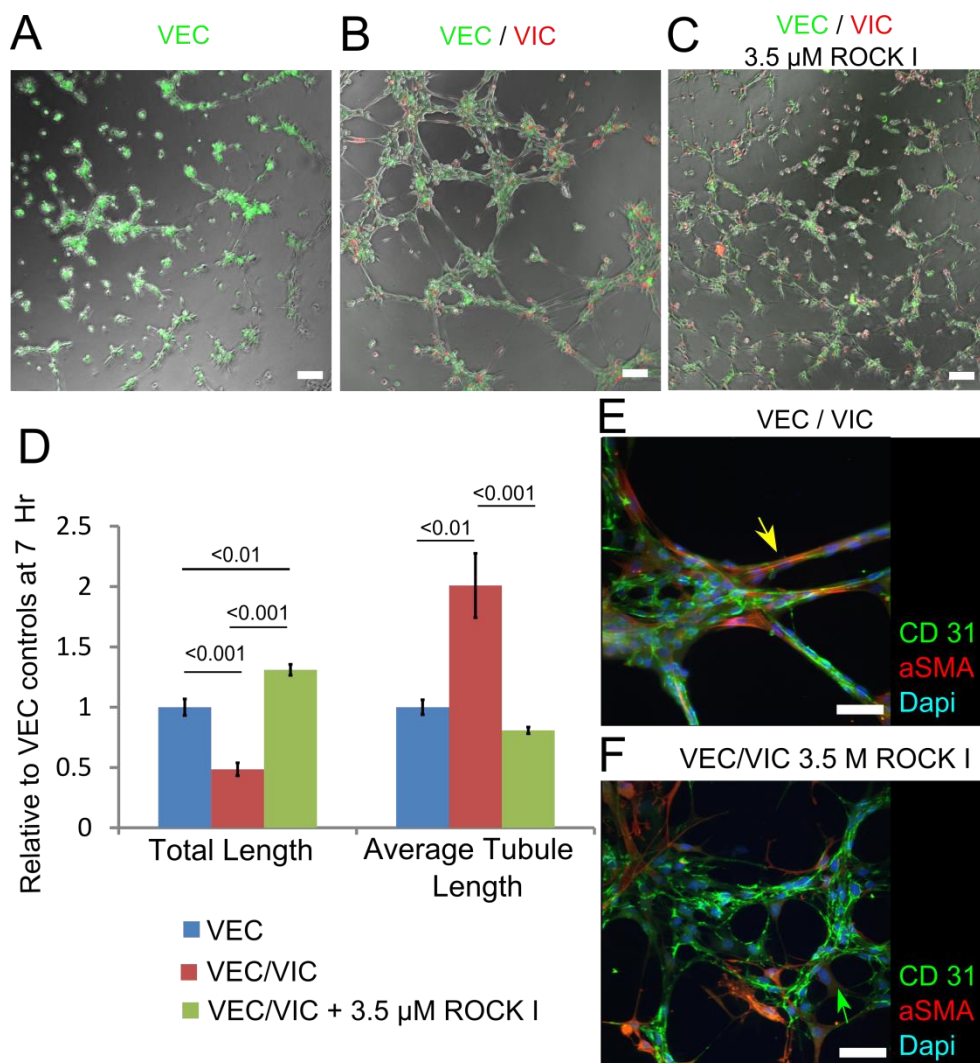


**Figure 4-2. VICs altered VEC vasculogenic network formation in a ROCK-dependent manner at 7 hours after seeding. A) VECs cultured alone formed complex networks. B) PKH-stained VECs (green) and VICs (red) formed complex**

vasculogenic networks when co-cultured. VICs were found connected to VEC tubules and in the nodes between tubules. C) Treatment of co-cultures with ROCK inhibitor Y-27632 (3.5  $\mu\text{M}$ ) eliminated macro changes to network architectures, although localization of VICs along VEC tubules and nodes was still found. Scale bars: 100  $\mu\text{m}$  in A-C. D) Quantification of changes to total network lengths and average tubule length in the co-cultures compared to VEC-only controls. Data shown as mean  $\pm$  standard error across 15 independently seeded wells. The p-value for comparison between groups is displayed above the denoted pairs. Immunocytochemistry of E) VEC/VIC co-cultures and F) VEC/VIC co-cultures treated with Y-27632 stained for CD31 (green),  $\alpha\text{SMA}$  (red), and cell nuclei (blue). E) Polymerized  $\alpha\text{SMA}^+$  VICs (yellow arrow) were found wrapped around and in contact with several elongated CD31+/ $\alpha\text{SMA}^-$  VECs. F) Treatment with the ROCK inhibitor did not affect VIC expression of  $\alpha\text{SMA}$ , but it was present diffusely and not in polymerized stress fibers (green arrow). ROCK inhibition did not eliminate VIC-to-VEC connections, demonstrated by the multiple connections to VECs made by each VIC in panel F. Co-cultures treated with the ROCK inhibitor displayed notably fewer VICs covering VEC network vertexes. Scale bars: 50  $\mu\text{m}$  in E-F.

#### 4.4.2. VEC/VIC Long Term Co-cultures Form 3D Invasive Spheroids

As demonstrated by the MCEC/10T1/2 co-culture in Figure 4-3A and quantified in Figure 4-4, network organization and stabilization is a major characteristic of EC/PC interactions *in vitro*. These results, in which the 10T1/2 cells stabilized the MCEC networks long-term, provided a benchmark of vascular EC/PC behavior for direct comparison with the effects of VIC co-culture on VECs in the same angiogenic assay. In contrast to the vascular controls, VEC/VIC co-cultures collapsed into spheroids at the network nodes by 24 hours in culture (Figure 4-3B). After 48 hours in culture, the VECs and VICs began to invade into the Matrigel. VICs were generally, though not exclusively, the first cells to migrate into the Matrigel in an angiogenic-like sprout. In these sprouts, the VIC would lead the way in a manner consistent with a tip cell, whereas the VECs acted more like the stalk cells of the new sprouts. The VEC/VIC spheroids continued to sprout into the gels, reaching a maximum invasion depth 5-7 days post-seeding. To demonstrate the dynamic VEC/VIC invasive spheroid (VEVIS) relationships, live cell imaging was performed using confocal fluorescence microscopy with an environmental chamber for periods of 4-6 hours; Supplemental Movies 3-9 show representative movies of significant time periods in the transition. After initial sprouting, VECs and VICs displayed a dynamic plasticity of roles in competing for the tip cell position, similar to how vascular ECs compete during angiogenic root formation.<sup>179</sup> Similar to the MCEC-

only cultures, the networks of VECs cultured alone slowly regressed over the first 72 hours of culture. By 7 days in culture, the VECs coalesced into spheroids and exhibited sprouts similar to VEVIS sprouts, but these sprouts tended to be fewer in number and smaller in size compared to the co-cultures as shown by Figure 4-5.

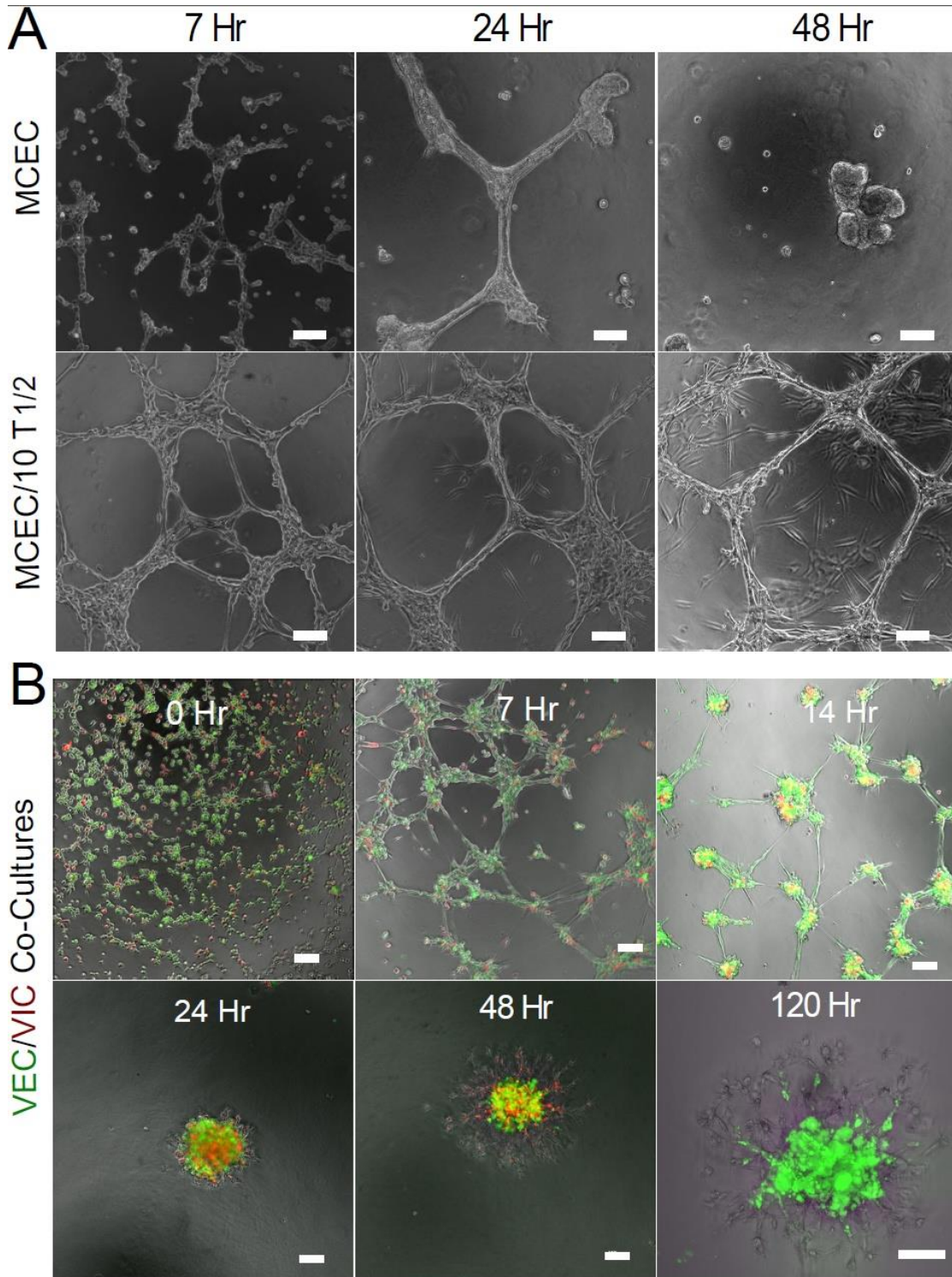


**Figure 4-3. Figure 2. VEC/VIC co-cultures form 3D invasive spheroids during sustained culture in a pro-angiogenic environment. A) MCECs cultured alone form networks that regress after 48 hours. MCEC/ 10T1/2 co-cultures display typical**

EC/PC dynamics by sustaining MCEC networks after 48 hours of culture. Scale bars: 100  $\mu\text{m}$ . B) Representative images of PKH-stained VEC (green)/VIC (red) co-cultures over long-term culture. Within 24 hours of seeding, VIC/VEC co-cultures formed EC/PC-like vasculogenic networks, spontaneously regressed, and reorganized into spheroid-like structures. After another 24 hours, the VICs begin to invade into the Matrigel, generally acting as tip cells with the VECs acting as the stalk cells. VIC/VEC co-cultures continued to sprout radially for 5 to 7 days. In the 120 hr panel, only the VECs (green) are highlighted to demonstrate their distribution throughout the VEVIS. Scale bars: 100  $\mu\text{m}$ . Images were taken from 4 independent experiments. 0 and 7 hr panels were taken from the same position in the same well, as were the 24 and 48 hr panels.

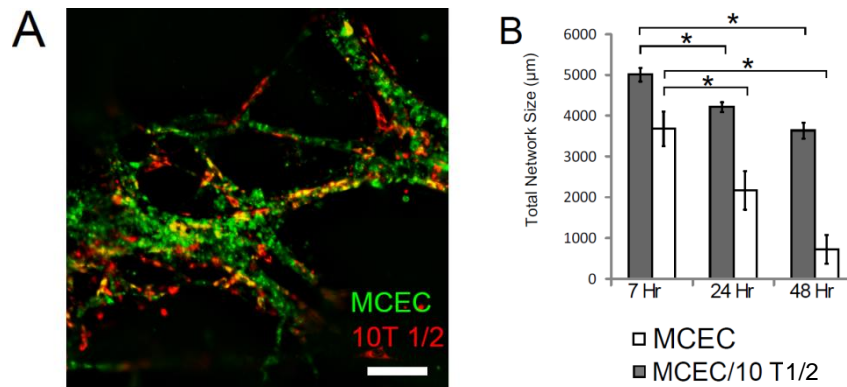


**Figure 4-4.** In order to compare the longer term co-culture of VICs and VECs to a known endothelial-pericyte co-culture, MCECs and 10T1/2 cells (to serve as pericytes) were co-cultured on matrigel. **A)** Similar to previous reports of vascular endothelial/pericyte co-cultures<sup>176</sup>, the MCEC (green) and 10T1/2 (red) cells formed interwoven vasculogenic networks. Scale bar represents 100 $\mu\text{m}$ . **B)** Quantification of MCEC/10T1/2 network size over time. MCEC-only cultures formed nascent networks at 7 hours, with a structure similar to VECs alone<sup>175</sup>. By 24 hours, the MCEC networks had consolidated with smooth node-to-tubule transitions. By 48 hours, the MCEC-only network structure had regressed substantially. Co-culturing with the 10T1/2 cells maintained network stability over this time period as demonstrated by the slowed network size decrease over time. \* represents p-value <0.05.

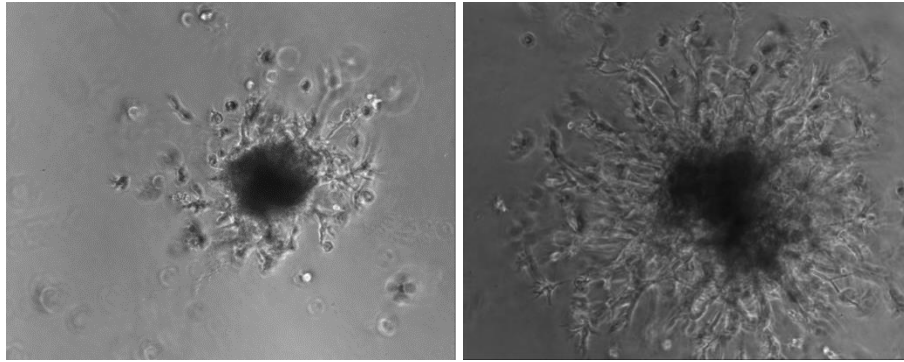


**Figure 4-5. Representative images of valve spheroid formation after 7 days in culture when seeded as VECs alone (left) or co-cultured with VICs (right).**

#### **4.4.3. A Subpopulation of VICs Guide VECs During Network Reorganization**

Upon further investigation of these co-cultures, it became evident that a subpopulation of VICs was attracting and guiding the organization of VECs during the time period before spheroid formation (7-24 hours) and it was hypothesized that there was a subpopulation of VICs significantly chemoattracting VECs. Therefore, a dual color PKH fluorescent speckle tracking method was implemented to track movement of VECs in relation to nearby VICs (Figure 4-6A) to quantify three relative chemotaxis metrics. The average cosine similarity measurements of VEC movements showed a narrow radial distribution around  $0^\circ$  ( $\pm 30^\circ$ ), indicating movement in the direction of VICs, unlike the simulated Brownian motion control, which had an even radial distribution (Figure 4-6B). The measured average directionality of VECs and their average Lagrangian Forward Migration Index (LaFMI) were significantly larger than in the simulated Brownian motion data sets, again indicating the movement of VECs in the direction of nearby VICs. Assuming that a LaFMI  $> 0.17$  represents a lower threshold for a chemoattractant effect (as demonstrated in prior chemotaxis studies<sup>178</sup>), 46% of VICs demonstrated this effect on nearby VECs, whereas this chemoattractant proportion was only 0.14% in the simulated Brownian motion data set. An example of a VIC demonstrating a LaFMI  $> 0.17$  (a chemoattractive effect on local VECs) is shown in Figure 4-6C and in Supplemental Movie 10.

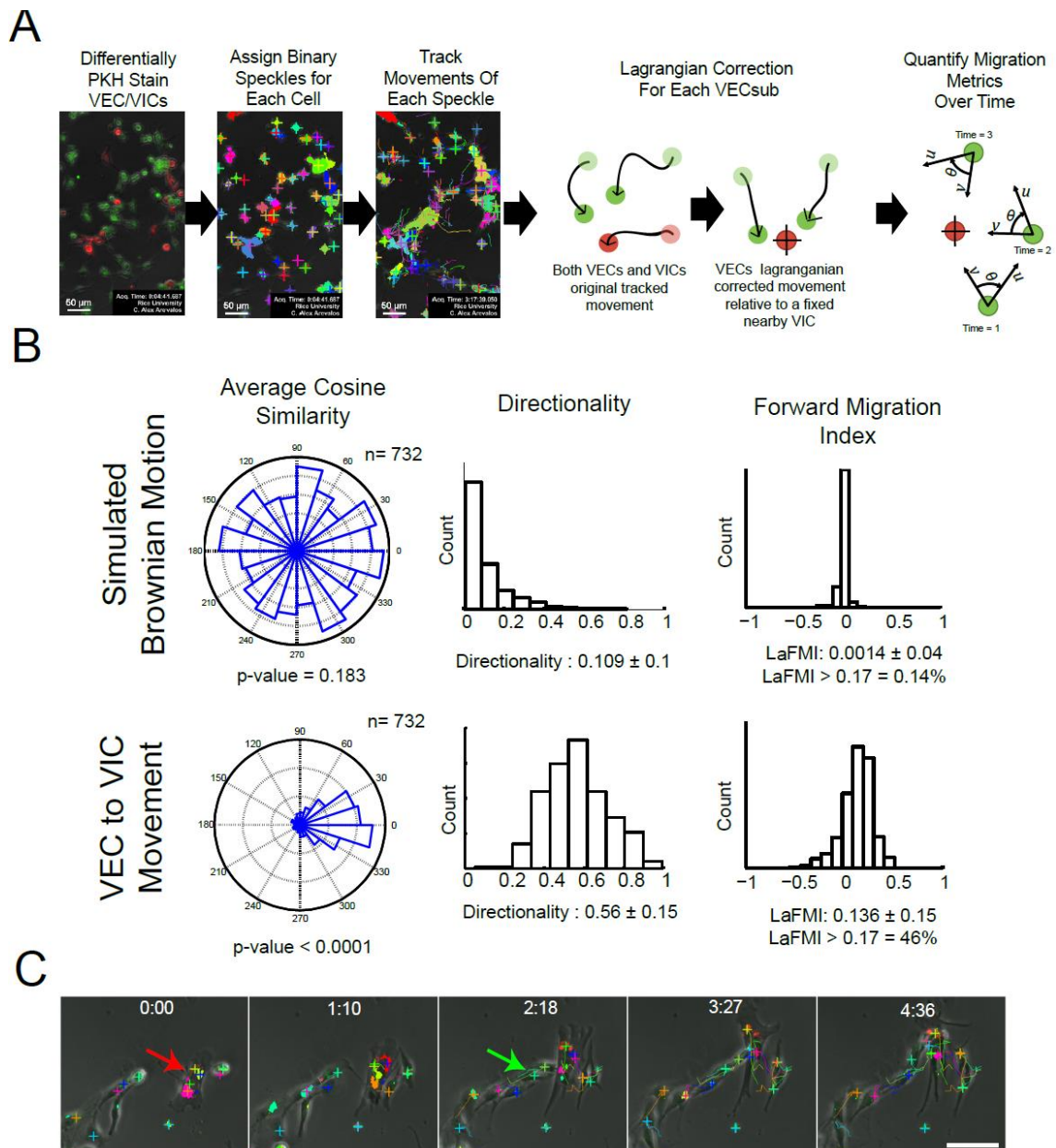


**Figure 4-6.** During organization into spheroids, tracking of VEC movement in relation to nearby VICs reveals a subpopulation of VICs that demonstrate chemoattraction. **A)** Illustration of method to quantify chemotaxis metrics. Confocal microscopy images of differentially stained VECs and VICs were reconstructed into z-stacks at each time point. For each color channel, the PKH staining was assigned a binary threshold, and each cell was tracked by its resultant unique speckle pattern. For each VIC, all nearby VECs were grouped together and a Lagrangian transformation was performed on their movements relative to the VIC of interest. Lagrangian-corrected chemotaxis metrics were then



calculated. B) Resultant chemotaxis metrics for a Brownian motion simulation (negative control) and the measured VEC and VIC movements. Compared to the independent-motion negative control simulation, VECs demonstrated a pronounced movement toward VICs in terms of average cosine similarity, directionality, and forward migration index. As defined by a forward migration index  $> 0.17$ , 46% of VICs had an overall positive chemotaxis effect on nearby VECs. C) Representative time track of a VIC (red arrow) exhibiting positive chemoattraction on nearby VECs (green arrow) during network contraction and reorganization into spheroids.

#### 4.4.4. VICs Promote VEC Invasion and Are Found Throughout VEVIS Sprouts

VECs cultured alone formed spheroids that displayed a limited amount of invasive sprouts after 7 days in culture. In contrast, VEVIS spheroids displayed a significantly larger invasion ratio (area of invasion/ area of core) by spreading more from the core spheroid into the Matrigel (Figure 4-7A). Quantification of the radial position of VECs and VICS revealed that a higher percentage of VICs were localized on the exterior of the spheroids (75% and 100% quartile rings) compared to VECs, whereas a higher percentage of VECs were found in the inner 25% quartile ring of the spheroid compared to VICs (Figure 4-7C). The PKH-labeled VICs were observed throughout the VEVIS. As demonstrated by the red arrows in Figure 4-7, VICs were frequently found wrapped around early 2D networks (Figure 4-7E), on the leading edge of invading sprouts (Figure 4-7F, yellow arrow), and wrapped around 3D invasive sprouts (Figure 4-7G, red arrow). Interestingly, VICs often displayed direct cell-to-cell contact to the leading edge of 3D invading VECs, as shown by Figure 4-7H. As shown by the Z-stack reconstructed confocal microscopy images (Figure 4-7H and Figure 4-7I), VEVIS sprouts formed complex geometries spreading in 3D. The continued dynamic plasticity of the sprout edge after 7 days of co-culture is shown in Supplemental Movie 11.

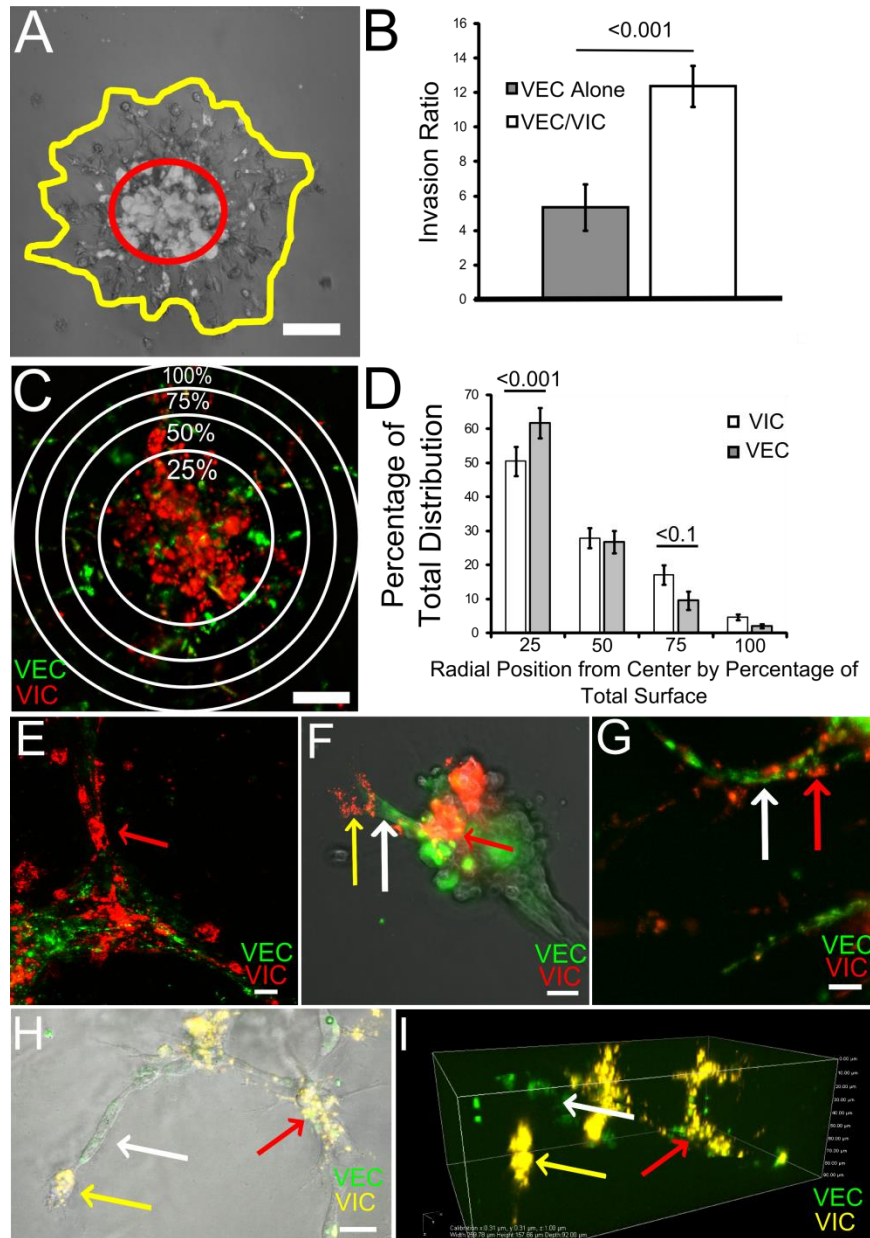


**Figure 4-7. VICs display a pericyte-like phenotype promoting and stabilizing VEC invasive angiogenic root formation throughout VEVIS. A) Representative image of quantification of sprouting ratio after 7 days. Scale bar: 100  $\mu$ m. B) Sprouting was significantly greater in VEC/VIC spheroids than in VEC-only spheroids. C) Representative image of the segmentation of a VEVIS into four quartile rings of equal surface area. Scale bar: 100  $\mu$ m. Both VECs and VICs were found throughout the VEVIS. D) A significant relationship was found between cell type and position by two-way ANOVA ( $p < 0.05$ ). The inner quartile ring contained a significantly larger percentage of VECs than VICs, whereas a larger percentage of**

VICs tended to be located in the third quartile ring. Throughout the VEC/VIC Matrigel co-culture, VICs were found in diverse locations that included E) wrapping around VEC tubules at 7 hours (red arrow); F) leading (yellow arrow) VEC angiogenic stalk-like cell (white arrow) sprouting from spheroids after 24 hours and co-localized with VEC spheroid nodes; G) wrapping (red arrow) around and stabilizing formed VEC invasive stalks (white arrow); and H) occupying the leading edge (yellow arrow) of VEC sprouts (white arrow) after 5 days in co-culture. Direct VIC-to-VEC contacts could also be found on invasive sprouts. I) 3D reconstruction of panel H demonstrating the 3D nature of VEVIS sprouts. Each arrow in panel I points to the same cell as in panel H. Scale bars represent 25  $\mu\text{m}$  in C and 50  $\mu\text{m}$  in D-F.

#### 4.4.5. VEVIS Sprouts Display Characteristics of Vascular Angiogenesis Sprouts

The VEVIS sprouts demonstrated several of the characteristics found in vascular sprouts, including DLL4 polarization, activated AKT, organized actin, 3D invasion, branching, lamellipodia at the tips, and multicellular tube formation (Figure 4-8). VECs maintained the ability to uptake acetylated LDL (Figure 4-8A). Most cells in VEVISs displayed low levels of unpolarized  $\alpha\text{SMA}$  (blue arrows, Figure 4-8B and Supplemental Movie 12) as opposed to the polarized  $\alpha\text{SMA}$  found in VICs but not in CD31+ VECs during the network formation at earlier time points (Figure 4-2C). VECs demonstrated continued expression of CD31 after 7 days of co-culture (magenta arrows in Figure 4-8C and in Supplemental Movie 13). Interestingly, both CD31- (green arrows) and CD31+ cells could be found on the tips of VEVIS sprouts (Figure 4-8D). These tip cells displayed direct cell-cell contact with CD31+ stalk cells emerging from the core VEVIS (magenta arrows in Figure 4-8D). VEVIS sprouts displayed DLL4+ polarization from tip to stalk, i.e., the expression of DLL4 was strongest at the leading cell and decreased toward the origin of the sprout (red arrows for tip and white arrows for origin in Figure 4-8E and Supplemental Movie 14). Interestingly, phosphorylated AKT+ cells were found prevalently on the tips of sprouts (yellow arrows in Figure 4-8F). The linear and tube-like organization of actin structures along VEVIS sprouts is recognizable in the higher magnification images (white arrows in Figure 4-8D,E,F). As shown by Figure 4-9, all cells in the VEVIS are pMLC+. In addition, VEVIS display  $\beta\text{-Catenin}$  polarity down the angiogenic like-sprouts.

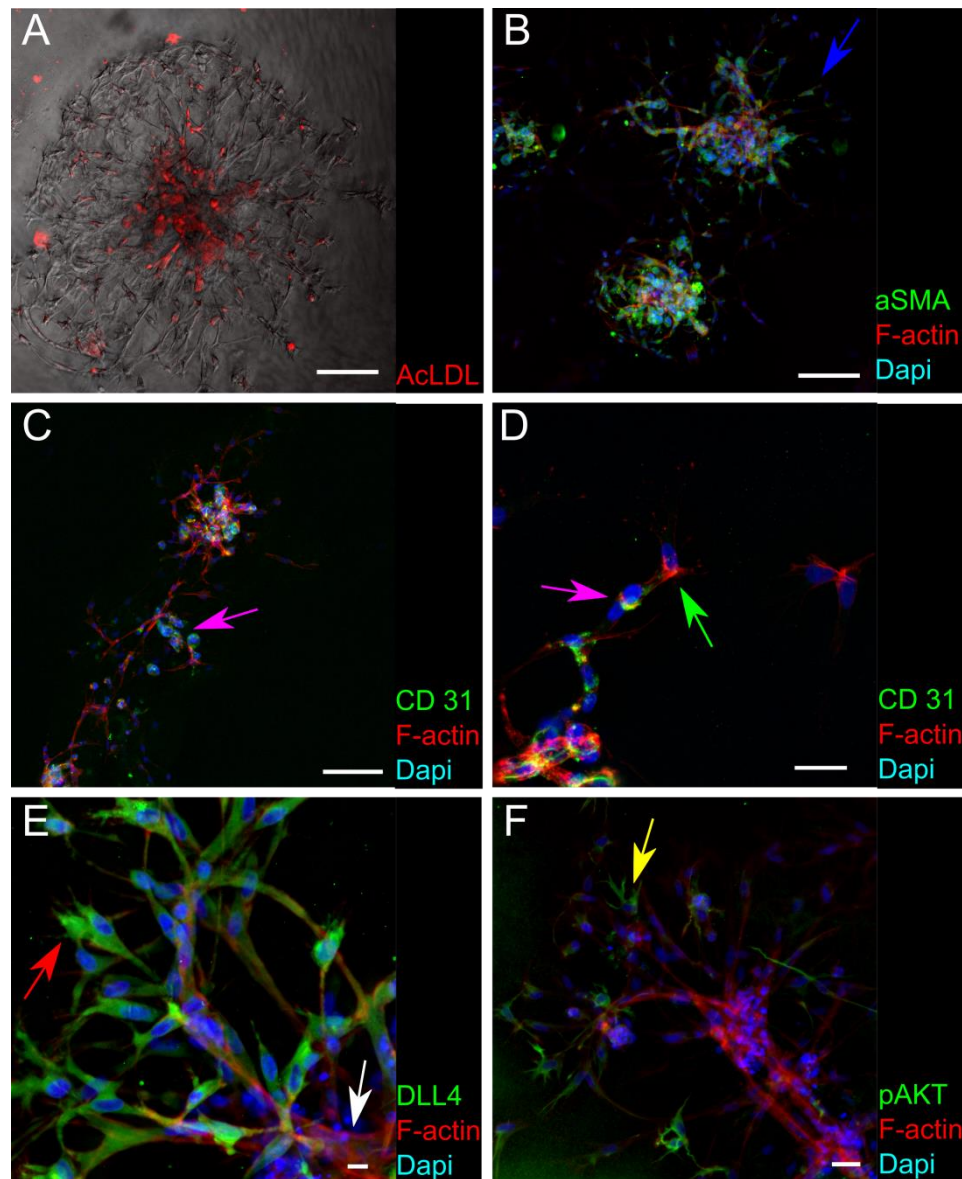


**Figure 4-8. VEVIS sprouts display characteristics of vascular angiogenesis sprouts after 7 days in co-culture. A)** VECs maintained endothelial phenotype as demonstrated by acetylated LDL uptake (red). Scale bar: 100  $\mu$ m. **B)** Most cells throughout the VEVIS, including tip and stalk cells, stained positive for diffusive non-polymerized aSMA (red; indicated by blue arrow). Counterstained with phalloidin (green) and DAPI (blue). Scale bar: 200  $\mu$ m. **C)** VECs maintained CD31 (red) expression in VEVIS core and sprouts (magenta arrow). Counterstained with phalloidin (green) and DAPI (blue). Scale bar: 200  $\mu$ m. **D)** CD31- VIC (green arrow) displayed direct cell-to-cell contact (white arrow) and organized actin on the tip of a stalk of CD31+ (red) VECs (magenta arrow). Counterstained with phalloidin (green) and DAPI (blue). Scale bar: 25  $\mu$ m. **E)** DLL4 (green) expression is polarized

from tip of the invasive root to the core spheroid (red arrow). In addition, linear and tube-like organized actin structures were recognizable along VEIS sprouts (white arrow). Cells are counterstained with phalloidin (red) and DAPI (blue). Scale bar: 25  $\mu\text{m}$ . F) pAKT+ (green) expression is localized on the tip cells of VEIS sprouts (yellow arrow). Counterstained with phalloidin (yellow) and DAPI (blue). Scale bar: 100  $\mu\text{m}$ .

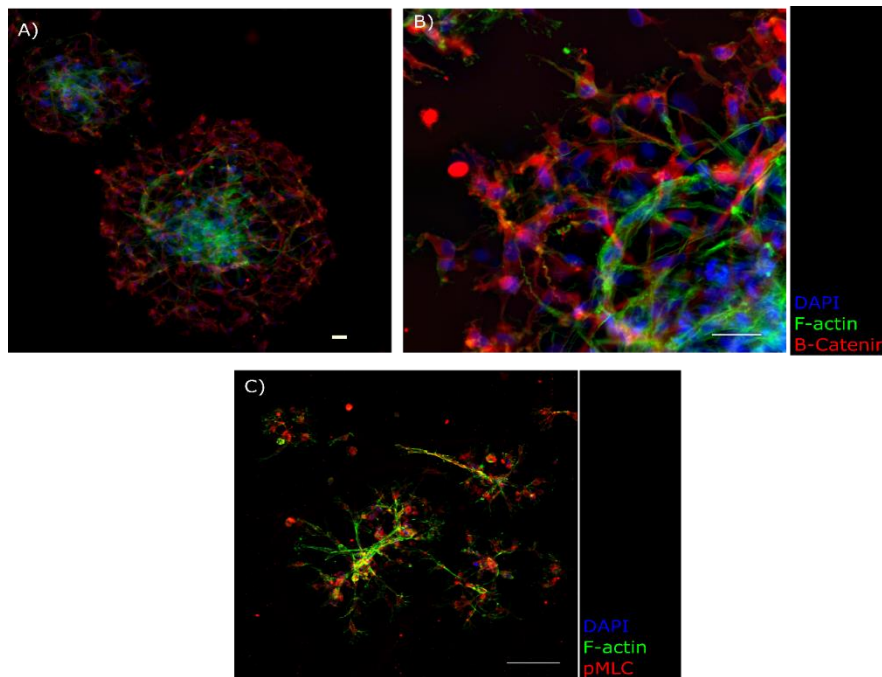


**Figure 4-9. VEIS demonstrate  $\beta$ -Catenin polarity down angiogenic-like root when visualized at A) 10x and B) 40x. Scale bars represent 25  $\mu\text{m}$ . As shown in panel C), pMLC was present in most cells with no appreciable pattern. Scale represents 200  $\mu\text{m}$ .**

#### 4.4.6. Tie2-Angiopoietin Signaling Is Important in Valve Cell Organization

VEC-only cultures treated with Ang1 displayed no significant change in total network size after 7 hours ( $93\pm 11\%$  of untreated control, Figure 4-10A-B). In contrast, treatment with Tie2 Inhibitor or pAKT inhibitor in addition to Ang1 resulted in significantly smaller networks relative to untreated controls at 7 hours ( $12\pm 7\%$  and  $50\pm 9\%$  respectively). After 3 days of culture, VECs treated with Ang1 demonstrated significantly larger total network size compared to controls ( $218\pm 3\%$ ), indicating the networks of Ang1-treated VECs were more stable than those of untreated VECs. This network size

effect was significantly abated with the addition of the Tie2 kinase inhibitor ( $62\pm 4\%$ ) and the pAKT inhibitor ( $86\pm 3\%$ ).

Treatment with Ang1 was insufficient to prevent VIC-mediated contraction into the VEVIS structures during 7 day cultures, as there was no significant difference in size between the VEVIS formed from untreated VEC/VIC co-cultures and the Ang1-treated group ( $91\pm 7\%$  of control). Treatment with the Tie2 inhibitor, either alone or in addition to Ang, significantly reduced VEVIS size ( $4\pm 1\%$  and  $11\pm 1.9\%$ , respectively) compared to control VEVIS. Treatment with the pAKT inhibitor in combination with Ang1 significantly reduced VEVIS formation ( $20\pm 7\%$ ) compared to the control.

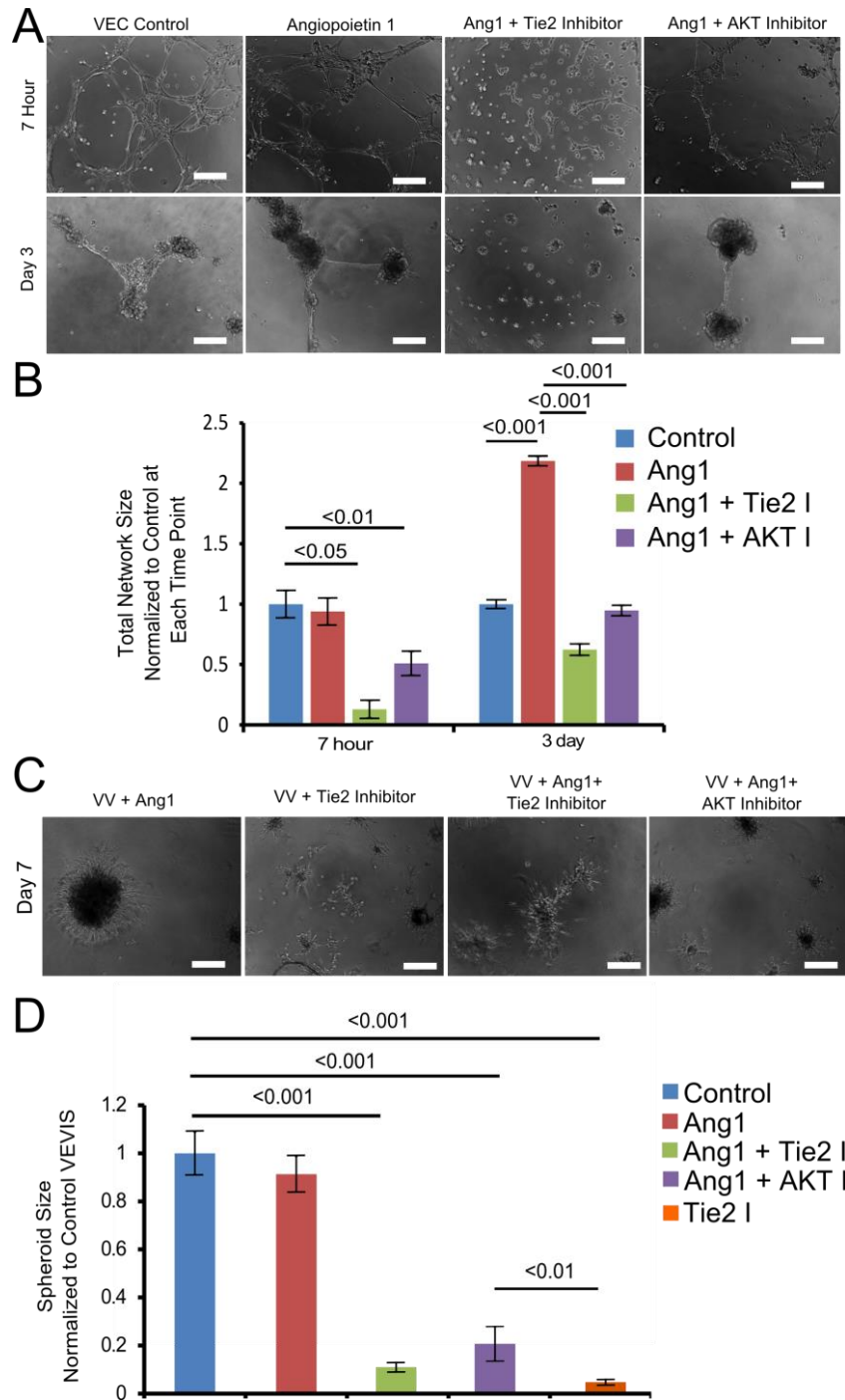


**Figure 4-10. Angiopoietin-Tie2 signaling regulates organization of VIC-VEC co-cultures. A) Representative images of the effects of Ang1 and its downstream inhibitors on VEC network formation over 3 days. Scale bars: 100  $\mu$ m. B) Quantification of the effects of Ang1 and its downstream inhibitors on VEC network formation over time. Results are presented as mean  $\pm$  SE for 12**

independently seeded wells.  $p < 0.05$  between groups. C) Representative images of the effects of Ang1 and its downstream inhibitors on VEVIS formation after 7 days in culture. Scale bars: 100  $\mu\text{m}$ . D) Quantification of the effects of Ang1 and its downstream inhibitors on VEC/VIC co-culture after 7 days. Results are presented as mean  $\pm$  SE of the VEVIS of 12 independently seeded wells.  $p < 0.05$  between groups.

#### 4.4.7. Long Term Co-Culture in the TLS Assay $\pm$ VICs Significantly Increases the Expression of Angiogenesis and Pericyte Related Genes

VECs and VICs demonstrated elevated levels of several angiogenesis- and pericyte-related markers after long term culture in the Matrigel model. When VECs were cultured alone in the Matrigel model, they showed significantly greater expression of FGFR2 and Tie2 compared to VECs cultured on tissue culture plastic. Angiopoetin1 expression was undetectable in control or Matrigel cultured VECs. No change in Periostin expression was measured between control and Matrigel cultured VECs. When VECs and VICs were co-cultured for 7 days in the Matrigel model, there was significantly greater expression of the angiogenesis and pericyte related markers FGFR2, Angiopoetin1, Tie2, NG2, and Periostin compared to a control 3:1 mixture of VECs and VICs mixed together prior to co-culture.



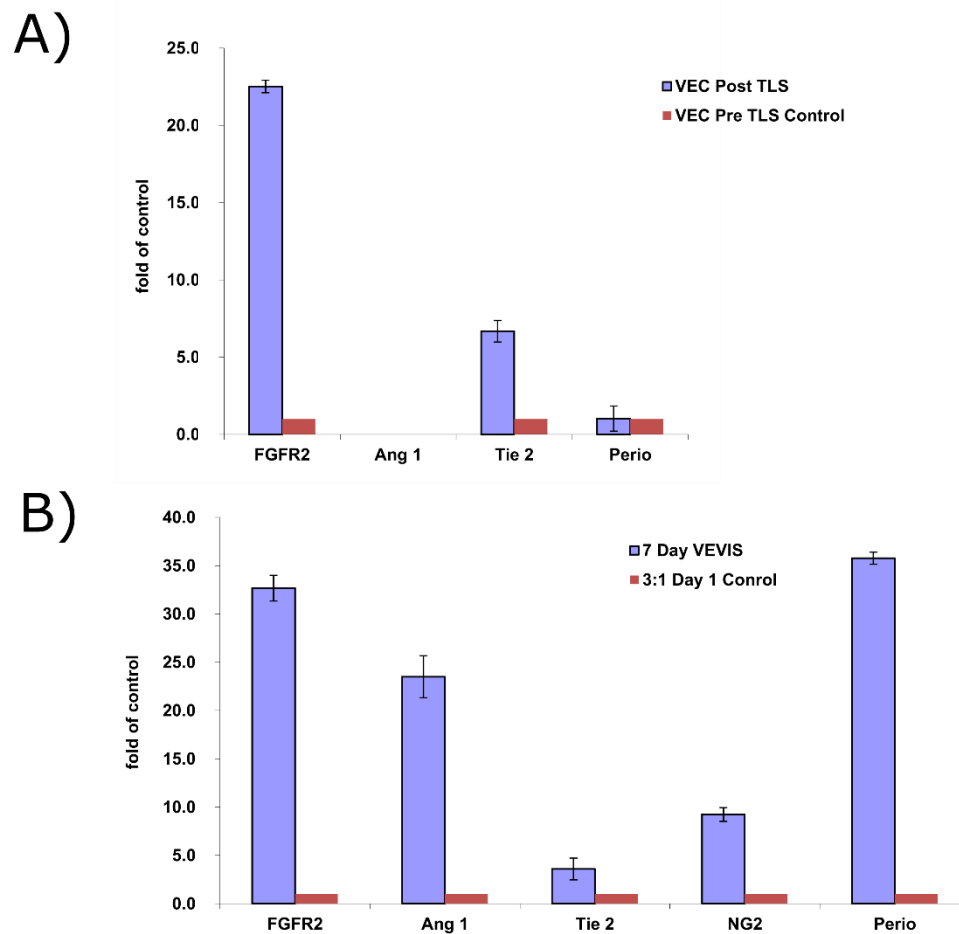


**Figure 4-11. VECs and VICs demonstrate several increases in angiogenesis and pericyte related markers after long term culture in the matrigel model. A) Significant increases in FGFR2 and Tie2 were measured when comparing VECs cultured in the matrigel model after 7 days compared to Day 0 control VECs. Angiopoetin1 did not prime in isolated culture or after 7 days in the matrigel model. No significant change in periostin was measured. B) Significant increases in the angiogenesis and pericyte related markers of FGFR2, Angiopoetin1, Tie2, NG2, and Periostin were measured after 7 days in co-culture in the matrigel model when compared to a control 3:1 mixture of VECs and VICs before co-culture.**

## 4.5. Discussion

During CAVD, the valve tissue undergoes an important change from an anti-angiogenic environment to a pro-angiogenic environment.<sup>170,171,180</sup> This change is

demonstrated by the presence of neovasculature in the normally avascular adult aortic valve.<sup>37</sup> These neovessels show characteristics of vascular microvessels, such as a CD31+ endothelial cell lining with aSMA+ pericytes wrapped circumferentially.<sup>37</sup> Although it would be ideal to confirm the valvular origin of these cells *in vivo*, it is compelling to investigate whether VECs and VICs have the potential to be the source of the endothelial cells and pericytes in these microvessels *in vitro* first, but there has been no previous study on whether VEC/VIC co-cultures could form 3D angiogenic structures.

This study was designed to quantify the extent to which VECs and VICs demonstrate characteristics representative of dynamic endothelial-pericyte interactions within a long-term Matrigel co-culture model that introduces the cells to a pro-angiogenic microenvironment. Directly comparing these aspects of the behavior of valve cells to vascular-derived endothelial cells and pericyte precursors elucidated several typical and atypical vasculogenic/angiogenic behaviors of the valve cells. The main findings were that the VICs do act like pericytes in stabilizing early VEC vasculogenic network formation, but later drive network collapse in a manner involving chemoattraction of VECs. In time, the co-cultured VIC and VECs form a spheroid, from which the VICs lead invasive angiogenic sprouting. Lastly, it was shown that these processes were regulated by ROCK and the Ang-Tie2 pathway. It should be noted that there are caveats associated with the use of this Matrigel model, it is unclear whether these invasive sprouts are indicative of functional *in vivo* angiogenesis complete with lumen formation and blood carrying capacity. Future studies should include an *in vitro* angiogenesis assay which incorporates flow to better demonstrate an EC lumen<sup>181</sup> and an *in vivo* model to test VIC ability to support vessel formation<sup>182</sup>. However, this work expands our understanding of valve cell-cell organization and communication with implications for valve homeostasis, heart valve tissue engineering, and the pathology of CAVD.

This study was centered on the ability of VICs to act as pericytes. During vascular angiogenesis, pericyte-endothelial signaling plays a very important role in the organization and stabilization of neovascularization. Pericytes guide vessel formation through paracrine and direct contact signaling mechanisms, several of which have been investigated in regards to valve cells.<sup>160,183–186</sup> Despite the evidence for a subpopulation

of cells in calcified valves that have pericyte-like characteristics,<sup>157</sup> VIC-endothelial cell studies to date have yet to induce quantifiable pericyte-mimicking behavior.

In this study, VICs demonstrated characteristics of pericyte phenotypes throughout sustained co-culture with VECs in the Matrigel model. During the initial network formation, co-culture with VICs led to a quantifiably smaller VEC network size, which was reversed by inhibition of ROCK. ROCK inhibition prevented  $\alpha$ SMA polymerization while maintaining VEC-VIC direct cell-cell contacts (Figure 1E compared to 1F), similar to how pericytes have been previously described *in vitro*.<sup>176</sup> This effect of ROCK inhibition on network size of VIC-VEC co-cultures is consistent with previous reports that ROCK inhibition increases vasculogenic network size in VEC-only cultures.<sup>175</sup> Given that ROCK also regulates contraction of collagen gels by VICs,<sup>132</sup> this data suggests that early VIC-mediated VEC network organization is ROCK dependent.

By tracking and quantifying cell motion to determine chemotaxis metrics, this study demonstrated that a subpopulation of VICs (46%) possessed a chemoattractant phenotype, attracting VECs. This behavior was demonstrated during VEC/VIC self-organized into spheroids by 24 hours after seeding in Matrigel. In contrast, co-culturing of the vascular mimetic cells (MCECs and 10T1/2 cells) led to sustained networks over time. Although not all VICs showed this chemoattractive behavior ( $\text{LaFMI} > 0.17$ ), it is unclear if VICs with a  $\text{LaFMI} < 0.17$  were unable to attract local VECs due to another VIC nearby with a stronger chemoattraction. It is currently not fully understood whether dysfunction of VECs, VICs, or both leads to initiation of CAVD.<sup>160</sup> These results indicate that VICs cultured in Matrigel develop a pro-angiogenic and chemoattractant phenotype. These VICs are then capable of driving VECs from their physiologically quiescent phenotype toward a more pro-angiogenic and invasive phenotype. These results suggest that under the proper stimuli VICs have the ability to organize VECs into pathological structures and, thus, the capacity to disrupt valve homeostasis.

Tracking of differentially-stained valve cell types in co-culture revealed several pericyte-like behaviors of VICs towards VECs. After our first observations of the spontaneous formation of VEVIS structures, we hypothesized that VECs would be the first cell type to invade the gel from the spheroids, and implemented PKH tracking to monitor cell behavior during this culture period. Unexpectedly, PKH tracking revealed

that VICs tended to be the first cell to leave the spheroid and invade the Matrigel, were found preferentially on the exterior of the VEVIS compared to the VECs, and facilitated greater invasion by VECs. These results reveal that the significant differences between the localization and arrangement pattern of VECs and VIC was not random, and these interactions were likely driven by a combination of cell-cell and cell-matrix signaling. These results were also distinct from the MCEC/10T1/2 co-cultures, which did not form spheroids. In the future, it will be important to elucidate further the key molecular regulators in valve cells that are responsible for their atypical translation of these angiogenic signals compared to the vascular controls.

The invading VEVIS sprouts were similar in some ways to classic angiogenic sprouts, but also demonstrated unique characteristics. The VICs on the leading edges of the sprouts were CD31- and  $\alpha$ SMA+, but the VICs maintained cell-cell adhesions with following CD31+ VECs. As shown by Figure 4-11, VECs demonstrated a pronounced elevation in periostin expression during the culture period, but that elevation was only in co-culture. This result suggests an association between the greater degree of cell invasion of Matrigel in the VEVIS condition and expression of this ECM protein, which has been strongly linked to neo-angiogenesis in aortic valve sclerosis.<sup>45</sup> Interestingly, the VEVIS sprouts demonstrated DLL4 and  $\beta$ -catenin polarity from the tip to stalk of sprouts, thus exhibiting evidence of cell-cell contact-mediated DLL4 as well as  $\beta$ -catenin linked<sup>187</sup> regulation of angiogenic-like sprout initiation. Further studies are required to investigate if manipulation of NOTCH or DLL4 expression in valve cells affects VEC/VIC tip cell dynamics. In vascular angiogenesis, DLL4 to NOTCH signaling plays an important role in cell-cell contact-mediated initiation and tip-stalk cell organization in neovessel formation.<sup>84</sup> NOTCH is the expected ligand for the DLL4 receptor, and there is a reported role for NOTCH signaling in VEC-VEC signaling, VIC-induced calcification, and valvulogenesis.<sup>186,188</sup> However, it is unclear if the same downstream pathways previously related to calcification and NOTCH are at play in this model. Further studies are needed to examine whether sustained angiogenic signaling leads towards valve calcification through angiogenic-related cell-cell contact NOTCH inhibition.

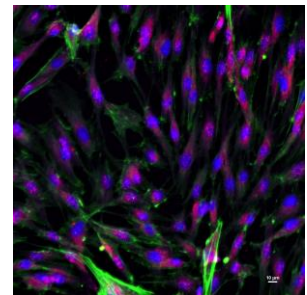
Since there is growing evidence for significant involvement of nitrous oxide (NO) signaling in VEC-VIC interactions,<sup>158,160</sup> this study examined the role of the Ang1-Tie2 pathway (an upstream regulator of NO via eNOS and AKT) in valve cell signaling and

organization into networks and VEVISs. Stimulation with Ang1, the ligand for Tie2 receptor, had no significant effect on early network formation in VIC-VEC co-cultures, but inhibition of direct and downstream signaling via inhibitors for Tie2 and AKT markedly reduced network formation. After 3 days in culture Ang1 stimulation significantly slowed network collapse and, correspondingly, inhibitors for Tie2 or AKT prevented this slowing. Long-term ROCK inhibition had a similar effect as Ang1 stimulation on VIC-VEC network stabilization (data not shown), which is not surprising given that ROCK inhibition is a downstream effect of Tie2 activation.<sup>189</sup> Ultimately, this network stabilizing effect of Ang1 could not prevent the VIC-mediated network collapse and eventual formation of VEVIS. Tie2 inhibition, however, completely ablated VEVIS formation suggesting that basal levels of Ang-Tie2 signaling are significant contributor to VEC/VIC signaling during VEVIS formation. Although treatment with the AKT inhibitor failed to prevent VEVIS formation, the resulting VEVIS were much smaller, suggesting a role for basal levels of AKT activation in VEC/VIC communication. . In addition, RT-qPCR demonstrated a large increase in both Tie2 and Ang1 expression in the co-culture model but only Tie2 increased in the VEC-only culture. These results suggest that long term culture of VECs in a proangiogenic environment primes VECs for vessel stabilization with local pericyte-produced Ang1, as shown by the increase in Tie2 expression. VECs cultured alone produce sufficient Ang1 stimulation to maintain vessel-like invasion to the same degree as the co-culture model. However, sustaining the vessels requires Ang1 stimulation, which was found only in the co-culture model (Figure 4-11). Interestingly, treatment of VEVIS co-cultures with PMA, which was shown to induce release of Ang2 in this work and other studies (data not shown), strongly inhibited vessel stabilization without affecting nucleation of VEVIS spheroids. Although it is unlikely that the Ang-Tie2 pathway is alone in affecting VEC-VIC behavior in this assay, collectively these results suggest that Angiotensin signaling, via the Tie2 and AKT pathways, mediates VIC pericyte behavior towards VEC organization, as well as evolution towards invasive angiogenic behavior. This finding is significant due to the role of Ang-Tie2 signaling in initial vascular destabilization,<sup>190</sup> and therefore suggests a role for this pathway in initial VEC dysfunction and the sustained vessel formation found during CAVD. Further studies are required to confirm the role and source of Tie2 signaling activity *in vivo*, and its effects on VEC monolayer homeostasis during CAVD.

## 4.6. Conclusion

Angiogenesis has long been associated with valvulogenesis and the pathology of CAVD. This study sought to identify the phenotypic changes of valve cells cultured long term in a pro-angiogenic model to provide further insight to the role of angiogenic signaling in VEC/VIC dynamics. Tracking of the cells revealed a subpopulation of VICs with chemoattractant behavior towards VECs and a novel invasive spheroid phenotype of these valve cells compared to their vascular counterparts. Lastly, this study identified a new set of angiogenic regulators, the Ang-Tie2 family, affecting valve cell communication and organization. This study contributed to the growing understanding of valve cell biology and how a sustained pro-angiogenic environment in the aortic valve could lead to an atypical translation of angiogenetic signaling in valve cells enabling angiogenic invasion of the valve through coordinated valve cell behavior contributing to the pathology of CAVD through increased inflammatory infiltrates and blood flow to the normally avascular aortic valve.

## Cyclic Strain Inhibits Valve Endothelial Cell Vasculogenic Network Formation Independent of Piezo1



### 5.1. Abstract

**Objective:** Valve endothelial cells (VECs) undergo unique mechanical stimulation compared to peripheral vascular endothelial cells. During the progression of CAVD, thickening and hardening of the aortic valve alters the mechanical environment of the VECs. Angiogenesis is a known important contributor to the progression of CAVD in the normally avascular aortic valve. However, it is unknown how mechanical strain contributes to maintaining the avascularity of the aortic valve or how disturbance of the normal mechanical strain contributes to the progression of CAVD. Therefore, this study examined the effect of mechanical stimulation, and the role of Piezo1, a mechanically active  $Ca^{+}$  channel, in regulating the response of valve endothelial cells to uniaxial strain in an angiogenesis Matrigel model.

**Method:** CD31+ porcine aortic VECs were uniaxially stretched at 0.5 Hz at 0%, 5%, or 10% strain for 24 hours using the Flexcell uniaxial strain system. The VECs were then seeded on matrigel, and the resultant vasculogenic tubule-like-networks were quantified after 7 hours. Piezo1 was silenced by treating VECs with siRNA for 48 hours, cyclically stretching them for 24 hours, and then testing the VECs in the Matrigel model.

**Results:** Network analysis revealed a strong pattern of strain to decrease the propensity of VECs to form networks. Quantification showed a significant decrease in junction and vessel segment density when cyclically strained at 5% or 10%. Lastly, silencing of Piezo1 significantly reduced network formation compared to a scrambled siRNA treatment, but showed no significant difference between cyclic stretch or static cultures.

**Conclusion:** These results suggest that a mechanically altered valve, such as those calcified by CAVD, are more prone to worsening disease conditions through increased angiogenesis. These results suggest that Piezo1 has a role in regulating angiogenesis signaling in VECs, but this effect was independent of stretch in this study. Further investigation of the mechanisms underlying VEC vessel formation and CAVD development will help pave the way for the development of an interventional treatments that target these valve-specific mechanisms.

## 5.2. Introduction

The trilayer structure of the aortic valve imparts the tissue with the mechanical properties necessary to withstand an extremely dynamic mechanical environment. Over the course of a person's lifetime, their aortic valve will open and close approximately three billion times, fully loading and unloading each time. Throughout this active life, the valve cells are subject to tension, compression, shear stress and hemodynamic pressure.

During systole, the ventricle ejects blood through the aortic valve, forcing it open. The strain of valve opening is largely borne by tension of the elastic fibers of the ventricular side, which can accommodate large strains due to their elastomeric nature. On the aortic side, collagen fibers of the fibrosa crimp to accommodate the corrugation-like folding and compression associated with the surface of the valve. Furthermore, systole induces uniform laminar shear stress of up to 80 dyne/cm<sup>2</sup> to VECs the ventricular side, while aortic side VECs experience highly turbulent oscillatory shear stress of much lower magnitudes: -8 to 10 dyne/cm<sup>2</sup>.<sup>13</sup>



During diastole, there is turbulent back-flow, causing the valve to close and preventing regurgitation of blood back into the ventricle. As the valve closes, it experiences peak tension of 50-100 N/m, which induces areal strains of up to 30% that are applied at rates as high as 1000%/sec. When strained, the collagen fibers of the fibrosa are uncrimped and stressed, and act as the main load-bearing elements. Their high stiffness resists strain circumferentially (the fiber direction), but not radially (perpendicular to fibers). However, the radially-aligned ventricular elastin becomes stressed at strains of 40%, protecting the tissue from over-distension. There is thus a highly uniaxial strain applied to the tissue in the radial direction<sup>2,191</sup>.

The mechanical environment may also play a large role in the development of pathological angiogenesis in valves. Mechanical stimulation has been shown to alter both the morphology and gene expression of VECs, as well as increase the angiogenic behavior of vascular endothelial cells (ECs). Vascular endothelial cells align axially along vessel walls, in line with blood flow and against circumferential strain. In contrast, VECs have been shown to align perpendicular under the same conditions although those results are considered controversial.<sup>192</sup> Furthermore, angiogenic studies of vascular endothelial cells show that physiologic cyclic strain increases production of MMPs and pro-angiogenic growth factors such as VEGF, angiopoietin-2, Tie-2, and PDGF. Stretch and shear also stimulate the development of angiogenic sprouts and capillaries by vascular endothelial cells *in vitro* and *in vivo*.<sup>193-195</sup> Collectively, these studies indicate that mechanical stimulation can increase the potential for angiogenesis by vascular cells as a function of where they are located in the vasculature, although it is unknown how these same forces affect VEC angiogenic capacity.

Recent studies have documented the influence of mechanical shear and strain on VECs. Under uniform laminar shear, they produce more anti-inflammatory proteins and down-regulate chondrogenic and osteogenic factors, creating a protective barrier to degeneration. Cyclic strain was shown to increase VEC expression of VE-cadherin,  $\beta$ 1-integrin and vinculin, all of which are vital in cell-cell and cell-matrix signaling<sup>196</sup>.  $\beta$ 1-integrin in particular is vital for the ROCK and periostin pathways<sup>192</sup> which were previously shown in this thesis to be important in VEC angiogenic capacity.

For years, the molecular mechanism in which endothelial cells sense and transduce mechanical stimuli, such as strain and shear, into an internal signal was unknown. Recently, the mechanically active  $\text{Ca}^{2+}$  ion channel Piezo1 was identified to be expressed uniformly by vascular endothelial cells. This channel was identified to play a major role in vascular remodeling, which is heavily influenced by blood flow. Loss of Piezo1 expression through siRNA gene silencing led to deficits in actin regulation and cellular morphology in response to mechanical stimuli<sup>197</sup>. Since VECs had been previously demonstrated to control actin regulation in ways that differed somewhat from peripheral vascular endothelial cells under various stimuli<sup>21,175</sup> and similar to vascular endothelial cells under some stimuli like in Chapter 3, this study investigated the effects of Piezo1 silencing on cyclic strain-induced changes in VEC vasculogenic network formation.

Lastly, a topic of growing interest in valve biology is the importance of side specificity on valve endothelial cell biology<sup>191198</sup>. As VECs from the inflow and outflow sides of the leaflet experience different levels of mechanical and biochemical stimuli, several studies have investigated how these effects translate to functional differences between VECs from the atrialis or ventricularis side of the valve<sup>20</sup>. As several of the reported genotypic differences were related to angiogenesis, a method was developed to isolate VECs in a side specific manner. Differences in gene expression were compared to previous studies, and the capacity of the resultant VEC populations to form vasculogenic networks was tested in the Matrigel model as in previous chapters.

Since the expression of genes and proteins in angiogenic pathways of valve endothelial cells have been previously shown to be altered under mechanical stimulation, this specific aim was inspired to provide insights on the effect of cyclic stretch on the vasculogenic capacity of VECs. These results from this study will provide further insights regarding how mechanical strain contributes to maintaining the avascularity of the aortic valve or how disturbance of the normal mechanical strain contributes to the progression of CAVD.

## 5.3. Materials and Methods

### 5.3.1. Cell culture

VECs were harvested and cultured as previously described in chapters 3 and 4.

### 5.3.2. Side Specific Isolation of VECs

Leaflets were excised from the aortic valves of adult pigs as per previous protocols in chapter 3 and 4. To ensure side specificity, a pin was used to pierce the leaflets through the fibrotic side during the leaflet harvest. Leaflets were rinsed with warm PBS and placed on a petri dish with the fibrosa side facing up. During the normal harvest of VECs, the pin was used to keep track of which side the VECs were being harvested from. P0 cells were magnetically sorted CD31+ and side-specificity was verified via qRT-PCR for vWF and FGFR2, which were previously identified to show differences between leaflet sides.

### 5.3.3. Cyclic Straining of Cells

VECs between passage 2-5 were seeded at 150,000 cells per well onto six well UniFlex™ culture plates pre-coated with collagen type 1 (Flexcell International, Hillsborough, NC, USA). Cells were seeded in PDMS inserts designed to seed cells only on to the area of the Flexcell plate which underwent stretch. After 7 hours, PDMS inserts were removed and the cells were washed with EGM-2 full bullet kit media. VECs were grown on Flexcell plates for a total of 24 hours before their media was replaced with fresh media. The UniFlex plates were then placed in a Flexcell® FX4000-TTM Tension Plus System (Flexcell International). The Flexcell system applies negative pressure behind the UniFlex plates via a vacuum pump that is monitored by a pressure transducer. Arctangle® Loading Stations™ (Flexcell International) were used to translate this reverse pressure to uniaxial strains along the major axis. With this system, the strain can be applied at any waveform and a range of frequencies. In this study a 0.5 Hz sinusoidal waveform was chosen to mimic the cardiac cycle. Cells were stretched for 24 hours at cyclic strains from 0-10% or 0-5%. This duration matched previous studies where a significant effect was measured after only 24 hours of

stretching.<sup>196</sup> In all studies, a static unstretched control set of VECs was seeded on a Uniflex plates and later processed in parallel with the stretched samples.

#### 5.3.4. Matrigel Tube-like Structure Assay

After 24 hours of cyclic stretching, VECs were harvested using trypsin and seeded on to the Matrigel assay as described in chapter 3. Network formation after 7 hours was then imaged and quantified as in chapter 4. For each 5% and 10% run, these values were normalized against their respective static controls to calculate a relative change in length and junction number. Results across the three conditions (static, 5%, and 10%) were compared using single-factor ANOVA followed by Tukey's HSD test ( $\alpha = 0.5$ ) using JMP statistical software.

#### 5.3.5. ICC Imaging

In order to perform ICC directly on stretched cells, one well from the 6 well Flexcell plate was cut out and the cells were fixed in 4% paraformaldehyde for 30 min, and permeabilized with 0.25% v/v Triton-X for 15 min at RT. Next, samples were blocked in PBS with 3.5% bovine serum albumin (BSA) for 1 hour at RT. The samples were incubated with primary antibodies for endothelial and angiogenic phenotypes (shown in Table 5-1) at 1:100 in PBS and 0.35% BSA overnight at 4 °C. Gels were then washed, and incubated with fluorescent secondary antibodies at 1:100 for 1 hour at RT. After washing, samples were counterstained with DAPI and phalloidin for 20 minutes prior to mounting with fluoromount and imaging with confocal microscopy (Nikon A1-Rsi or Zeiss LSM 510).

**Table 5-1. Antibody Targets for FlexCell Study**

<b>Antibody Target</b>	<b>Function</b>
CD31 <sup>a</sup>	Endothelial cell marker
Delta Like Ligand 4 (DLL4)	Tip cell designation marker
pAKT	Proangiogenesis marker

### 5.3.6. qRT-PCR

After 24 hours of cyclic stretch or static culture, mRNA was harvested directly from 100,000 cells using a Quick-RNA Micro Prep (Zymo Research). 100 ng of RNA was then converted to cDNA using a PrimeScript™ 1st strand cDNA Synthesis Kit (Clontech). qRT-PCR was then performed at a 1:100 dilution using the SYBR® Advantage® qPCR Premix for the targets in Table 5-2. Ubiquitin was used as the housekeeping gene in each run. Fold change was then calculated pairwise between stretched and static cultured VECs before seeding into the Matrigel model in order to compare expression changes in the system as a function of the different levels of flex.  $\Delta Ct$  was averaged between runs of the same condition. This averaged  $\Delta Ct$  was then used to calculate the fold increase between the reference condition and the target by taking the ratio of  $(\text{Efficiency of amplification})^{\text{avg}\Delta Ct}$  for the target and the Ubiquitin reference. The error was represented by the square root of the average of the variances of the reference condition and the target.

**Table 5-2. Angiogenesis related genes for RT-qPCR**

Gene	Primer
Ubiquitin FWD	TGA CCA GCA GCG TCT GAT T
Ubiquitin REV	TCT TGT CGC AGT TGT ATT TCT GAG
Ang1 FWD	TTT CCA GAG AGG TTG GAA AGA A
Ang1 REV	GTA CTG CCT CTG ACT GGT TAT G
Ang2 FWD	TGG AAC CTC GAA CAG AAT ATG AG
Ang2 REV	GGA GGA GGA AGA CCG ATA GAA
Tie2 FWD	CCG TCA ACT GCA TCA CTT AAA C
Tie2 REV	TTA TCT TCC CAC AGG CTT TCT C
VEGF FWD	TAT GCG GAT CAA ACC TCA CC
VEGF REV	CTT GCC TCG CTC TAT CTT TCT T
vWF FWD	GGT CAG CGG TGT GGA CGA G
vWF REV	ACA AAC TCC GTG CTC CTG TTG AAG

### 5.3.7. Piezo1 siRNA Treatment Protocol

Dicer-substrate siRNAs (DsiRNA) targeting porcine Piezo1 were designed to specifically down-regulate Piezo1 expression. Traditional siRNAs are designed to mimic Dicer products and therefore bypass interaction with the enzyme Dicer. Dicer has been recently shown to be a component of RISC and involved with entry of the siRNA duplex into RISC. Dicer-substrate siRNAs are designed to be optimally processed by Dicer and

show increased potency by engaging this natural processing pathway. Using this approach, sustained knockdown has been demonstrated for up to 8 days *in vitro* according to the manufacturer. The DsiRNAs and the negative control DsiRNA (DS NC1) were purchased from Integrated DNA Technologies. 10  $\mu$ M of each pair of siRNAs were transfected into VECs by complexing them first with 1.5  $\mu$ l of Lipofectamine® RNAiMAX transfection reagent for 5 minutes in Opti-MEM medium (Lonza). Multiple Piezo1-targeting DsiRNA sequence pairs were designed from different coding regions of Piezo1 in order to improve silencing efficiency. The sequence of the DsiRNA primers were CAGAGCAGCAGCACGAAGGUCAGCCAG, GGCUGACCUUCGUGCUGCUGCUCTG, AGCAGGAGCCAGAAGGUCAGGGUGCAC, GCACCCUGACCUUCUGGCUCUGCT. To verify the transfection protocol, VECs were transfected with 10  $\mu$ M of TYE™ 563 DS Transfection Control (IDT) to confirm the entry of the complexed unit in > 80% of treated cells. VECs were transfected with the complexed DsiRNA as they were plated on to the Flexcell plate. After 48 hours of transfection, the media was changed with fresh EGM-2 media and the seeded cells were cyclically strained at 0-5% for 24 hours as described previously. Efficiency of gene silencing was verified 24 hours after silencing in a separately seeded VEC population by qRT-PCR specific for the target of interest using the scrambled DS NC1 product as a negative control.

## 5.4. Results

### 5.4.1. Cyclic Strain Inhibits VEC Network Formation as a Bimodal Function

VEC network formation on Matrigel was influenced by strain, but in a monotonic manner. Compared to static conditions, cyclic strain significantly decreased network formation of VECs on Matrigel by both the metrics of segment length and junction number, but the lowest amount of network formation was seen in the 5% strained VECs. For 0-5% and 0-10% stretch, the total segment length was 9.6% and 63%, respectively, of the total segment length of the static cultures. The relative junction number for 0-5% and 0-10% was 7% and 53% strain respectively compared to static controls. P-values between all conditions are <0.01 as depicted in Figure 5-1.

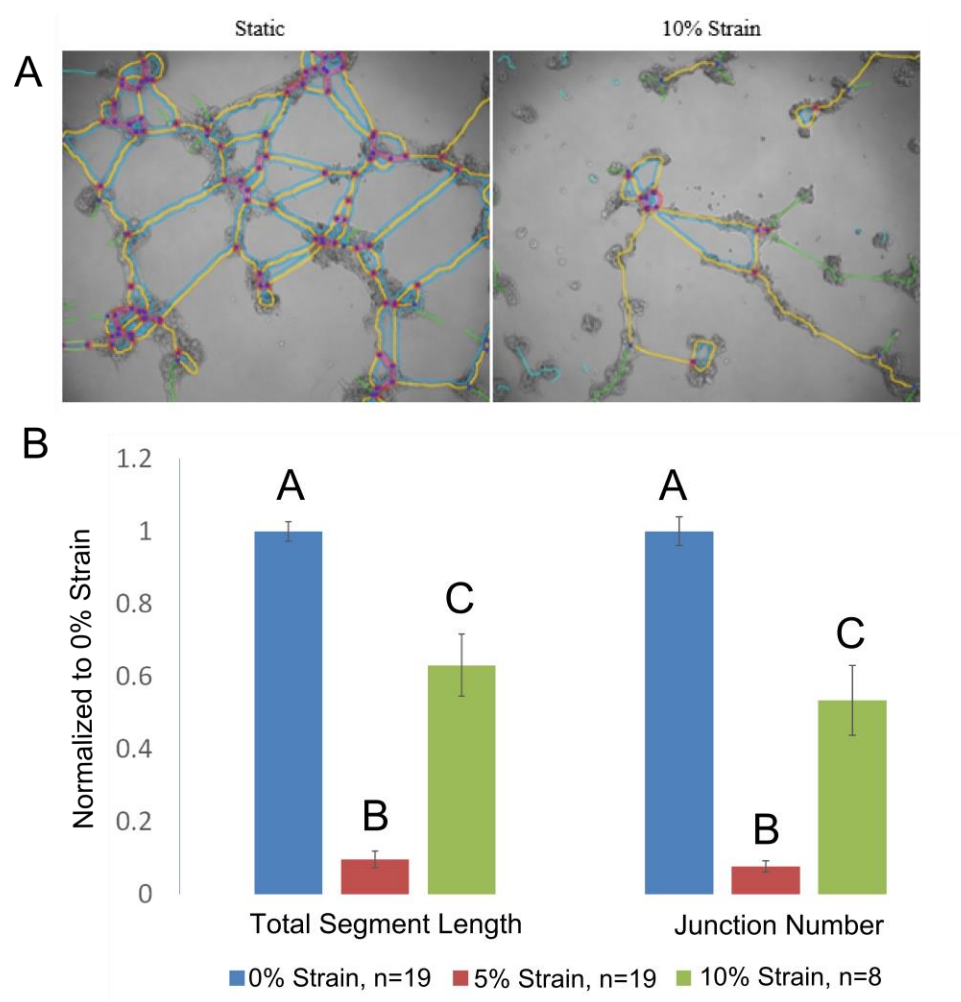


**Figure 5-1. VECs demonstrated a complex relationship between network formation and cyclic strain. A) Representative images of VEC vasculogenic network formation after 7 hours in the Matrigel model after static (left) and 0-10% (right) cyclic strain at 0.5 Hz for 24 hours. B) Quantification of the effect of static, 0-5%, and 0-10% strain on total network length and junction number. 0-5% strain demonstrated the largest decrease in total network length and junction number. All treatment groups not connected by the same letter were significantly different from one another in each network metric.**

#### 5.4.2. Cyclic Stretching Alters VEC Expression of Angiogenesis Related Genes

Several studies have demonstrated the effects of various mechanical stimuli on aortic valves from varying system levels from cellular to tissue scales<sup>20,192,196,199,200</sup>. As

demonstrated in Figure 5-2A, a significant decrease in VEGF and Tie2 were measured as a result of 24 hours of 0-5% cyclic stretch. No significant differences were measured in Ang2 or vWF. However as shown in Figure 5-2B, no significant differences in the genes of interest were measured for 0-10% stretch. Since the greatest measured effect on network change was at 0-5% strain and no significant gene expression changes were measured at 0-10%, the rest of the study was carried out a 0-5% strain.

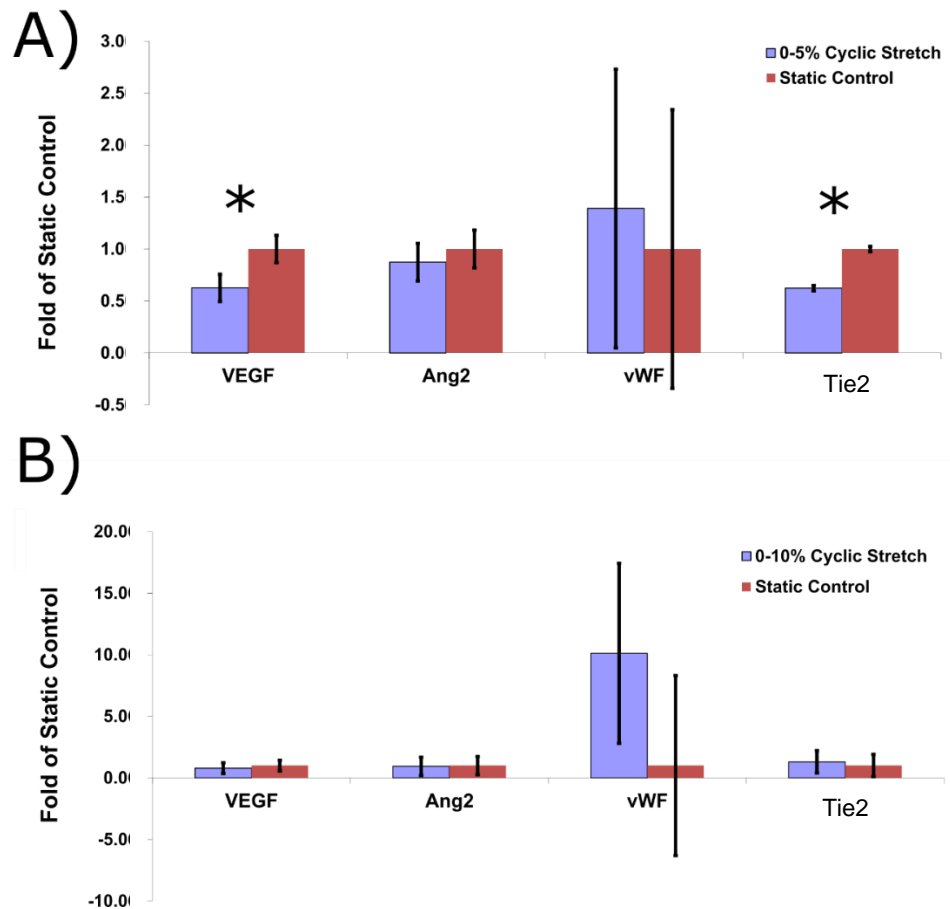


**Figure 5-2. Quantification of changes in angiogenesis related genes as a function of degree of cyclic stretch. \* represents a p-value < 0.05 between groups. A) Significant decreases in VEGF and Tie2 expression were seen after 24 hours of 0-5% cyclic strain. B) There were no significant differences in the genes investigated in this study after 24 hours of 0-10% cyclic strain. N = 4 independent biological runs paired for each treatment group.**



#### 5.4.3. Cyclic Stretching Alters VEC pAKT Expression and Localization

No apparent differences in Dll4 or CD31 were witnessed as an effect of 5% cyclic strain when investigated with immunocytochemistry. pAKT, however, appeared to move from mostly being expressed in the nuclei to being expressed greatly in the cytosol and the nucleus.

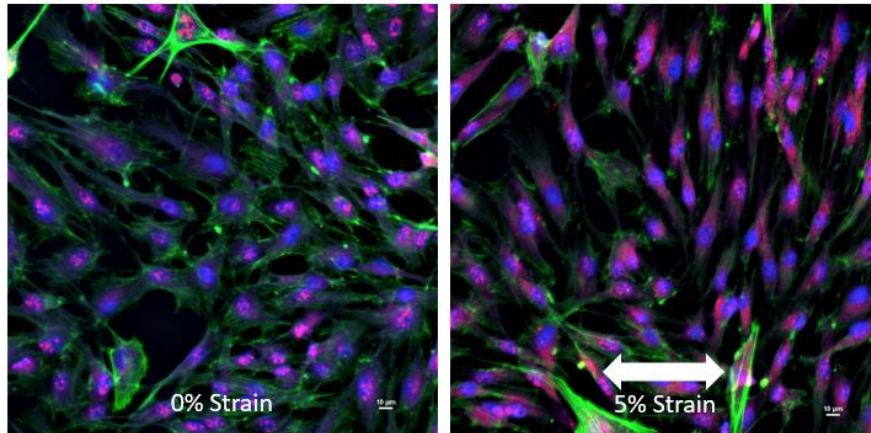


**Figure 5-3. Representative image of pAKT localization without (left) or with (right) 24 hours of cyclic strain. pAKT expression (red) localized to the cytosol as well as the nucleus in the 5% strain condition while pAKT appeared generally just in the nuclei (DAPI, blue) in the control condition. Cells were counter stained with phalloidin (green).**

#### 5.4.4. VECs Display Side Specific Differences in Network Formation

As previous investigations have established the gene expression profile difference between VECs harvested from the fibrosa and ventricularis side of the aortic valve leaflet, it was important to verify that our method of side-specific isolation produced cell populations with similar trends in the differences between their genes. Two angiogenesis-related genes with the largest changes in expression were FGFR2 and vWF in prior reports<sup>20</sup>, and in this study VECs showed a significant difference in vWF expression and a trending difference in FGFR2 expression between the cells from the fibrosa and the ventricularis. Both of these expression changes as shown in Table 5-3 were in the same direction as in previous studies<sup>20</sup>.

**Table 5-3: qRT-PCR data comparing expression fold changes of previously identified differentially expressed angiogenic related markers between side specifically harvested populations of VECs. Data is displayed as the ratio between the Fibrosa/Ventricularis delta CT values to the Ubiquitin reference.**

Gene	$\frac{\Delta}{\Delta}$ CT Value	P-Value	Function
<b>FGFR2</b>	1.21	0.14	Proangiogenic growth factor
<b>vWF</b>	2.21	0.046	Antiangiogenic factor <sup>201</sup>

Upon verification of the differences in the two isolated cell populations, passage 1 side-specific VECs were tested in the Matrigel assay to determine whether the fibrosa or the ventricularis microenvironments predisposed the VECs to form vasculogenic networks in the Matrigel assay. Both cell populations formed complex networks in this study. VECs from the ventricularis formed significantly larger networks than did cells from the fibrosa. However, there were no significant differences in junction number between groups.

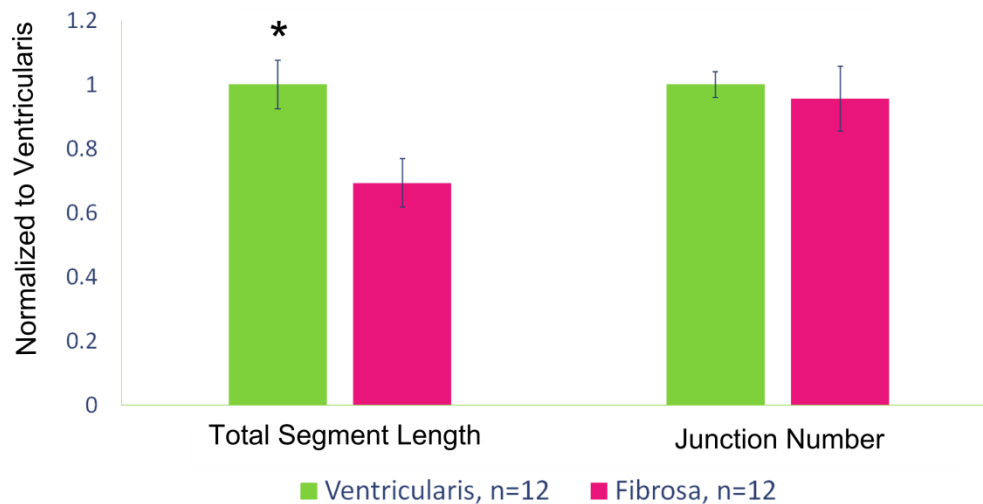


**Figure 5-4. Quantification of changes in VEC vasculogenic networks as a function of side specificity. VECs harvested from the ventricularis displayed significantly larger networks, but they did not display any significant differences in junction number.**

#### 5.4.5. VEC Network Formation Due to Cyclic Stretch is Independent of Piezo1

We next sought to determine whether DsiRNA knockdown of Piezo1 in VECs would rescue the stretch-dependent loss in network formation induced by 5% cyclic stretch. Figure 5-5A demonstrates that the DsiRNA treatment resulted in a 90% knock-down of Piezo1 expression by VECs down to  $10\% \pm 3\%$ . Piezo1 gene knock-down for at least 48 hours at this level had been shown to be sufficient to induce functional decreases in mechanically-induced calcium influx in previous studies<sup>197,202–204</sup>. As Figure 5-5B demonstrates by comparing the Piezo1 siRNA treatments  $\pm$  stretch, treatment of VECs with the scrambled control DsiRNA did not affect stretch-dependent inhibition of network formation. However, DsiRNA silencing of Piezo1 by itself was sufficient to reduce network formation in the static condition to levels comparable to the scrambled stretched controls, and there was no significant difference between VECs cyclically stretched or statically cultured once treated with Piezo1 siRNAs. Both Piezo1 treatments resulted in network lengths that were significantly reduced compared to the scrambled static controls.

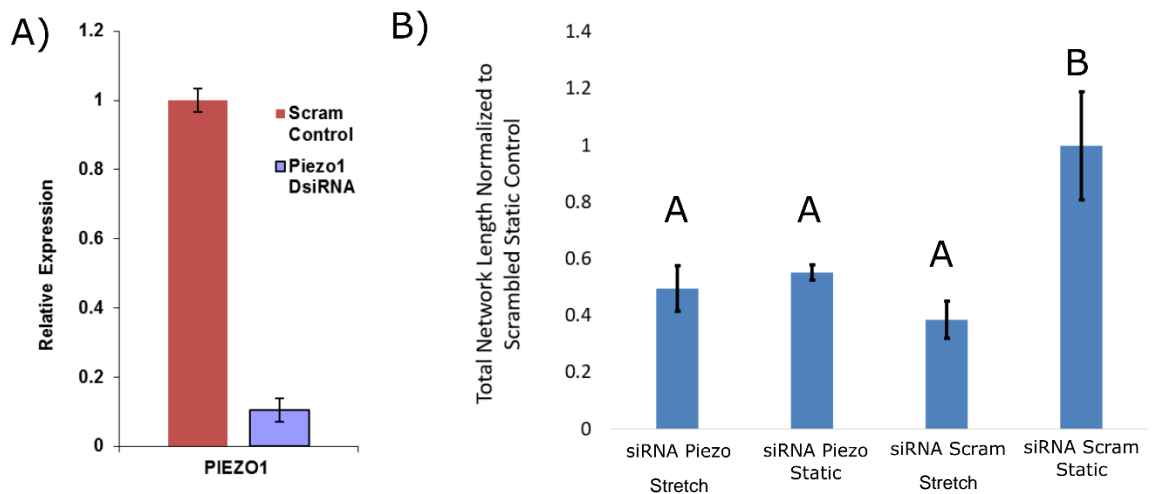


**Figure 5-5. A) Piezo1 expression was measured by RT-qPCR after siRNA treatment. Expression analysis showed a reduction in gene expression by  $90\% \pm 3$ . B) Quantification of the effect of Piezo1 silencing and cyclic stretch on VEC network formation. Treatment with Piezo1 DsiRNAs  $\pm$  stretch were sufficient to reduce network formation to levels comparable to stretched scrambled controls. Groups not connected by the same letter are significantly different from one another (p-value < 0.05).**

## 5.5. Discussion

The fundamental purpose of the aortic valve is to open and close efficiently in response to its unique mechanical environment. Mechanical stimulation is known to be strong motivator of endothelial cell angiogenic capacity. Several studies have investigated the various effects of strain and shear on vascular derived cells demonstrating significant changes in several angiogenic markers such as VEGF, angiopoietin-2, Tie-2, and PDGF *in vitro and in vivo*<sup>193-195</sup>. These studies indicate that mechanical stimulation can increase the potential for angiogenesis by vascular cells as a function of where they are located in the vasculature, although it is unknown how these same forces affect VEC angiogenic capacity. Similarly, mechanical strain has also been demonstrated to be an important regulator of VEC biology, with strong ties to direct causes of valve calcification.<sup>17,20,192</sup> Therefore, this study examined the effect of cyclic uniaxial strain on VEC network formation to better understand how the avascular nature of the adult aortic valve is regulated. In this study, we found that VEC network formation was strongly dependent on the levels of strain preconditioning, in a non-linear relationship.

Non-linear relationships between endothelial cells and cyclic strain were found in this study since 0-5% strain inhibited network formation to a greater degree than did the 0-10% condition, although the 0-0% (static) exhibited the largest network formation in comparison. However, non-linear relationships between mechanical stimulation and endothelial cells are not unprecedented.<sup>192</sup> In this study, no gene expression changes were observed in 0-10% stretch, but significant decreases in Tie2 and VEGF were found in 0-5% stretch. The lack of significant decrease in these pro-angiogenic markers could explain why this condition had the strongest knockdown of networks as both have been shown to regulate VEC activity in this work (Chapter 4) and in prior VEC studies<sup>186</sup>. Ultimately, this data suggests that the natural motion of the valve directly contributes to its avascularity. In addition, strain-shielded areas of the valve, either due to their location or to early stiff calcific nodules, could act as a trigger to greater angiogenesis. As has been previously hypothesized, this increase in angiogenesis could cause a major

influx of calcification and inflammatory infiltrates ultimately leading to the stenosis becoming symptomatic enough to require aortic valve replacement. Providing treatments that could prevent the progression of the disease and the reversal of the pathology at this time could potentially be used to prevent this catastrophic dysregulation of valve structure and prevent the need for a valve replacement.

In this study, side-specific cell isolation allowed for a method to model the effects of side-specific strain differences that the VECs had been preconditioned with throughout their lifespan in order to gain insights into the specific localization of calcification in the fibrosa layer. As demonstrated in this study, VECs harvested from the ventricularis exhibited greater network formation compared to VECs from the fibrosa. These results align with previous studies that suggested that valve cells from the ventricularis have a higher angiogenic capacity as a greater concentration of neovascularization was found in the ventricularis and middle layers of the valve.<sup>171</sup> In addition, prior studies have demonstrated differences in the expression of Rho protein signal transducers and actin cytoskeletal organizers between fibrosa-derived and ventricularis-derived VECs<sup>196</sup>. As shown by the results from Chapter 3, these factors could explain differences in the network formation between the two populations. These results suggest that VECs derived from the ventricularis are predisposed to pro-angiogenic invasion and therefore predisposed to contribute greater to aortic valve calcification. However, there is likely a multitude of factors contributing to the side-specific differences. Several caveats exist in this study, one of which is that some of the effect of the *in vivo* preconditioning could be lost in the short time that the cells are cultured. In addition, the effect of cyclic stretch in isolation using the Flexcell system was not tested on the side specifically harvested VECs.

Piezo1 is an important mechanically-active calcium channel in endothelial cells required for vascular development<sup>197,202–204</sup>. Piezo1 activation leads to calcium influx, calpain activity changes, and ultimately to several transcriptional changes and actin/integrin regulation changes. However in this study, Piezo1 DsiRNA treatment did not rescue the effects of stretch on network formation as hypothesized. Instead, a 90% gene expression knockdown of Piezo1 was sufficient to inhibit network formation by VECs when stretched or statically cultured. The resultant Piezo1 DsiRNA treated networks were similar in size to networks formed by VECs treated with a scrambled

control and stretched. These results suggest that Piezo1 plays a role in regulating VEC network formation, but that this effect is independent of cyclic stretch. This is not unprecedented as the same response was seen in HUVECS silencing in static culture.<sup>203</sup> However, the effect of Piezo1 silencing along with stretch in vascular endothelial cells remains unknown. Future studies would need to integrate shear along with Piezo1 silencing for the complete picture of the role in Piezo1 in valve endothelial cell regulation.

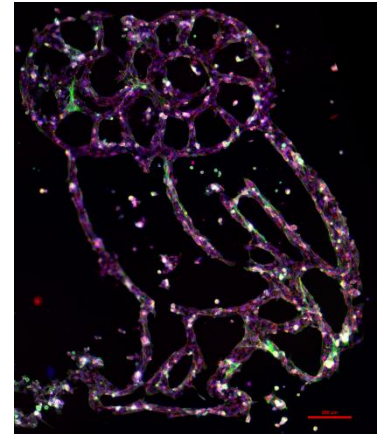
Previous studies have investigated the effect of biaxial strain on VECs using the Flexcell system<sup>196</sup>, and in these biaxial studies 0-10% and 0-20% strain were used to model physiological and pathological strain rates respectively based on prior reports<sup>199,200</sup>. In this study, uniaxial strain was applied to model the anisotropic stress differences experienced by VECs. Since the Flexcell system reports strains as a function of changes in area, a strain of 20% in the biaxial system modeled in the unidirectional uniaxial system would be approximately the equivalent of a displacement in one axial direction of  $\sqrt{1.2}$  or a strain of ~9%. Therefore, in this model 0-5% can be interpreted to model physiological strains while 0-10% strain and the static control strain can be interpreted to model pathological strains. However, it is important to note the caveat that the cells are experiencing the forces from the Flexcell system in isolation. Cells *in vivo* in the aortic valve are stress-shielded by their surrounding ECM and neighboring cells. Given this caveat, it remains difficult to make direct conclusions on the exact strains experienced by cells *in vivo* based on physiological strains and therefore difficult to make 1 to 1 predictive conclusions from the effect of strains used in this study back to *in vivo* effects. Nonetheless, these results provide directly controlled insights to the effect of cyclic strain on the vasculogenic and angiogenic capacity of VECs.

## 5.6. Conclusion

Mechanical strain has been demonstrated to be an important regulator of valve endothelial cells biology with strong ties to direct causes of valve calcification.<sup>17,20,192</sup> This work expands on the current understanding of valve endothelial cell biology, by demonstrating that cyclic uniaxial strain modulates VEC network formation, VEC side specificity influences their inherent angiogenic capacity, and establishing the stretch

independent role of Piezo1 in regulating VEC network formation. These results indicate that the cyclically stretching nature of the valve directly contributes to its avascularity. In addition, a mechanically disrupted valve, such as those calcified by CAVD, are more prone to worsening disease conditions through increased angiogenesis. Further understanding of the mechanically dependent mechanisms underlying VEC vessel formation can help pave the way for the development of aortic valve specific interventional treatments that target how VECs translate mechanical stimuli since the aortic valve has a unique mechanical environment compared to the rest of the body.

## Geometry – Dependent Regulation of VEC Angiogenic Phenotype



### 6.1. Abstract

**OBJECTIVE:** The development of complex engineered tissues is currently limited by the ability to incorporate functional microvasculature to encourage survival and growth. This issue is particularly relevant to pediatric tissue engineered heart valves. Vascular networks of varying complexity can be designed within engineered tissues, but the amount of biological complexity necessary for proper biological functionality is unclear. Prior work has identified that the geometric lacunarity of a network of valve endothelial cells (VECs) in an in vitro angiogenesis model can be tuned by manipulating the activity of the actin regulator ROCK with small molecule inhibitors. To examine the fundamental relationship between network structure and VEC biology, this work cultured VECs atop varied lacunarity patterns using biomaterial patterning strategies, then assessed the expression of several angiogenesis related markers.

**METHODS:** Polyethylene glycol diacrylate hydrogels (8 kDa) were patterned with RGDS into 15  $\mu\text{m}$  deep tubule networks using photolithography. VECs were then seeded on a vessel-mimicking pattern, a higher lacunarity hexagon-based pattern, or a lower lacunarity triangle-based pattern. After 24 hours of culture, levels of pMLC, pAKT,



pMAPK,  $\beta$ -catenin, VEGFR2, CD31,  $\alpha$ SMA, NCadherin, VECadherin, and perlecan was investigated using immunocytochemistry. Changes in tubule circularity and actin alignment were quantified after F-actin staining.

**RESULTS:** Notable differences in several angiogenesis related markers were found depending on the cell seeding pattern. VEC pMLC activity was lowest when seeded in the triangle pattern, while pMAPK was highest in the hexagon pattern. Actin organization and tubule circularity was highest in the vessel mimicking tubules. No significant differences were apparent in the other markers.

**CONCLUSIONS:** Controlling the geometric pattern of VEC networks mimicked changes in signaling previously observed in angiogenesis models with VECs. These results suggest a more biomimetic vessel pattern in a tissue engineered valve would stimulate a more biomimetic and functional endothelial response. Addition of further valve-specific elements such as periostin or chondromodulin will enable the creation of structured biomaterial scaffolds for application to pediatric TEHV development as well as models of calcific aortic valve disease, in which angiogenesis plays a role.

## 6.2. Introduction

The formation of a physiological microvascular system requires precise coordination between cells and their environment to produce vastly complex functional networks. In order to develop higher order tissue engineered constructs, rapid vessel formation and perfusion into the construct will be essential to ensure the survival and growth of the construct.<sup>205</sup> In order to achieve this goal, several strategies have been developed to pattern vascular networks into tissue engineered constructs. These strategies fall into two different categories. In one strategy, the vascular pattern is defined either through photolithography<sup>122</sup>, stereolithography<sup>206</sup>, or more recently 3D printing<sup>207</sup>. The second involves embedding cells in a properly proangiogenic 3D environment to encourage self-assembly into a vascular network<sup>119</sup>. Both strategies have been used to successfully engineer vasculature of varied lengths, junction densities, lacunarity, and in general levels of complexity. However a missing piece of insight from these studies is the amount of biological complexity necessary for proper long term biological functionality, because increased complexity is often accepted as

more successful<sup>114,115,208</sup>. However, more complex vasculature is not necessarily more functional; for example, the highly tortuous vasculature produced by proangiogenic tumors is functionally improved by certain vessel-normalizing anti-cancer treatments.<sup>209</sup> The necessary degree of complexity in these tissue engineered networks, and how that affects the internal cell biology independent of the initial stimuli that assembled the networks, remains a question of interest.

This fundamental question is relevant for tissue engineered heart valves and, in particular, for pediatric tissue engineered heart valves. A pediatric TEHV would ideally have the ability to grow, repair itself, and remodel as the child grows, eliminating the need for the repetitive surgeries and greatly increasing their overall quality of life and long term prognosis<sup>2</sup>. However, as in any tissue engineered material, achieving rapid host integration is an important step. The tissue would require rapid neovascularization to encourage incorporation into the host tissue and to increase the viability of the implanted cells. On the other hand, as reviewed in detail in this thesis, poorly regulated angiogenesis is hypothesized to lead to various heart valve pathologies such as CAVD. Therefore, any optimal TEHV would require angiogenesis that is spatially and temporally controlled as it is in the native valve. This control of the angiogenesis would likely involve patterning proangiogenic environments near the annulus and anti-angiogenic agents such as chondromodulin near the free edge. Over time, the encapsulated VICs would produce their own native anti-angiogenic compounds when necessary, which would switch off the angiogenesis at the appropriate time and location.

In the first specific aim of this thesis, the geometric lacunarity of a network of VECs was tuned by manipulating the activity of the actin regulators ROCK and Rac with small molecule inhibitors. That work demonstrated that the final complexity and potential functionality of such networks could be tuned by altering the internal biology of the cell using a chemical/pharmacological approach. To examine the fundamental relationship between network structure and VEC angiogenic-related biology from a different perspective, this chapter aims to provide proof-of-principle evidence that the internal VEC biology can be altered by growing them on patterned geometries of vascular networks. Several previous works have investigated the effects of patterned stripes of varying thicknesses, adhesiveness, and growth factor composition on the behavior of

endothelial cells patterned on top of hydrogels but those had not yet been applied to VECs.<sup>210,211</sup>

Because straight lines are less common in native vasculature, this work cultured VECs atop 8 kDa polyethylene glycol diacrylate hydrogels patterned using photolithography into 15  $\mu\text{m}$  deep tubule networks. This approach was termed a synthetic tubule like structure assay (syTLS). VECs were then seeded on to either a vessel-mimicking pattern, a higher lacunarity hexagon-based pattern, or a lower lacunarity triangle-based pattern. After 24 hours of culture, the VECs were assessed to determine several aspects their angiogenic phenotype using immunocytochemistry.

## 6.3. Methods and Materials

### 6.3.1. PEGDA Synthesis

Preparation and purification of PEGDA was performed as previously described.<sup>110</sup> A PEG powder of 8 kDa molecular weight was acrylated by mixing 0.4 mmol of PEG with 0.016 mol of acryloyl chloride and 0.8 mmol of triethyl amine in anhydrous dichloromethane (DCM) under argon gas overnight. Next, the PEGDA solution was washed and mixed vigorously with 2 M  $\text{K}_2\text{CO}_3$  until the solution was a milky white emulsion. The solution was then allowed to separate by gravity into an aqueous phase and a DCM phase overnight. The organic phase was then separated from the other phases by carefully draining into a beaker, and then mixed with anhydrous  $\text{MgSO}_4$  to remove any residual solution. The  $\text{MgSO}_4$  was then filtered from the solution, and the PEGDA was precipitated from the DCM and filtered with cold diethyl ether. The resulting PEGDA powder was then dried overnight under vacuum. The powder was stored at  $-20^\circ\text{C}$  under argon until use.

### 6.3.2. PEGylation Reaction

PEGylation of proteins and peptides was performed as previously described<sup>114</sup>. In brief, 3400 Da molecular weight Acrl-PEG-SVA (Laysan Bio) was mixed with the RGDS peptide (American Peptide Company) at a 1.2:1 molar ratio in PBS. The pH of the solution was brought up to 8.0 using 1 N NaOH and transferred to a 40 ml amber

vial. The mixture was vortexed for 1 hour, and the pH was re-adjusted to 8.0 every hour for four hours. The reaction was then allowed to react overnight. The reaction was dialyzed from free PEG-SVA and remaining salts overnight in ultrapure water the cold room protected from light. Afterwards, the dialyzed liquid was sterilized and lyophilized sterile. Dry PEG-RGDS was stored under sterile argon until it was eventually used.

### 6.3.3. Creation of Photomask Patterns

In order to recreate a vessel mimicking pattern, a phase contrast image of a representative VEC 7 hour network was converted to a binary image using ImageJ. The binary image was imported into a 2D CAD software (DraftSight) and vectorized by tracing each vertex with a 50  $\mu\text{m}$  line. The resultant vectorized image was then repeated as shown in Figure 6-1. The pattern was then printed out on to a transparency emulsion side down (CadArt). The hexagon and triangle pattern were designed by repeating the desired shape with 200 x 25  $\mu\text{m}$  thick patterns. 25  $\mu\text{m}$  thickness pattern edges were chosen to stimulate tubule formation by VECs.<sup>210,212</sup> The lacunarity of the final patterns were quantified using Angiotool as in Chapter 3 to confirm that the lacunarity of the hexagon and triangle pattern were greater than and less than the lacunarity of the vessel mimicking pattern<sup>175</sup>.

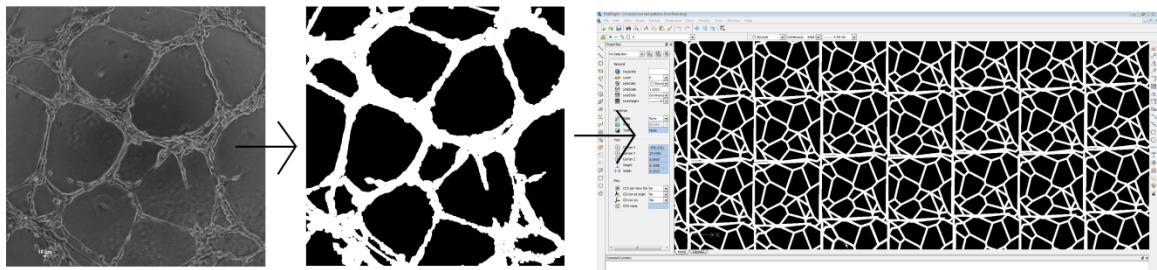


**Figure 6-1: Flow diagram demonstrating conversion of an image of VEC network to a repeating vectorized pattern.**

### 6.3.4. Construction of Synthetic Tubule Like Structures

Patterned hydrogels were constructed as depicted in Figure 6-2A. First, base gels were constructed in a sterile manner as previously described.<sup>213</sup> In brief, 10% w/v 8 kDa PEGDA was dissolved in a white light photoinitiator precursor solution consisting of 1.5% v/v triethanolamine (TEOA), 10  $\mu\text{M}$  Eosin Y, and 0.35% v/v 1-vinyl-2-pyrillidinone

(NVP) in HEPES buffered saline. 40  $\mu$ l of activated PEGDA precursor solution was pipetted between two 1 mm PDMS slabs separated by a 1 mm silicone spacer. Base gels were then photo-crosslinked under 160 kLux of white light (UltraTow LED Floodlight, Northern Tool and Equipment, Burnsville, MN) for 35 s. The molecular weight of 8 kDa was chosen for the base gels based on prior VEC hydrogel work to promote adhesion and maintenance of VEC endothelial characteristics during the study period.<sup>159</sup> Resultant hydrogels were then swollen in ultrapure water for 12 hours to remove any uncrosslinked PEGDA. Hydrogels were then swollen in a secondary polymer solution consisting of 1 mM PEG-RGDS, 1% 8 kDa PEGDA, 1.5% TEOA, 10  $\mu$ M Eosin Y, and 0.35% v/v NVP in a HEPES buffered saline solution overnight. Photomasks were then UV sterilized and placed directly on to the surface of the hydrogels and crosslinked for 2 minutes under a 290 kLux white light source collimated by a N-BK7 plano-convex  $\varnothing$ 2" lens with a focal distance of 60.0 mm (Edmund Optics). A light absorbing black-out flock velvet-like paper was placed underneath a 0.5 inch glass spacer to block any non-incident or reflected light. Patterned hydrogels were then swollen overnight in sterile PBS + 1% v/v PenStrap. The sterile collimated light source is diagrammed in Figure 6-2B. To test the specificity of the surface modification, 0.04% wt/v Acryloxyethyl thiocarbamoyl Rhodamine B (Acryl-Rhodamine) was added to the secondary solution and imaged with fluorescence microscopy (Polysciences, Inc., Warrington, PA).<sup>214</sup> A representative image of the pattern specificity is shown in Figure 6-2C.

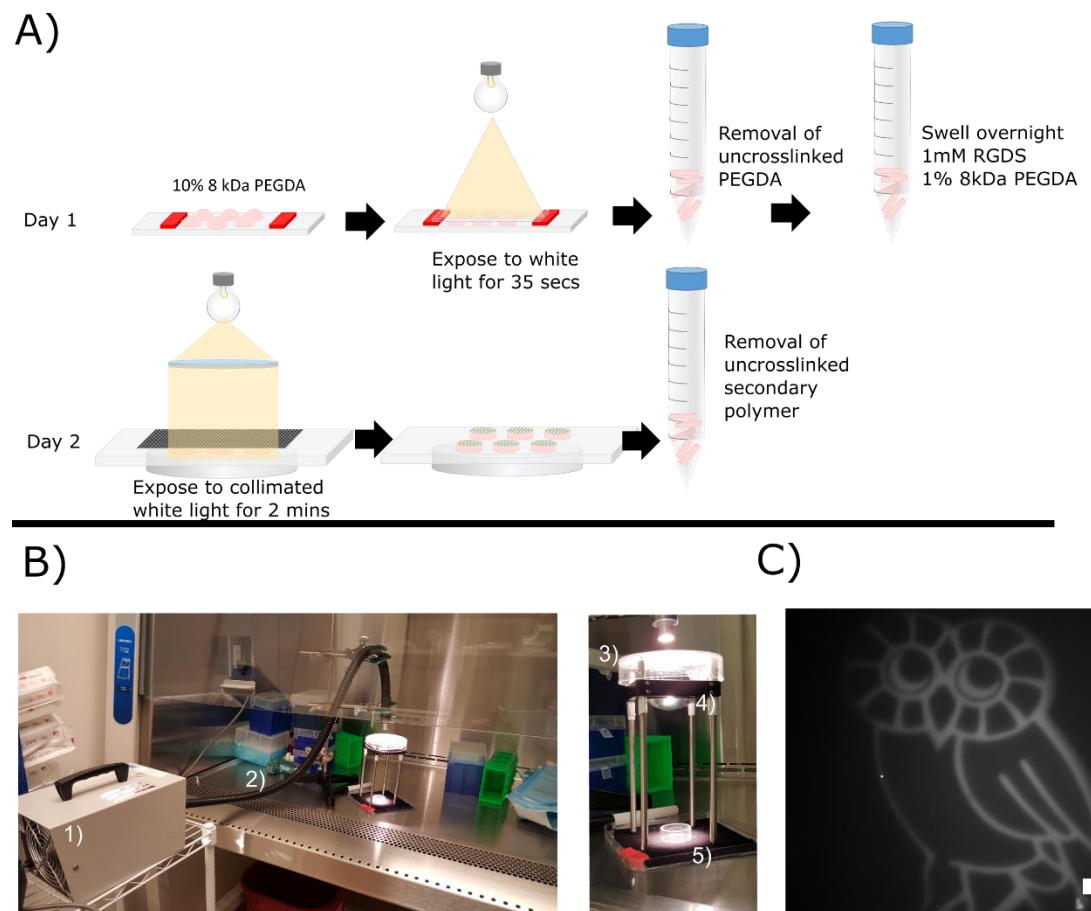


**Figure 6-2. A) Diagram of construction of patterned PEGDA hydrogels. B) Diagram of the sterile collimated light source. 1) Fiber optic light source. 2) Fiber optic cable. 3) Light diffuser. 4) 1.2 numerical aperture plano-convex collimating lens. 5) Light absorbing black flock velvet paper. C) Patterned Acryl-Rhodamine demonstrating pattern specificity. Scale bar represents 200  $\mu\text{m}$ .**

### 6.3.5. Seeding of VECs on syTLS

Cloning columns 6.8 mm in diameter were placed on top of the patterned hydrogels, and the exterior of the gels were flooded with EGM-2 media. The hydrogels were placed in a 37° incubator for 10 minutes. Next, 35,000 cells were seeded into the middle of the cloning columns. After 12 hours, the columns were removed, and the hydrogels were washed with EGM-2 to remove any non-adherent cells. Adhered cells were then cultured for 24 hours before further processing.

### 6.3.6. Quantification of Actin Alignment

After staining with F-actin, 100  $\mu\text{m}$  segments of each network patterns were cropped from Z-stacked confocal fluorescence microscopy images of each pattern as shown in Figure 6-6B. 12 segments were chosen randomly for each pattern from 3 independent gel constructions and VEC seedings. All analysis was done blindly in a single randomized batch. Actin alignment was quantified using a custom written Matlab script.<sup>215</sup>

### 6.3.7. Immunocytochemistry of syTLS

After 24 hours of culture, patterned cells were fixed in 4% v/v paraformaldehyde for 30 min, and permeabilized with 0.25% v/v Triton-X for 15 min at RT. Next, samples were blocked in PBS with 3.5% w/v bovine serum albumin (BSA) for 1 hour at RT. The samples were incubated with the primary antibodies shown in Table 6-1 at 1:100 in PBS and 0.35% w/v BSA overnight at 4 °C. Gels were then washed and incubated with fluorescent secondary antibodies at 1:100 for 1 hour at RT. After washing, samples were counterstained with DAPI and phalloidin for 20 minutes prior to mounting with fluoromount and imaging with confocal microscopy (Nikon A1-Rsi or Zeiss LSM 510).

**Table 6-1. Angiogenesis markers of interest investigated on the syTLS**

Antibody Target	Function
CD31 <sup>a</sup>	VEC Marker
Perlecan <sup>a</sup>	Basement Membrane Proteoglycan
VEGR2	Proangiogenesis Marker
N-Cadherin	AKT activation Marker
Dll4	Tip Cell Designation Marker
pAKT	Proangiogenesis Marker
pMAPK	Proangiogenesis Marker
pMLC	ROCK Activation Marker
B-Catenin	Wnt Signaling Marker

## 6.4. Results

### 6.4.1. Two Stage Photolithography Can Reliably and Repeatedly Produce Highly Specific Patterns of Varied Lacunarity

Previous studies have demonstrated the capacity to pattern hydrogels using photolithography<sup>210</sup>. Several of these studies have investigated changes in endothelial morphogenesis as a function of several variables such as pattern thickness, adhesiveness, adhesion moiety, and attachment chemistry. The work in this aim builds on the understanding from these past studies as well as other VEC hydrogel studies from our lab<sup>159</sup> to understand the effects of higher order spatial changes in the local microenvironment on valvular endothelial cell tubule morphogenesis, angiogenic marker expression, and actin regulation.

As demonstrated by Figure 6-3, the method used in this study is not limited to repeated geometric shapes. Although the theoretical feature resolution limit is 10  $\mu\text{m}$  due to resolution limits in printing the photomask, in practice the resolution in which the cells will remain true to the pattern is larger than the optical limit. This cellular limit is due in part to the ability of cells to stretch across gaps and chasms when their local environment instructs them to do so. This effect can be appreciated in Figure 6-5B where VECs can be seen rounding out the corners of the triangle pattern as the cells tighten into the rounded tubule shape.



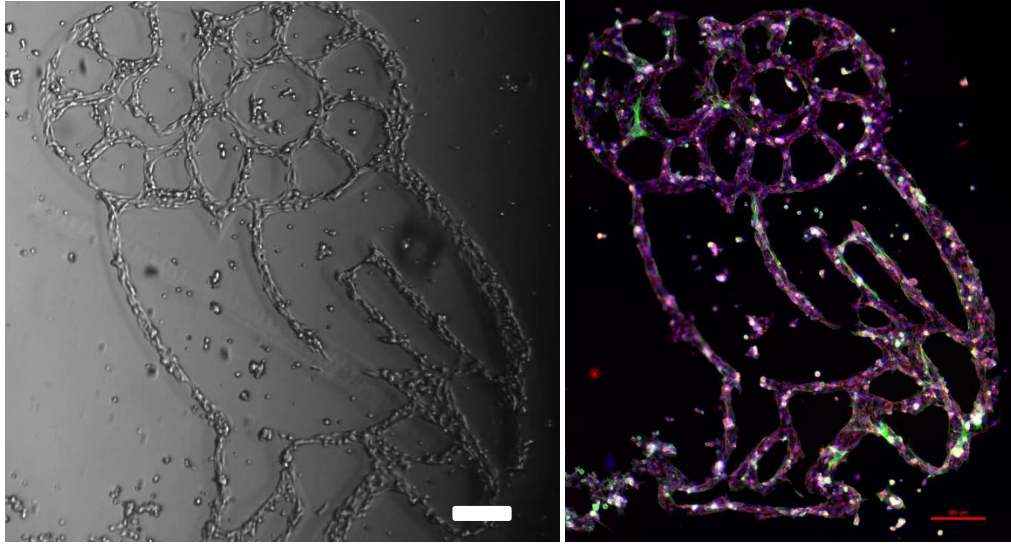


**Figure 6-3.** Representative images of the pattern specificity capable with the syTLS method imaged in phase contrast (left) and after staining with ICC (right) for CD 31(red), vimentin (purple), phalloidin (green), and DAPI. Addition of 1% PEGDA in the secondary solution allows for channel creation appreciable in the phase contrast image on the left which leads to increased pattern specificity. Scale bars represent 200  $\mu\text{m}$ .

In order to compare the effects of changing the spatial microenvironment by patterning different geometric shapes on endothelial cell morphogenesis, it was important to ensure that the only variable between groups was the pattern themselves. In order to ensure this, each batch of syTLS were created from the same batch of base gels and from the same formulation of secondary solution. As each pattern is swollen with the same secondary polymer formulation, the final ligand concentration per area was held constant as all cross linking was performed along a single plane and would not saturate at the given parameters<sup>159210</sup>. As demonstrated in Figure 6-4, no significant differences were measured between the widths of the tubules that the VECs produced on each pattern.

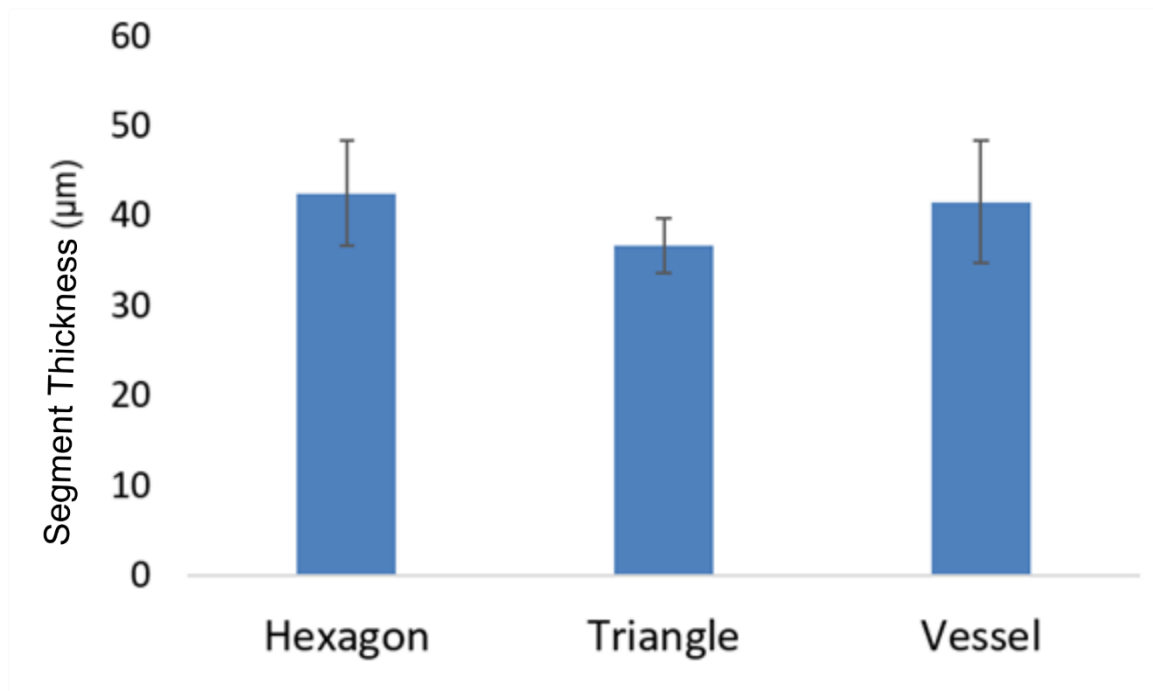
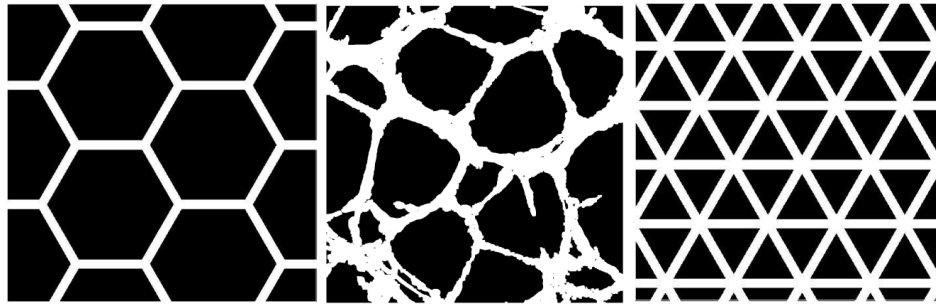


**Figure 6-4. Quantification of syTLS pattern edge thickness as a function of pattern. No significant difference was measured between the thicknesses of 12 randomly chosen VEC tubule segments for each condition. Data is displayed as the mean thickness  $\pm$  the standard deviation.**

As demonstrated in Figure 6-5A, automated image analysis of the three patterns confirmed that the lacunarity decreased as a function of the average sizes of the gaps in each pattern with the hexagon lacunarity being greater than the vessel-mimicking pattern and triangle lacunarity being less than that of the vessel pattern. As shown in Figure 6-5B, VECs demonstrated strong specificity to the patterned areas, although some non-specific adherence to non-patterned regions can be found in each pattern. Interestingly, smooth VEC tubule transitions from pattern vertex to segment can be appreciated in the 40x images, similar to the MCEC tubules formed in chapter 3 and demonstrated in Figure 3-10, suggesting that entrapment of VECs in the 3D tubule arrangement in the syTLS promotes a more angiogenic prone phenotype.

A)



D = 1.917

D = 1.877

D = 1.78

B)

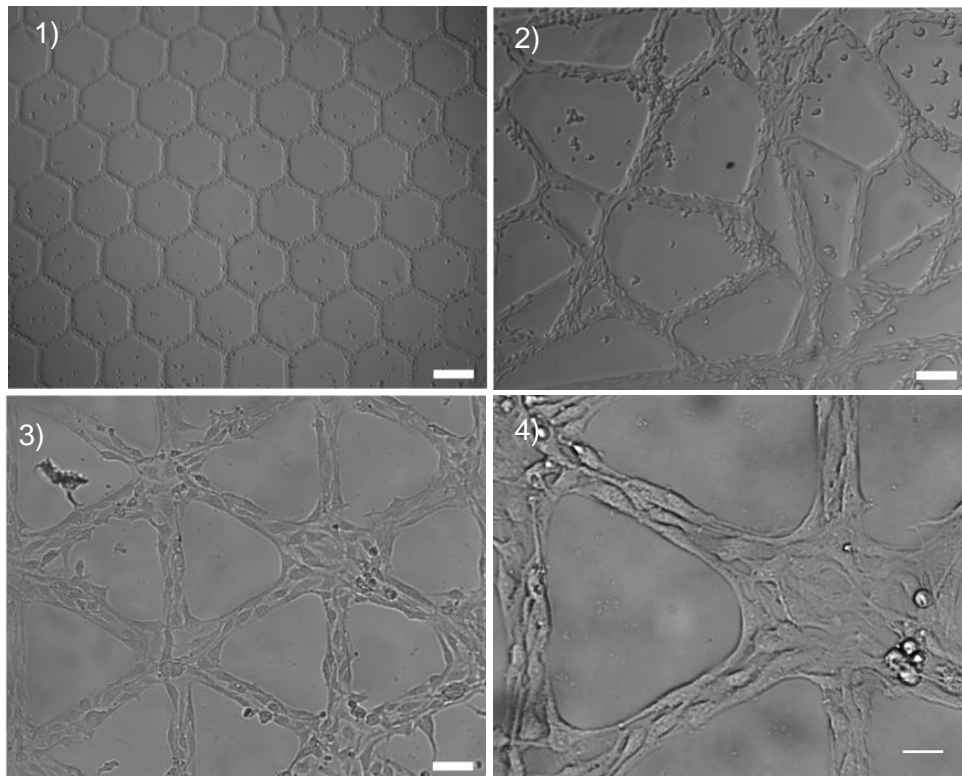


**Figure 6-5. A) Quantification of varied lacunarity (represented as D) patterns used for patterning of syTLS. B) Representative images of VECs patterned in syTLS imaged with DIC at 1) 4x, 2) 10x, 3) 20x, and 4) 40x images. Scale bars represent 250, 100, 50, and 25  $\mu\text{m}$ . Although some non specific adherence to non-patterned regions can be found in each pattern, VECs demonstrate strong specificity to the patterned areas. The 40x image in panel D shows the rounded appearance of tubule borders at the vertices.**

#### 6.4.2. Altering Lacunarity Alone is Enough to Alter Tubule Actin Alignment

As demonstrated by Figure 6-6A, altering the syTLS pattern was sufficient to cause gross changes in endothelial cell tubule-like-structure shape and actin alignment in a manner that resembled the pharmacological studies of Specific Aim 1 (Figure 3-3 through Figure 3-6). The hexagon-seeded VECs demonstrated a rounded phenotype with few cells that demonstrated organized actin alignment along the pattern segments similar to higher levels of Rac-inhibited VECs in Figure 3-4. The vessel-mimicking syTLS seeded VECs demonstrated greater actin alignment along each pattern edge and through each vertex similar to control TLS structures in Figure 3-6. VECs seeded in the triangle pattern mimicked the actin alignment of ROCK-inhibited VEC TLS networks, demonstrating reduced actin alignment along network edges compared to the vessel pattern and unorganized actin at the vertexes. As demonstrated in Figure 6-6, differences in actin alignment were measured between each pattern's segments.

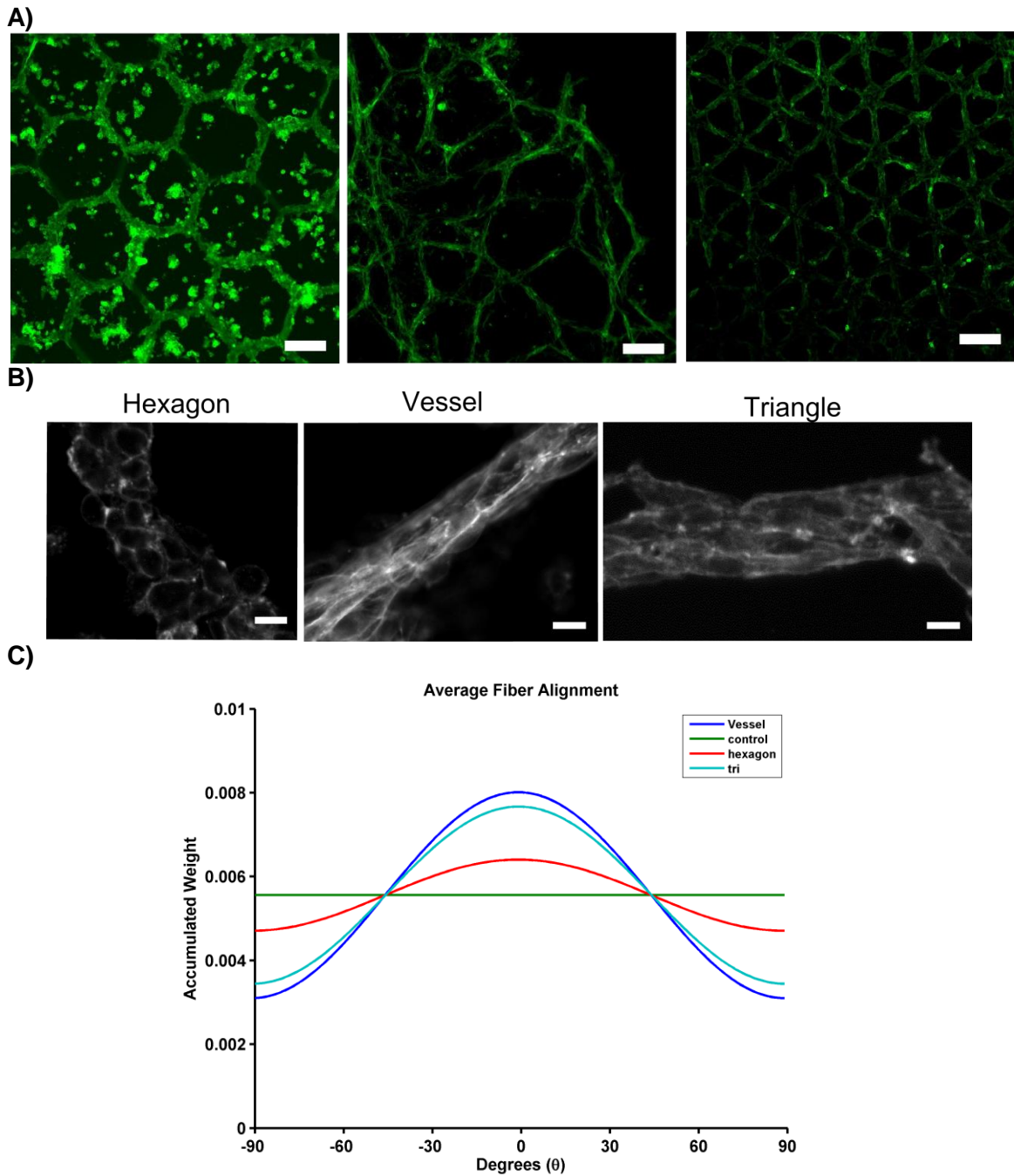


**Figure 6-6. A) Representative images of changes in phalloidin (green) staining as a function of pattern. VECs patterned in the hexagon pattern demonstrated a more rounded phenotype, while vessel-mimicking patterned VECs appeared the most aligned. Scale bars represent 200  $\mu\text{m}$ . B) Representative images of actin fibers as a function of syTLS pattern. Cells seeded on the hexagon patterns appeared rounded whereas the cells seeded on the vessel-mimicking appeared to**

be the most aligned. Scale bars represent 10  $\mu\text{m}$ . C) Quantification of the distribution of fiber alignment as a function of syTLS pattern demonstrating differences in the fiber alignment as a function of pattern.

#### 6.4.3. CD31, aSMA, VEGFR2, Perlecan, N-Cadherin, Dll4 Display Pattern Independent Expression

VECs cultured for 24 hours on the syTLS maintained their endothelial markers throughout the study period. Expression of CD31, VEGFR2, perlecan, N-cadherin, or Dll4 did not appear to change in amount or localization during the 24 hour time period. As demonstrated by Figure 6-7, VECs maintained strong cell-cell expression of CD31 in each tested. Unlike in the Matrigel TLS described in Chapter 3 and 4, no network contraction was observed in any of the patterns after 24 hours of culture. Given that there was limited to no expression of aSMA in each pattern, the syTLS approach appeared to promote VEC organization without induction of EndMT. As demonstrated by Figure 6-8, within 24 hours of seeding, VECs on all patterns began producing basement membrane proteins as demonstrated by strong staining of perlecan in each condition.

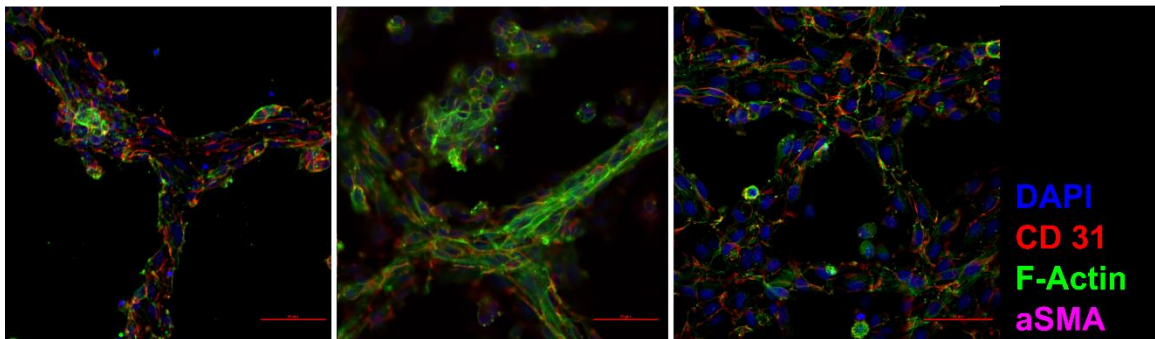


**Figure 6-7.** All cells demonstrated strong cell-cell staining for CD 31 (Red) and little to no staining for aSMA (purple) . Scale bars represent 50  $\mu\text{m}$ .

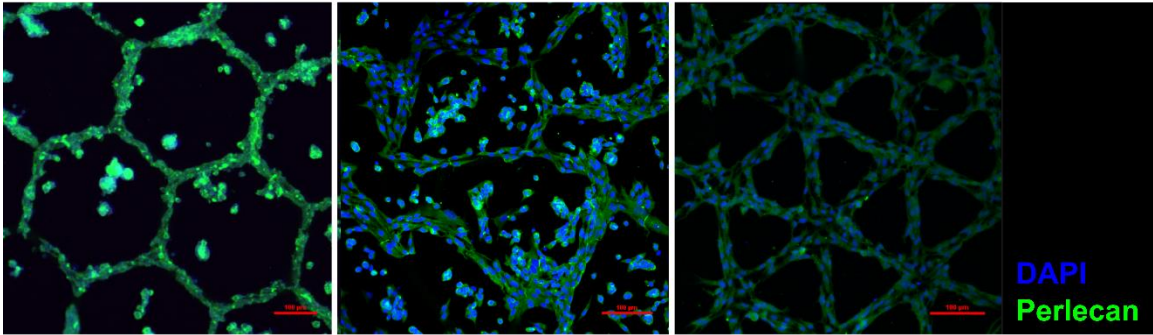
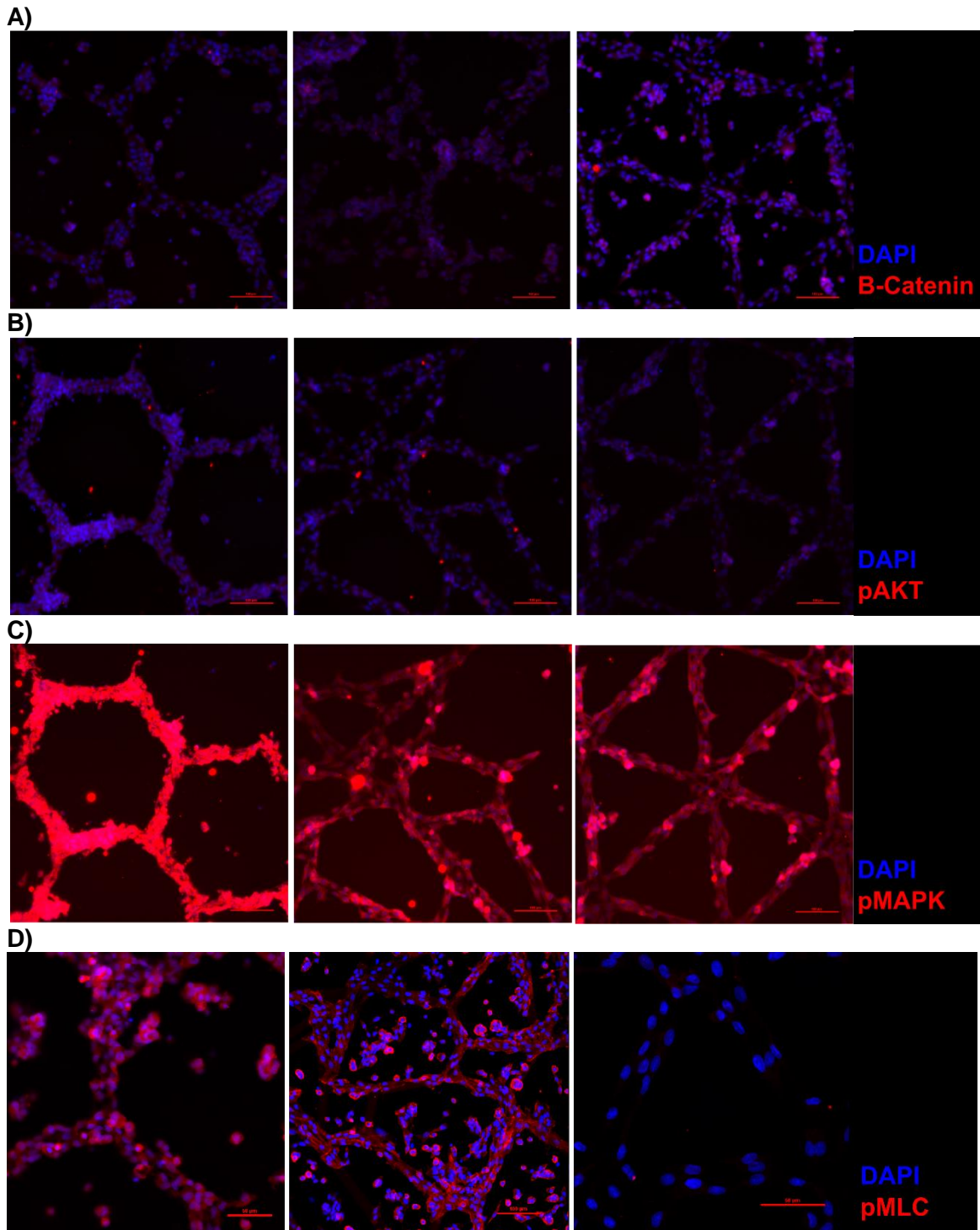


**Figure 6-8.** Within 24 hours of seeding, VECs on all patterns begun producing basement membrane proteins as demonstrated by strong staining of perlecan in each condition. Scale bars represent 100  $\mu$ m.

**6.4.4. VECs demonstrate active perception of their environment by displaying pattern-specific differences in their expressions of  $\beta$ -Catenin, pAKT, pMAPK, and pMLC**

As demonstrated in Figure 6-9,  $\beta$ -Catenin expression was strongest in the triangle pattern with no differences between the hexagon and vessel patterns. pAKT staining appeared stronger in the hexagon and triangle patterns compared to the vessel mimicking patterns. pMAPK stained strongest in the hexagon pattern, while both the vessel and triangle patterns demonstrated similar levels of pMAPK. VEC pMLC expression correlated with lacunarity of resultant syTLS. This pattern of a decrease in pMLC expression as a function of decreasing lacunarity aligns with the pattern in Figure 3-3, which previously demonstrated a decrease in the lacunarity of VEC TLS networks as a function of increased ROCK inhibition (decreased pMLC activity). A summary of the changes in actin regulators is shown in Table 6-2.





mimicking patterns. C) pMAPK stained strongest in the hexagon pattern, while both the vessel and triangle patterns demonstrated similar levels of pMAPK. D) VEC pMLC expression correlated with lacunarity of resultant syTLS. Scale bars represent 100  $\mu\text{m}$  in A-C and the middle panel of D. Scale bars represent 50  $\mu\text{m}$  in the remaining panels in D.

**Table 6-2: Compilation of changes in expression of actin and angiogenesis regulators relative to the vessel pattern.**

Marker	Hexagon	Triangle
<b>B-Catenin</b>	—	↑
<b>pAKT</b>	↑	—
<b>pMAPK</b>	↑	—
<b>pMLC</b>	↑	↓

## 6.5. Discussion

The formation of a physiological microvascular system requires precise coordination between cells and their environment to produce vastly complex functional networks. A fundamental question remaining in tissue engineering is the amount of biological complexity necessary to be recreated by the tissue engineer for proper long term biological functionality. Since prior work in this thesis had identified that the geometric complexity of a network of VECs in an *in vitro* angiogenesis model can be tuned with small molecule inhibitors of actin regulators, this study cultured VECs in a synthetic TLS hydrogel assay with predefined spatial arrangements as a framework to examine the fundamental relationship between network structure and VEC biology. In this study, controlling the geometric pattern of VEC networks mimicked changes in signaling previously observed in angiogenesis models with VECs.

Several studies have investigated the effects of endothelial morphogenesis as a function of patterned surfaces. These studies have reported difference in endothelial cell morphogenesis as a function of time, pattern width, adhesive ligand concentration, or growth factor composition on the behavior of non-valvular endothelial cells patterned on top of hydrogels<sup>210,211</sup>. This study built on these prior studies and techniques to produce highly specific synthetic vascular networks. Similar to these prior studies, entrapment of the VECs in confined patterns promoted the formation of aligned tubule

like structures as shown in Figure 6-6. In comparison, VECs seeded on non-patterned hydrogels simply grew to confluency.<sup>213</sup> Novel to this study was the variable of the lacunarity of the pattern of the synthetic vascular network. Surprisingly, seeding VECs on different lacunarity patterns was sufficient to promote significant differences in endothelial cell morphogenesis. In this study, simply increasing the complexity of the pattern did not produce more aligned cells. The vessel mimicking patterns demonstrated the most aligned actin and lumen formation compared to the higher lacunarity hexagon and the lower lacunarity triangle syTLS patterns, while still demonstrating activation of all of the necessary angiogenesis and actin regulators found in Table 6-2. These results suggest that there are functional biological reasons for engineering biomimetic patterns into tissue engineered constructs although the question of the required threshold of mimicry remains.

Interestingly, no significant changes in endothelial or EndMT markers were found in this study. This absence was surprising because VECs in the Matrigel model began network contraction into invasive spheroids by 24 hours in culture, and there were no signs of network contraction during this study. The lack of contraction could be explained by the lack of growth factors and ECM components found in the Matrigel model such as TGF- $\beta$  or perlecan. The lack of EnMT in the syTLS assay demonstrates that vasculogenic network organization by VECs in isolation does not signal VECs to undergo EnMT. However, it is still unknown if VECs can produce angiogenic invasions without partial EnMT. However, there are other tissue engineering methods that could be incorporated in the syTLS to investigate this fact further. One such future method could involve specific patterning of EnMT inducing growth factors such as TGF-  $\beta$  or other factors of the Matrigel such as perlecan, to investigate which combination of these signals is essential in driving VEC transformation into a pro-angiogenic invasive phenotype. Since periostin was found to be highly upregulated only in the highly invasive VEVIS co-culture and has been previously tied to neovascularization during CAVD<sup>45</sup>, another potentially significant future study would involve the patterning of periostin into a MMP-degradable<sup>213</sup> syTLS to provide direct causal evidence in its role in promoting 3D VEC angiogenic invasive phenotype. These studies would be able to answer the significant remaining question of whether VEC angiogenic invasion requires the preliminary activation of EnMT signals. Although the Matrigel model is a useful tool

in providing a potent complex mix of proangiogenic signals to endothelial cells, the complexity of these input signals makes it difficult to test any variable in isolation. Since any combination of these signals can be incorporated in any spatial arrangement into the syTLS demonstrates its strength as an *in vitro* platform to better understand VEC biology.

There remain several limitations of the use of the syTLS in this study. For one, most of the analysis done in this study is based off of immunocytochemistry staining. Although ICC allows for detailed actin morphological analysis, it is difficult to quantify any of the changes in the expression of the angiogenesis markers beyond general qualitative assessments. True quantification of these changes would require western blotting analysis of total protein harvesting from the entire hydrogel. However, the hydrogels designed in this study were not large enough to supply enough protein for such analysis. However, future versions of the syTLS design could be scaled up to allow for such detailed analysis.

## 6.6. Conclusion

Tissue engineering is a growing field with much promise, but many challenges and questions remain. As demonstrated by this work, vascular networks of varying complexity can be patterned into tissue engineered constructs, but the amount of biological complexity necessary for proper biological functionality was unclear. This study used VECs as framework to provide proof of principle insights to this question. This work found that the internal biology and morphogenesis of endothelial cells can be affected simply by their local spatial arrangement. Controlling the geometric pattern of VEC networks mimicked changes in signaling previously observed in angiogenesis models with VECs. These results suggest a more biomimetic vessel pattern in a tissue engineered valve would stimulate a more biomimetic and functional endothelial response. Addition of further valve-specific elements such as periostin or TGF- $\beta$  will enable further understanding of how valve cells translate angiogenic signals with greater specificity. The major novelty of this work stems from it being the first and only attempt to date at patterning VECs in specific patterns in order to better understand their response to angiogenic signaling. Novelty also extends to the tissue engineering field in

general in its attempt to better understand the effects of higher spatial arrangements of endothelial cells on their internal biology. Ultimately this work has implications for the creation of functional vasculature in pediatric TEHVs and of development of specific treatments for CAVD.

## Chapter 7

### Conclusion

This thesis detailed the characterization of the typical and atypical translation of several angiogenesis related signals by aortic valve cells. VEC angiogenic capacity was observed to be regulated by actin regulators similar to vascular endothelial cells, VICs acting in a pericyte manner, cyclic stretch, and side-specific origin. Lastly a PEGDA-based synthetic angiogenic assay was developed to characterize the geometric dependent regulation of the angiogenic capacity of VECs. The following section highlights the results found in the course of this thesis work and the conclusions drawn from these studies.

*VECs form complex vasculogenic networks tunable by small molecule ROCK and Rac inhibitors similar to vascular endothelial cells.*

Applying automated analytical tools for quantifying networks allowed for a detailed assessment of the biological response of valve endothelial cells to a model *in vitro* angiogenic model. VECs harvested from healthy aortic valves were found to form complex vasculogenic networks similar to vascular endothelial cells. Although these networks were quantitatively and morphologically different from the vascular endothelial networks, they were similarly tunable by ROCK and Rac inhibitors. These results suggest that VECs contain the inherent machinery to form functional neovascularization found during CAVD, but they require a specific mix of signals, atypical compared to vascular endothelial cells, in order to properly coordinate themselves into a functional vascular network. The novelty in this study derived from studying the factors that induce specifically isolated VECs from healthy aortic valves to undergo vasculogenic network

formation, direct analytical comparison to vascular derived endothelial cells, and demonstration of the tunable nature of VEC networks with small molecule inhibitors.

*Sustained co-culture of VICs in a model proangiogenic environment promote a pericyte-like phenotype that promotes angiogenic characteristics and invasion by VECs.*

With the knowledge that VECs could form complex vasculogenic networks similar to vascular endothelial cells and said networks were manipulable through similar methods of vascular endothelial cells, the pericyte capabilities of VICs were investigated. Initial studies with VEC and VIC co-cultures demonstrated the formation of VEVIS structures. Fluorescently tracking VECs and VICs over time revealed the pericyte-like behavior of VICs and the VIC dependent angiogenic-like behavior of VECs. Using a novel method to quantify the Lagrangian corrected chemoattraction of one cell type towards another in a mixed population, a subpopulation of VICs was identified and the degree of chemoattraction towards VECs was quantified. This method is not just limited to valve cell studies. The same methodology could be applied to any system requiring specific tracking of the interrelationships of multi-bodied system in 3D and over time such as performed in several cancer models. Surprisingly, the 3D sprouts formed by VEVIS were found to have several markers typical of *in vivo* angiogenic root sprouts, such as delta-like ligand 4 and  $\beta$ -catenin polarity. In addition, this study was the first to demonstrate the effect of partial EnMT, suggested to occur during CAVD, to induce VECs into a proangiogenic phenotype, suggesting that this transition is essential to the progression of CAVD. This study was the first to characterize this preprogrammed organization into VEVIS by any endothelial cells, let alone by valve cells, and comprehensively demonstrated their atypical behavior compared to vascular derived cells. Further novelty in this study stemmed from using valve endothelial cells and valve interstitial cells together, as many prior angiogenic-related valve studies have applied would apply valve specific elements, such as VIC co-culture or chondromodulin, in combination with non-valve derived endothelial cells. These results highlighted the importance of using VECs in any valve related research, since they translate many typical endothelial cells signals very differently from other vascular derived endothelial cells. Additionally innovation existed in demonstration of the importance of

Angiopoietin1-Tie2 signaling in regulating valve cell organization. This was the first study to demonstrate that valve cells produce these markers and are functionally affected by changing their activity. Ultimately, this work found that a change in phenotype to an invasive sprouting spheroid by valve cells, which suggests that both cell types undergo phenotypic changes during long-term culture in the model angiogenic environment to a more proangiogenic phenotype. This study also contributed to the growing understanding of valve cell biology and addressed the questions of how a sustained pro-angiogenic environment in the aortic valve could lead to an atypical translation of angiogenetic signaling in valve cells, thus enabling angiogenic invasion of the valve through coordinated valve cell behavior. This increase in angiogenic invasion, in turn, would contribute to the pathology of CAVD through increased inflammatory infiltrates and blood flow to the normally avascular adult aortic valve.

*Cyclic strain regulates VEC angiogenic capacity independent of Piezo1.*

Mechanical cyclic strain is known to be an important regulator of valve endothelial cells biology with strong ties to direct causes of valve calcification. This work expanded on the current understanding of valve endothelial cell biology, by demonstrating that cyclic uniaxial strain modulates VEC network formation, that VEC side specificity influences their inherent angiogenic capacity, and that there is a stretch independent role of Piezo1 in regulating VEC network formation. These results indicate that the cyclically stretching nature of the valve directly contributes to its avascularity. In addition, areas of stress shielding, such as regions near calcified nodules by CAVD, are more prone to worsening disease conditions through increased angiogenesis. The novelty of this study stemmed from quantifying the significant functional effect of cyclic stretch on VECs in the context of angiogenesis. In addition, this study was the first to identify the presence of Piezo1 in VECs and its role in regulating VEC network formation. The results of this study provided an explanation to a pervasive question of the side specific differences of the localization of calcification and neovascularization found during CAVD, suggesting that the greatest increase in oxygen transport to an internal calcific nodule would be more likely to come from back side neovascular invasion into the valve. These results therefore suggest a means for the targeting of ventricularis

VECs by taking advantage of their unique translation of angiogenic signals and mechanical environment in the development of interventional treatments for CAVD.

*Network geometry alone is sufficient to regulate the angiogenic phenotype of VECs.*

This study used VECs as a framework to examine this fundamental relationship between network structure and endothelial cell biology to provide proof of principle evidence that the internal signaling biology of endothelial cells could be tuned based upon culture in a spatially defined network. PEGDA hydrogels were then patterned into varied lacunarity patterns to create a model synthetic *in vitro* angiogenesis assay. When VECs were seeded on these patterns, notable differences in several angiogenesis related markers were found as function of the pattern where the cells were seeded. These changes included several markers for actin activity regulators as well as significant changes in actin alignment, whereas some notable angiogenesis markers showed no change. Controlling the geometric pattern of VEC networks mimicked changes in signaling previously observed in chapter 3. A vessel-mimicking pattern demonstrated the most aligned actin and lumen formation compared to the higher lacunarity hexagon and the lower lacunarity triangle syTLS patterns while demonstrating activation of all of the investigated angiogenesis and actin regulators. The major innovation of this work stems from it being the first and only attempt to date at patterning VECs in specific patterns in order to better understand their response to angiogenic signaling. Novelty also includes the use of tissue engineering tools in general in an attempt to better understand the effects of higher spatial arrangements of endothelial cells on their internal biology. In applying these results to the more fundamental question behind this Specific Aim 4, they suggest there are functional biological reasons for engineering biomimetic patterns into tissue engineered constructs although the question of the required threshold of mimicry remains. Therefore, the success of the design shows great potential as a platform to investigate both vascular and valvular endothelial biology and strategies necessary in future tissue engineering constructs.

In summary throughout this work, valve cells translated angiogenic stimuli typically and atypically in several ways. The typical behavior of valve cells compared to



vascular and previously studied pericyte-like cells included the formation of complex vasculogenic networks by VECs, susceptibility of those networks' formation to be inhibited by Rac inhibitors, and the increase junction density of VEC networks when treated with ROCK inhibitors. Inhibition of migration and proliferation were also tunable with ROCK and Rac inhibitors similar to prior work with vascular derived endothelial cells. The important role of the Ang-Tie2 pathway in VEC network formation and in VIC pericyte-like behavior was also discovered as a typical feature similar to vascular derived cells. This pathway was also traced to signal through the AKT molecule as it is traditionally described to be. Other typical pericyte-like behavior of VICs included wrapping around VEC tubule like structures and VEC invasive sprouts, production of Ang1, chemoattraction to and of VECs, and support of sustained VEC angiogenic-like invasive behavior. Silencing of Piezo1 was also found to have a similar effect in the static cultures compared to reports of vascular endothelial cells. Lastly, the formation of tubule like structures on the synthetic TLS compared to flat PEGDA gels was similar to prior reports of endothelial cells where entrapment of the endothelial cells encouraged endothelial tubule morphogenesis. Several atypical valve cell behaviors in response to angiogenic signals was also discovered in this work. For one, morphological and numerical differences in basal VEC network formation were found compared to vascular derived cells. Valve cell co-culture lead to a time dependent collapse of VEC network formation compared to the network stabilization that was found when culturing vascular and pericyte mimetic cells. The most unique valve cell behavior discovered in this work was the formation of the VEVIS during long term co-culture as no other endothelial cell was identified to have the same behavior. Better understanding of this unique phenotype could lead to a potential valve specific pathway to be targeted pharmacologically as an interventional treatment for CAVD. Lastly, cyclic stretch was found to inhibit network formation while previously it had been found to promote angiogenesis in vascular endothelial cells; however, the reason for this contrasting behavior was not identified in this work.

In total, this thesis creates a compelling argument for the capabilities of VECs as a potential source of the neovascularization found during CAVD. However, there remains several future studies that could improve our understanding of VEC angiogenic capacity. A crucial angiogenic process that has remained unstudied in this context of

valve cells is lumen formation. Although VECs were promoted to form 3D mimicking angiogenic sprouts, and aligned actin structures, in this study, VECs have yet to be demonstrated to be able to form functional lumens nor microvasculature. *In vitro* microfluidic devices as described previously have demonstrated the ability create functional microvasculature *in vitro*.<sup>181</sup> These devices are able to expose a tube of endothelial cells to shear and growth factor gradients sufficient to induce functional lumen formation between channels. Applying these devices to valve biology would be able to definitively answer the question of the functional angiogenic capacity of VECs. Patterning of valve specific elements such as chondromodulin, periostin, TGF- $\beta$  into a MMP-degradable PEGDA hydrogel core would allow for definitive expansion of our current understanding of VEC angiogenic related biology. Although the original construction of these devices would require complex microphotolithography techniques for fabrication, preliminary work has demonstrated the ability to recreate prior designs by molding PDMS around 3D printed masters. Another pathway for future study not previously discussed would be the further adaption of DsiRNA treatment of VECs and VICs as in chapter 5. For example, silencing the expression of DLL4 or its receptor NOTCH in either VECs or VICs in the Matrigel model from chapter 4 would help elucidate the role of this signaling system in deciding tip cell fate designation similar to work done in the vascular endothelial field. Thus in general, future studies can build from the insights and methods described in detail in this thesis to enhance understanding of the role of the translation of angiogenic signals by valve cells to the pathobiology of CAVD.

The overall impact of this thesis can be summarized by: (1) the basal characterization of VEC vasculogenic networks, (2) demonstration of the pericyte-like behavior of VICs, (3) demonstration of the antiangiogenic effect of cyclic stretch on VECs, and (4) the design and implementation of a synthetic PEGDA based *in vitro* angiogenesis assay to investigate the geometric dependent changes in VEC angiogenic potential as a function of pattern complexity.

## References

1. Hinton, R. B. & Yutzey, K. E. Heart valve structure and function in development and disease. *Annu. Rev. Physiol.* **73**, 29–46 (2011).
2. Mendelson, K. & Schoen, F. J. Heart valve tissue engineering: concepts, approaches, progress, and challenges. *Ann. Biomed. Eng.* **34**, 1799–819 (2006).
3. Sacks, M. S., Schoen, F. J. & Mayer, Jr., J. E. Bioengineering challenges for heart valve tissue engineering. *Annu. Rev. Biomed. Eng.* **11**, 289–313 (2009).
4. Butcher, J. T. *et al.* Transcriptional profiles of valvular and vascular endothelial cells reveal phenotypic differences: influence of shear stress. *Arterioscler. Thromb. Vasc. Biol.* **26**, 69–77 (2006).
5. Kalluri, R. Basement membranes: structure, assembly and role in tumour angiogenesis. *Nat. Rev. Cancer* **3**, 422–33 (2003).
6. Yacoub, M. H. & Cohn, L. H. Novel approaches to cardiac valve repair: from structure to function: Part I. *Circulation* **109**, 942–50 (2004).
7. Duran, C. M. & Gunning, A. J. The vascularization of the heart valves: a comparative study. *Cardiovasc. Res.* **2**, 290–6 (1968).
8. Taylor, P. M., Batten, P., Brand, N. J., Thomas, P. S. & Yacoub, M. H. The cardiac valve interstitial cell. *Int. J. Biochem. Cell Biol.* **35**, 113–8 (2003).
9. Liu, A. C., Joag, V. R. & Gotlieb, A. I. The emerging role of valve interstitial cell phenotypes in regulating heart valve pathobiology. *Am. J. Pathol.* **171**, 1407–18 (2007).
10. Paranya, G. *et al.* Aortic valve endothelial cells undergo transforming growth factor-beta-mediated and non-transforming growth factor-beta-mediated transdifferentiation in vitro. *Am. J. Pathol.* **159**, 1335–43 (2001).
11. Yoshioka, M. *et al.* Chondromodulin-I maintains cardiac valvular function by preventing angiogenesis. *Nat. Med.* **12**, 1151–9 (2006).

12. Skowasch, D. *et al.* Cells of primarily extra-valvular origin in degenerative aortic valves and bioprostheses. *Eur. Heart J.* **26**, 2576–80 (2005).
13. Yip, C. Y. Y. & Simmons, C. A. The aortic valve microenvironment and its role in calcific aortic valve disease. *Cardiovasc. Pathol.* **20**, 177–82 (2011).
14. Rajamannan, N. M. *et al.* Calcified rheumatic valve neoangiogenesis is associated with vascular endothelial growth factor expression and osteoblast-like bone formation. *Circulation* **111**, 3296–301 (2005).
15. Rajamannan, N. M. *et al.* Human aortic valve calcification is associated with an osteoblast phenotype. *Circulation* **107**, 2181–4 (2003).
16. Cheung, W.-Y., Young, E. W. K. & Simmons, C. A. Techniques for isolating and purifying porcine aortic valve endothelial cells. *J. Heart Valve Dis.* **17**, 674–81 (2008).
17. El-Hamamsy, I. *et al.* Endothelium-dependent regulation of the mechanical properties of aortic valve cusps. *J. Am. Coll. Cardiol.* **53**, 1448–55 (2009).
18. Xu, S., Liu, A. C. & Gotlieb, A. I. Common pathogenic features of atherosclerosis and calcific aortic stenosis: role of transforming growth factor-beta. *Cardiovasc. Pathol.* **19**, 236–47 (2010).
19. Davies, P. F., Passerini, A. G. & Simmons, C. a. Aortic valve: turning over a new leaf(let) in endothelial phenotypic heterogeneity. *Arterioscler. Thromb. Vasc. Biol.* **24**, 1331–3 (2004).
20. Simmons, C. a, Grant, G. R., Manduchi, E. & Davies, P. F. Spatial heterogeneity of endothelial phenotypes correlates with side-specific vulnerability to calcification in normal porcine aortic valves. *Circ. Res.* **96**, 792–9 (2005).
21. Butcher, J. T., Penrod, A. M., García, A. J. & Nerem, R. M. Unique morphology and focal adhesion development of valvular endothelial cells in static and fluid flow environments. *Arterioscler. Thromb. Vasc. Biol.* **24**, 1429–34 (2004).
22. Chalajour, F. *et al.* Angiogenic activation of valvular endothelial cells in aortic valve stenosis. *Exp. Cell Res.* **298**, 455–64 (2004).
23. Mariscalco, G. *et al.* Imbalance between pro-angiogenic and anti-angiogenic factors in rheumatic and mixomatous mitral valves. *Int. J. Cardiol.* **152**, 337–44

(2011).

24. Roger, V. L. *et al.* Heart disease and stroke statistics--2012 update: a report from the American Heart Association. *Circulation* **125**, e2–e220 (2012).
25. Rajamannan, N. M., Gersh, B. & Bonow, R. O. Calcific aortic stenosis: from bench to the bedside--emerging clinical and cellular concepts. *Heart* **89**, 801–5 (2003).
26. Nathaniel, S., Saligram, S. & Innasimuthu, A. L. Aortic stenosis: An update. *World J. Cardiol.* **2**, 135–9 (2010).
27. Otto, C. M. Valvular aortic stenosis: disease severity and timing of intervention. *J. Am. Coll. Cardiol.* **47**, 2141–51 (2006).
28. HoffmanJIE, K. S. Theincidence of congenital heart disease. *J. Am.Coll. Cardiol.* **39**, 1890–900 (2002).
29. Costell, M. Hyperplastic Conotruncal Endocardial Cushions and Transposition of Great Arteries in Perlecan-Null Mice. *Circ. Res.* **91**, 158–164 (2002).
30. Rahimtoola, S. H. Choice of prosthetic heart valve for adult patients. *J. Am. Coll. Cardiol.* **41**, 893–904 (2003).
31. Jamieson, W. R. E. *et al.* Performance of bioprostheses and mechanical prostheses assessed by composites of valve-related complications to 15 years after mitral valve replacement. *J. Thorac. Cardiovasc. Surg.* **129**, 1301–8 (2005).
32. American Heart Association, Heart Disease and Stroke Statistics—2004 Update. *Am. Hear. Assoc.* (2004).
33. Mohler, III, E. R. Mechanisms of aortic valve calcification. *Am. J. Cardiol.* **94**, 1396–402, A6 (2004).
34. Stewart, B. F. *et al.* Clinical factors associated with calcific aortic valve disease. Cardiovascular Health Study. *J. Am. Coll. Cardiol.* **29**, 630–4 (1997).
35. Aronow, W. S., Ahn, C., Kronzon, I. & Goldman, M. E. Association of coronary risk factors and use of statins with progression of mild valvular aortic stenosis in older persons. *Am. J. Cardiol.* **88**, 693–5 (2001).

36. Mu, A. M. *et al.* Expression of endothelial cell adhesion molecules on heart valves : up-regulation in degeneration as well as acute endocarditis. *J. Pathol.* **1**, 54–60 (2000).
37. Syväranta, S. *et al.* Vascular endothelial growth factor-secreting mast cells and myofibroblasts: a novel self-perpetuating angiogenic pathway in aortic valve stenosis. *Arterioscler. Thromb. Vasc. Biol.* **30**, 1220–7 (2010).
38. Mazzone, A. *et al.* Neoangiogenesis, T-lymphocyte infiltration, and heat shock protein-60 are biological hallmarks of an immunomediated inflammatory process in end-stage calcified aortic valve stenosis. *J. Am. Coll. Cardiol.* **43**, 1670–6 (2004).
39. Mahler, G. J. & Butcher, J. T. Inflammatory regulation of valvular remodeling: the good(?), the bad, and the ugly. *Int. J. Inflam.* **2011**, 721419 (2011).
40. Chalajour, F. *et al.* Identification and characterization of cells with high angiogenic potential and transitional phenotype in calcific aortic valve. *Exp. Cell Res.* **313**, 2326–35 (2007).
41. Soini, Y., Salo, T. & Satta, J. Angiogenesis is involved in the pathogenesis of nonrheumatic aortic valve stenosis. *Hum. Pathol.* **34**, 756–63 (2003).
42. Poggio, P. *et al.* Osteopontin controls endothelial cell migration in vitro and in excised human valvular tissue from patients with calcific aortic stenosis and controls. *J. Cell. Physiol.* **226**, 2139–49 (2011).
43. Charest, a *et al.* Distribution of SPARC during neovascularisation of degenerative aortic stenosis. *Heart* **92**, 1844–9 (2006).
44. Chalajour, F. *et al.* Angiogenic activation of valvular endothelial cells in aortic valve stenosis. *Exp. Cell Res.* **298**, 455–64 (2004).
45. Hakuno, D., Kimura, N. & Yoshioka, M. Periostin advances atherosclerotic and rheumatic cardiac valve degeneration by inducing angiogenesis and MMP production in humans and rodents. *J. Clin. Invest.* **120**, (2010).
46. Helske, S. *et al.* Induction of local angiotensin II-producing systems in stenotic aortic valves. *J. Am. Coll. Cardiol.* **44**, 1859–66 (2004).
47. Baker, M. *et al.* Use of the mouse aortic ring assay to study angiogenesis. *Nat.*

*Protoc.* **7**, 89–104 (2012).

48. Ergün, S. *et al.* CEA-related cell adhesion molecule 1: a potent angiogenic factor and a major effector of vascular endothelial growth factor. *Mol. Cell* **5**, 311–20 (2000).
49. Arnaoutova, I. & Kleinman, H. K. In vitro angiogenesis: endothelial cell tube formation on gelled basement membrane extract. *Nat. Protoc.* **5**, 628–35 (2010).
50. Paruchuri, S. *et al.* Human pulmonary valve progenitor cells exhibit endothelial/mesenchymal plasticity in response to vascular endothelial growth factor-A and transforming growth factor-beta2. *Circ. Res.* **99**, 861–9 (2006).
51. Collett, G. D. M. & Canfield, a E. Angiogenesis and pericytes in the initiation of ectopic calcification. *Circ. Res.* **96**, 930–8 (2005).
52. Orock, Z. K. Z., Mahfouz, R. a R., Makarem, J. a & Shamseddine, A. I. Understanding the biology of angiogenesis: review of the most important molecular mechanisms. *Blood Cells, Mol. ...* **39**, 212–20 (2007).
53. Sage, E. H. Pieces of eight: bioactive fragments of extracellular proteins as regulators of angiogenesis. *Trends Cell Biol.* **7**, 182–6 (1997).
54. Eming, S. A. & Hubbell, J. A. Extracellular matrix in angiogenesis: dynamic structures with translational potential. *Exp. Dermatol.* **20**, 605–13 (2011).
55. Stupack, D. G. & Cheresh, D. A. in (ed. Biology, B. T.-C. T. in D.) **Volume 64**, 207–238 (Academic Press, 2004).
56. Clark, R. A., Tonnesen, M. G., Gailit, J. & Cheresh, D. A. Transient functional expression of alphaVbeta 3 on vascular cells during wound repair. *Am. J. Pathol.* **148**, 1407–21 (1996).
57. Soldi, R. *et al.* Role of [alpha]v[beta]3 integrin in the activation of vascular endothelial growth factor receptor-2. *EMBO J* **18**, 882–892 (1999).
58. Eliceiri, B. P. Integrin and Growth Factor Receptor Crosstalk . *Circ. Res.* **89** , 1104–1110 (2001).
59. Hood, J. D., Frausto, R., Kiosses, W. B., Schwartz, M. A. & Cheresh, D. A.

- Differential  $\alpha$  integrin-mediated Ras-ERK signaling during two pathways of angiogenesis. *J. Cell Biol.* **162**, 933–943 (2003).
60. Zcharia, E. *et al.* Heparanase accelerates wound angiogenesis and wound healing in mouse and rat models. *FASEB J.* **19**, 211–221 (2005).
  61. Carmeliet, P. *et al.* Impaired myocardial angiogenesis and ischemic cardiomyopathy in mice lacking the vascular endothelial growth factor isoforms VEGF164 and VEGF188. *Nat. Med.* **5**, 495–502 (1999).
  62. Rini B.I., S. E. J. Biology and clinical development of vascular endothelial growth factor-targeted therapy in renal cell carcinoma. *J. Clin. Oncol.* **23**, 1028–1043 (2005).
  63. Tischer E., M. R. H. T. S. M. G. D. F. J. C. A. J. A. The human gene for vascular endothelial growth factor: Multiple protein forms are encoded through alternative exon splicing. *J. Biol. Chem.* **266**, 11947–11954 (1991).
  64. Neufeld G., C. T. G. S. P. Z. Vascular endothelial growth factor (VEGF) and its receptors. *FASEB J.* **13**, 9–22 (1999).
  65. Byrne, A. M., Bouchier-Hayes, D. J. & Harmey, J. H. Angiogenic and cell survival functions of Vascular Endothelial Growth Factor (VEGF). *J. Cell. Mol. Med.* **9**, 777–794 (2005).
  66. Ferrara N., G. H.-P. L. J., Ferrara, N., Gerber, H.-P. & LeCouter, J. The biology of VEGF and its receptors. *Nat. Med.* **9**, 669–76 (2003).
  67. Hiratsuka S., M. O. K. J. N. T. S. M. Flt-1 lacking the tyrosine kinase domain is sufficient for normal development and angiogenesis in mice. *Proc. Natl. Acad. Sci. U. S. A.* **95**, 9349–9354 (1998).
  68. Holmes, K., Roberts, O. L., Thomas, A. M. & Cross, M. J. Vascular endothelial growth factor receptor-2: structure, function, intracellular signalling and therapeutic inhibition. *Cell. Signal.* **19**, 2003–12 (2007).
  69. Takahashi T., U. H. S. M. VEGF activates protein kinase C-dependent, but Ras-independent Raf-MEK-MAP kinase pathway for DNA synthesis in primary endothelial cells. *Oncogene* **18**, 2221–2230 (1999).
  70. Meadows K.N., B. P. P. K. Vascular Endothelial Growth Factor Induction of the



- Angiogenic Phenotype Requires Ras Activation. *J. Biol. Chem.* **276**, 49289–49298 (2001).
71. Shu X., W. W. M. R. D. B. D. Sphingosine kinase mediates vascular endothelial growth factor-induced activation of ras and mitogen-activated protein kinases. *Mol. Cell. Biol.* **22**, 7758–7768 (2002).
  72. Gerber, H.-P. *et al.* Vascular Endothelial Growth Factor Regulates Endothelial Cell Survival through the Phosphatidylinositol 3'-Kinase/Akt Signal Transduction Pathway: REQUIREMENT FOR FIK-1/KDR ACTIVATION. *J. Biol. Chem.* **273**, 30336–30343 (1998).
  73. VANDENDRIESCHE, S., MUMMERY, C. & WESTERMANN, C. Hereditary hemorrhagic telangiectasia: an update on transforming growth factor  $\alpha$  signaling in vasculogenesis and angiogenesis. *Cardiovasc. Res.* **58**, 20–31 (2003).
  74. Carmeliet, P. Angiogenesis in health and disease. *Nat. Med.* **9**, 653–660 (2003).
  75. Willis, B. C. & Borok, Z. TGF-beta-induced EMT: mechanisms and implications for fibrotic lung disease. *Am. J. Physiol. Lung Cell. Mol. Physiol.* **293**, L525–34 (2007).
  76. Welch-Reardon, K. M., Wu, N. & Hughes, C. C. W. A Role for Partial Endothelial-Mesenchymal Transitions in Angiogenesis? *Arterioscler. Thromb. Vasc. Biol.* **35**, 303–8 (2014).
  77. Gerhardt, H. & Betsholtz, C. Endothelial-pericyte interactions in angiogenesis. *Cell Tissue Res.* **314**, 15–23 (2003).
  78. Armulik, A., Abramsson, A. & Betsholtz, C. Endothelial/pericyte interactions. *Circ. Res.* **97**, 512–23 (2005).
  79. Cuevas, P. *et al.* Pericyte endothelial gap junctions in human cerebral capillaries. *Anat. Embryol. (Berl)*. **170**, 155–9 (1984).
  80. Gerhardt, H., Wolburg, H. & Redies, C. N-cadherin mediates pericytic-endothelial interaction during brain angiogenesis in the chicken. *Dev. Dyn.* **218**, 472–479 (2000).
  81. Díaz-Flores, L., Gutiérrez, R., Varela, H., Rancel, N. & Valladares, F. Microvascular pericytes: a review of their morphological and functional

- characteristics. *Histol. Histopathol.* **6**, 269–86 (1991).
82. Courtoy, P. J. & Boyles, J. Fibronectin in the microvasculature: localization in the pericyte-endothelial interstitium. *J. Ultrastruct. Res.* **83**, 258–73 (1983).
  83. De Smet, F., Segura, I., De Bock, K., Hohensinner, P. J. & Carmeliet, P. Mechanisms of vessel branching: filopodia on endothelial tip cells lead the way. *Arterioscler. Thromb. Vasc. Biol.* **29**, 639–49 (2009).
  84. Hellstrom, M. *et al.* Dll4 signalling through Notch1 regulates formation of tip cells during angiogenesis. *Nature* **445**, 776–780 (2007).
  85. Roca, C. & Adams, R. H. Regulation of vascular morphogenesis by Notch signaling. *Genes Dev.* **21**, 2511–2524 (2007).
  86. van Hinsbergh, V. W. M. & Koolwijk, P. Endothelial sprouting and angiogenesis: matrix metalloproteinases in the lead. *Cardiovasc. Res.* **78**, 203–212 (2008).
  87. Yana, I. *et al.* Crosstalk between neovessels and mural cells directs the site-specific expression of MT1-MMP to endothelial tip cells. *J. Cell Sci.* **120**, 1607–1614 (2007).
  88. Murakami, M. *et al.* The FGF system has a key role in regulating vascular integrity. *J. Clin. Invest.* **118**, 3355–3366 (2008).
  89. Phng, L.-K. *et al.* Nrarp Coordinates Endothelial Notch and Wnt Signaling to Control Vessel Density in Angiogenesis. *Dev. Cell* **16**, 70–82 (2009).
  90. Yang, J., Wylie-Sears, J. & Bischoff, J. Opposing actions of Notch1 and VEGF in post-natal cardiac valve endothelial cells. **374**, 512–516 (2008).
  91. Lamalice, L., Le Boeuf, F. & Huot, J. Endothelial cell migration during angiogenesis. *Circ. Res.* **100**, 782–94 (2007).
  92. Huber, A. B., Kolodkin, A. L., Ginty, D. D. & Cloutier, J.-F. Signaling at the growth cone: ligand-receptor complexes and the control of axon growth and guidance. *Annu. Rev. Neurosci.* **26**, 509–63 (2003).
  93. Pollard, T. D. & Borisy, G. G. Cellular Motility Driven by Assembly and Disassembly of Actin Filaments. *Cell* **112**, 453–465 (2003).

94. Defilippi, P. *et al.* Actin cytoskeleton organization in response to integrin-mediated adhesion. *Microsc. Res. Tech.* **47**, 67–78 (1999).
95. Mitra, S. K., Hanson, D. A. & Schlaepfer, D. D. Focal adhesion kinase: in command and control of cell motility. *Nat Rev Mol Cell Biol* **6**, 56–68 (2005).
96. Virmani, R., Burke, A. P., Farb, A. & Kolodgie, F. D. Pathology of the Vulnerable Plaque. *J. Am. Coll. Cardiol.* **47**, C13–C18 (2006).
97. Ribatti, D., Levi-Schaffer, F. & Kovanen, P. T. Inflammatory angiogenesis in atherogenesis—a double-edged sword. *Ann. Med.* **40**, 606–621 (2008).
98. Kolodgie, F. D. *et al.* Elimination of Neoangiogenesis for Plaque Stabilization. Is There a Role for Local Drug Therapy? *J. Am. Coll. Cardiol.* **49**, 2093–2101 (2007).
99. Junmin Zhu. Bioactive Modification of Poly(ethylene glycol) Hydrogels for Tissue Engineering. **31**, 4639–4656 (2011).
100. Langer, R. & Vacanti, J. P. Tissue engineering. *Science* **260**, 920–6 (1993).
101. Temenoff, J. S. & Mikos, A. G. Injectable biodegradable materials for orthopedic tissue engineering. *Biomaterials* **21**, 2405–2412 (2000).
102. Hahn, M. S., McHale, M. K., Wang, E., Schmedlen, R. H. & West, J. L. Physiologic pulsatile flow bioreactor conditioning of poly(ethylene glycol)-based tissue engineered vascular grafts. *Ann. Biomed. Eng.* **35**, 190–200 (2007).
103. Buxton, A. N. *et al.* Design and characterization of poly(ethylene glycol) photopolymerizable semi-interpenetrating networks for chondrogenesis of human mesenchymal stem cells. *Tissue Eng.* **13**, 2549–60 (2007).
104. Nerem, R. M. & Seliktar, D. Vascular tissue engineering. *Annu. Rev. Biomed. Eng.* **3**, 225–43 (2001).
105. Drury, J. L. & Mooney, D. J. Hydrogels for tissue engineering: scaffold design variables and applications. *Biomaterials* **24**, 4337–4351 (2003).
106. Hersel, U., Dahmen, C. & Kessler, H. RGD modified polymers: biomaterials for

- stimulated cell adhesion and beyond. *Biomaterials* **24**, 4385–4415 (2003).
107. Badylak, S. F. The extracellular matrix as a biologic scaffold material. *Biomaterials* **28**, 3587–3593 (2007).
  108. Mann, B. K., Schmedlen, R. H. & West, J. L. Tethered-TGF- $\beta$  increases extracellular matrix production of vascular smooth muscle cells. *Biomaterials* **22**, 439–444 (2001).
  109. Leslie-Barbick, J. E., Moon, J. J. & West, J. L. Covalently-immobilized vascular endothelial growth factor promotes endothelial cell tubulogenesis in poly(ethylene glycol) diacrylate hydrogels. *J. Biomater. Sci. Polym. Ed.* **20**, 1763–79 (2009).
  110. DeLong, S. A., Moon, J. J. & West, J. L. Covalently immobilized gradients of bFGF on hydrogel scaffolds for directed cell migration. *Biomaterials* **26**, 3227–34 (2005).
  111. Saik, J. E., Gould, D. J., Keswani, A. H., Dickinson, M. E. & West, J. L. Biomimetic Hydrogels with Immobilized EphrinA1 for Therapeutic Angiogenesis. *Biomacromolecules* **12**, 2715–22 (2011).
  112. Gobin, A. S. & West, J. L. Effects of Epidermal Growth Factor on Fibroblast Migration through Biomimetic Hydrogels. *Biotechnol. Prog.* **19**, 1781–1785 (2003).
  113. Lee, S.-H., Moon, J. J. & West, J. L. Three-dimensional micropatterning of bioactive hydrogels via two-photon laser scanning photolithography for guided 3D cell migration. *Biomaterials* **29**, 2962–8 (2008).
  114. Leslie-Barbick, J. E., Saik, J. E., Gould, D. J., Dickinson, M. E. & West, J. L. The promotion of microvasculature formation in poly(ethylene glycol) diacrylate hydrogels by an immobilized VEGF-mimetic peptide. *Biomaterials* **32**, 5782–9 (2011).
  115. Saik, J. E., Gould, D. J., Watkins, E. M., Dickinson, M. E. & West, J. L. Covalently immobilized platelet-derived growth factor-BB promotes angiogenesis in biomimetic poly(ethylene glycol) hydrogels. *Acta Biomater.* **7**, 133–43 (2011).
  116. Saik, J. E., Gould, D. J., Keswani, A. H., Dickinson, M. E. & West, J. L. Biomimetic hydrogels with immobilized ephrinA1 for therapeutic angiogenesis. *Biomacromolecules* **12**, 2715–22 (2011).

117. Zhu, J., Tang, C., Kottke-Marchant, K. & Marchant, R. E. Design and synthesis of biomimetic hydrogel scaffolds with controlled organization of cyclic RGD peptides. *Bioconjug. Chem.* **20**, 333–9 (2009).
118. Porter, A. Covalently grafted VEGF165 in hydrogel models upregulates the cellular pathways associated with angiogenesis. *Am. J. ...* 1086–1092 (2011). doi:10.1152/ajpccell.00090.2011.
119. Moon, J. J. J. *et al.* Biomimetic hydrogels with pro-angiogenic properties. *Biomaterials* **31**, 3840–7 (2010).
120. Zhu, J., He, P., Lin, L., Jones, D. R. & Marchant, R. E. Biomimetic poly(ethylene glycol)-based hydrogels as scaffolds for inducing endothelial adhesion and capillary-like network formation. *Biomacromolecules* **13**, 706–13 (2012).
121. Poché, R. & Saik, J. The mouse cornea as a transplantation site for live imaging of engineered tissue constructs. *Cold Spring Harb. ...* **2010**, (2010).
122. Julie E. Leslie-Barbick, Colette Shen, Christopher Chen, J. L. W. Micron-Scale Spatially Patterned, Covalently Immobilized Vascular Endothelial Growth Factor on Hydrogels Accelerates Endothelial Tubulogenesis and Increases Cellular Angiogenic Responses. *Tissue Eng. Part A* **12**, (2012).
123. Go, A. S. *et al.* Heart disease and stroke statistics--2014 update: a report from the American Heart Association. *Circulation* **129**, e28–e292 (2014).
124. Charest, a, Pepin, A., Shetty, R. & Côté, C. Distribution of SPARC during neovascularisation of degenerative aortic stenosis. *Heart* **92**, 1844–9 (2006).
125. Rajamannan, N. M. *et al.* Calcified rheumatic valve neoangiogenesis is associated with vascular endothelial growth factor expression and osteoblast-like bone formation. *Circulation* **111**, 3296–301 (2005).
126. Collett, G. D. M. & Canfield, A. E. Angiogenesis and pericytes in the initiation of ectopic calcification. *Circ. Res.* **96**, 930–8 (2005).
127. Yoshioka, M. *et al.* Chondromodulin-I maintains cardiac valvular function by preventing angiogenesis. *Nat. Med.* **12**, 1151–9 (2006).
128. Teo, K. K., Corsi, D. J., Tam, J. W., Dumesnil, J. G. & Chan, K. L. Lipid lowering on progression of mild to moderate aortic stenosis: meta-analysis of the

- randomized placebo-controlled clinical trials on 2344 patients. *Can. J. Cardiol.* **27**, 800–8 (2011).
129. Ishijima, M. *et al.* Perlecan modulates VEGF signaling and is essential for vascularization in endochondral bone formation. *Matrix Biol.* **31**, 234–45 (2012).
  130. Xu, S. *et al.* Rac inhibition reverses the phenotype of fibrotic fibroblasts. *PLoS One* **4**, e7438 (2009).
  131. Yang, J.-H., Wylie-Sears, J. & Bischoff, J. Opposing actions of Notch1 and VEGF in post-natal cardiac valve endothelial cells. *Biochem. Biophys. Res. Commun.* **374**, 512–6 (2008).
  132. Gu, X. & Masters, K. S. Role of the Rho pathway in regulating valvular interstitial cell phenotype and nodule formation. *Am. J. Physiol. Heart Circ. Physiol.* **300**, H448–58 (2011).
  133. Sakabe, M. *et al.* Rho kinases regulate endothelial invasion and migration during valvuloseptal endocardial cushion tissue formation. *Dev. Dyn.* **235**, 94–104 (2006).
  134. Hoang, M. V, Whelan, M. C. & Senger, D. R. Rho activity critically and selectively regulates endothelial cell organization during angiogenesis. *Proc. Natl. Acad. Sci. U. S. A.* **101**, 1874–9 (2004).
  135. Afek, A. *et al.* Increased endothelial cell expression of alpha3beta1 integrin in cardiac valvulopathy in the primary (Hughes) and secondary antiphospholipid syndrome. *Lupus* **8**, 502–7 (1999).
  136. Nakajima, Y., Mironov, V., Yamagishi, T., Nakamura, H. & Markwald, R. R. Expression of smooth muscle alpha-actin in mesenchymal cells during formation of avian endocardial cushion tissue: a role for transforming growth factor beta3. *Dev. Dyn.* **209**, 296–309 (1997).
  137. Stephens, E. H., Durst, C. A., West, J. L. & Grande-Allen, K. J. Mitral valvular interstitial cell responses to substrate stiffness depend on age and anatomic region. *Acta Biomater.* **7**, 75–82 (2011).
  138. Zudaire, E., Gambardella, L., Kurcz, C. & Vermeren, S. A computational tool for quantitative analysis of vascular networks. *PLoS One* **6**, e27385 (2011).

139. Gould, D. J., Vadakkan, T. J., Poché, R. A. & Dickinson, M. E. Multifractal and lacunarity analysis of microvascular morphology and remodeling. *Microcirculation* **18**, 136–151 (2011).
140. Takada, Y., Khuri, F. R. & Aggarwal, B. B. Protein farnesyltransferase inhibitor (SCH 66336) abolishes NF-kappaB activation induced by various carcinogens and inflammatory stimuli leading to suppression of NF-kappaB-regulated gene expression and up-regulation of apoptosis. *J. Biol. Chem.* **279**, 26287–99 (2004).
141. Ishizaki, T. *et al.* Pharmacological properties of Y-27632, a specific inhibitor of rho-associated kinases. *Mol. Pharmacol.* **57**, 976–83 (2000).
142. Lee, S.-H., Kunz, J., Lin, S.-H. & Yu-Lee, L. 16-kDa prolactin inhibits endothelial cell migration by down-regulating the Ras-Tiam1-Rac1-Pak1 signaling pathway. *Cancer Res.* **67**, 11045–53 (2007).
143. Rodriguez, L., Wu, X. & Guan, J. Wound-healing assay. *Cell Migr.* **294**, 23–29 (2005).
144. Davis, G. E. & Bayless, K. J. An integrin and Rho GTPase-dependent pinocytic vacuole mechanism controls capillary lumen formation in collagen and fibrin matrices. *Microcirculation* **10**, 27–44 (2003).
145. Bryan, B. A. *et al.* RhoA/ROCK signaling is essential for multiple aspects of VEGF-mediated angiogenesis. *FASEB J.* **24**, 3186–95 (2010).
146. Bijman, M. N. A., van Nieuw Amerongen, G. P., Laurens, N., van Hinsbergh, V. W. M. & Boven, E. Microtubule-targeting agents inhibit angiogenesis at subtoxic concentrations, a process associated with inhibition of Rac1 and Cdc42 activity and changes in the endothelial cytoskeleton. *Mol. Cancer Ther.* **5**, 2348–57 (2006).
147. Yin, L. *et al.* Fasudil inhibits vascular endothelial growth factor-induced angiogenesis in vitro and in vivo. *Mol. Cancer Ther.* **6**, 1517–25 (2007).
148. Colomba, A. *et al.* Inhibition of Rac controls NPM-ALK-dependent lymphoma development and dissemination. *Blood Cancer J.* **1**, e21 (2011).
149. Caira, F. C. *et al.* Human degenerative valve disease is associated with up-regulation of low-density lipoprotein receptor-related protein 5 receptor-mediated bone formation. *J. Am. Coll. Cardiol.* **47**, 1707–12 (2006).

150. Mohler, III, E. R. *et al.* Bone formation and inflammation in cardiac valves. *Circulation* **103**, 1522–8 (2001).
151. Mohler, E. R. *et al.* Identification and characterization of calcifying valve cells from human and canine aortic valves. *J. Heart Valve Dis.* **8**, 254–60 (1999).
152. O'Brien, K. D. *et al.* Osteopontin is expressed in human aortic valvular lesions. *Circulation* **92**, 2163–8 (1995).
153. Butcher, J. T., Mahler, G. J. & Hockaday, L. A. Aortic valve disease and treatment: the need for naturally engineered solutions. *Adv. Drug Deliv. Rev.* **63**, 242–68 (2011).
154. Jian, B., Narula, N., Li, Q., Mohler, E. R. & Levy, R. J. Progression of aortic valve stenosis: TGF-beta1 is present in calcified aortic valve cusps and promotes aortic valve interstitial cell calcification via apoptosis. *Ann. Thorac. Surg.* **75**, 457–65; discussion 465–6 (2003).
155. Tao, G., Kotick, J. D. & Lincoln, J. Heart valve development, maintenance, and disease: the role of endothelial cells. *Curr. Top. Dev. Biol.* **100**, 203–32 (2012).
156. Butcher, J. T. & Nerem, R. M. Valvular endothelial cells regulate the phenotype of interstitial cells in co-culture: effects of steady shear stress. *Tissue Eng.* **12**, 905–15 (2006).
157. Wang, H., Sridhar, B., Leinwand, L. A. & Anseth, K. S. Characterization of cell subpopulations expressing progenitor cell markers in porcine cardiac valves. *PLoS One* **8**, e69667 (2013).
158. Tseng, H. *et al.* A three-dimensional co-culture model of the aortic valve using magnetic levitation. *Acta Biomater.* **10**, 173–82 (2014).
159. Balaoing, L. R., Post, A. D., Liu, H., Minn, K. T. & Grande-Allen, K. J. Age-related changes in aortic valve hemostatic protein regulation. *Arterioscler. Thromb. Vasc. Biol.* **34**, 72–80 (2014).
160. Gould, S. T., Matherly, E. E., Smith, J. N., Heistad, D. D. & Anseth, K. S. The role of valvular endothelial cell paracrine signaling and matrix elasticity on valvular interstitial cell activation. *Biomaterials* **35**, 3596–606 (2014).
161. Benton, J. A. *et al.* Photocrosslinking of gelatin macromers to synthesize porous



- hydrogels that promote valvular interstitial cell function. *Tissue Eng. Part A* **15**, 3221–30 (2009).
162. Chen, M. B., Sriganapalan, S., Wheeler, A. R. & Simmons, C. A. A 3D microfluidic platform incorporating methacrylated gelatin hydrogels to study physiological cardiovascular cell-cell interactions. *Lab Chip* **13**, 2591–8 (2013).
163. Duan, B., Hockaday, L. A., Kapetanovic, E., Kang, K. H. & Butcher, J. T. Stiffness and adhesivity control aortic valve interstitial cell behavior within hyaluronic acid based hydrogels. *Acta Biomater.* **9**, 7640–50 (2013).
164. Eslami, M. *et al.* Fiber-reinforced hydrogel scaffolds for heart valve tissue engineering. *J. Biomater. Appl.* (2014). doi:10.1177/0885328214530589
165. Durst, C. A., Cuchiara, M. P., Mansfield, E. G., West, J. L. & Grande-Allen, K. J. Flexural characterization of cell encapsulated PEGDA hydrogels with applications for tissue engineered heart valves. *Acta Biomater.* **7**, 2467–76 (2011).
166. Kirschner, C. M., Alge, D. L., Gould, S. T. & Anseth, K. S. Clickable, Photodegradable Hydrogels to Dynamically Modulate Valvular Interstitial Cell Phenotype. *Adv. Healthc. Mater.* (2014). doi:10.1002/adhm.201300288
167. Gould, S. T. & Anseth, K. S. Role of cell-matrix interactions on VIC phenotype and tissue deposition in 3D PEG hydrogels. *J. Tissue Eng. Regen. Med.* (2013). doi:10.1002/term.1836
168. Duan, B., Hockaday, L. A., Kang, K. H. & Butcher, J. T. 3D bioprinting of heterogeneous aortic valve conduits with alginate/gelatin hydrogels. *J. Biomed. Mater. Res. A* **101**, 1255–64 (2013).
169. Weind, K. L., Ellis, C. G. & Boughner, D. R. Aortic valve cusp vessel density: relationship with tissue thickness. *J. Thorac. Cardiovasc. Surg.* **123**, 333–40 (2002).
170. Shworak, N. W. Angiogenic modulators in valve development and disease: does valvular disease recapitulate developmental signaling pathways? *Curr. Opin. Cardiol.* **19**, 140–6 (2004).
171. Hakuno, D., Kimura, N., Yoshioka, M. & Fukuda, K. Molecular mechanisms underlying the onset of degenerative aortic valve disease. *J. Mol. Med. (Berl)*. **87**, 17–24 (2009).

172. Mohler, E. R. *et al.* Bone formation and inflammation in cardiac valves. *Circulation* **103**, 1522–8 (2001).
173. Walker, G. A., Masters, K. S., Shah, D. N., Anseth, K. S. & Leinwand, L. A. Valvular myofibroblast activation by transforming growth factor-beta: implications for pathological extracellular matrix remodeling in heart valve disease. *Circ. Res.* **95**, 253–60 (2004).
174. van Meurs, M. *et al.* Bench-to-bedside review: Angiopoietin signalling in critical illness - a future target? *Crit. Care* **13**, 207 (2009).
175. Arevalos, C. A. *et al.* Regulation of valve endothelial cell vasculogenic network architectures with ROCK and Rac inhibitors. *Microvasc. Res.* **98C**, 108–118 (2015).
176. Bryan, B. A. & D'Amore, P. A. Pericyte isolation and use in endothelial/pericyte coculture models. *Methods Enzymol.* **443**, 315–31 (2008).
177. Petrie, R. J., Doyle, A. D. & Yamada, K. M. Random versus directionally persistent cell migration. *Nat. Rev. Mol. Cell Biol.* **10**, 538–49 (2009).
178. Martins, M. *et al.* Activity of PLC $\epsilon$  contributes to chemotaxis of fibroblasts towards PDGF. *J. Cell Sci.* **125**, 5758–69 (2012).
179. Jakobsson, L. *et al.* Endothelial cells dynamically compete for the tip cell position during angiogenic sprouting. *Nat. Cell Biol.* **12**, 943–53 (2010).
180. Armstrong, E. J. & Bischoff, J. Heart valve development: endothelial cell signaling and differentiation. *Circ. Res.* **95**, 459–70 (2004).
181. Nguyen, D.-H. T. *et al.* Biomimetic model to reconstitute angiogenic sprouting morphogenesis in vitro. *Proc. Natl. Acad. Sci. U. S. A.* **110**, 6712–7 (2013).
182. Melero-Martin, J. M. *et al.* In vivo vasculogenic potential of human blood-derived endothelial progenitor cells. *Blood* **109**, 4761–8 (2007).
183. Paranya, G. *et al.* Aortic valve endothelial cells undergo transforming growth factor-beta-mediated and non-transforming growth factor-beta-mediated transdifferentiation in vitro. *Am. J. Pathol.* **159**, 1335–43 (2001).

184. Witt, W. *et al.* Sphingosine-1-phosphate induces contraction of valvular interstitial cells from porcine aortic valves. *Cardiovasc. Res.* **93**, 490–7 (2012).
185. Fernández-Pisonero, I. *et al.* Synergy between sphingosine 1-phosphate and lipopolysaccharide signaling promotes an inflammatory, angiogenic and osteogenic response in human aortic valve interstitial cells. *PLoS One* **9**, e109081 (2014).
186. Stankunas, K., Ma, G. K., Kuhnert, F. J., Kuo, C. J. & Chang, C.-P. VEGF signaling has distinct spatiotemporal roles during heart valve development. *Dev. Biol.* **347**, 325–36 (2010).
187. Oubaha, M. *et al.* Formation of a PKC $\zeta$ / $\beta$ -catenin complex in endothelial cells promotes angiotensin-1-induced collective directional migration and angiogenic sprouting. *Blood* **120**, 3371–81 (2012).
188. Bosse, K. *et al.* Endothelial nitric oxide signaling regulates Notch1 in aortic valve disease. *J. Mol. Cell. Cardiol.* **60**, 27–35 (2013).
189. Lukasz, A., Kümpers, P. & David, S. Role of angiotensin/tie2 in critical illness: promising biomarker, disease mediator, and therapeutic target? *Scientifica (Cairo)*. **2012**, 160174 (2012).
190. Ucuzian, A. A., Gassman, A. A., East, A. T. & Greisler, H. P. Molecular mediators of angiogenesis. *J. Burn Care Res.* **31**, 158–75 (2010).
191. Sacks, M. S., Schoen, F. J. & Mayer, J. E. Bioengineering challenges for heart valve tissue engineering. *Annu. Rev. Biomed. Eng.* **11**, 289–313 (2009).
192. Butcher, J. T. & Nerem, R. M. Valvular endothelial cells and the mechanoregulation of valvular pathology. *Philos. Trans. R. Soc. Lond. B. Biol. Sci.* **362**, 1445–57 (2007).
193. Tressel, S. L., Huang, R.-P., Tomsen, N. & Jo, H. Laminar shear inhibits tubule formation and migration of endothelial cells by an angiotensin-2 dependent mechanism. *Arterioscler. Thromb. Vasc. Biol.* **27**, 2150–6 (2007).
194. Cuy, J. L., Beckstead, B. L., Brown, C. D., Hoffman, A. S. & Giachelli, C. M. Adhesive protein interactions with chitosan: consequences for valve endothelial cell growth on tissue-engineering materials. *J. Biomed. Mater. Res. A* **67**, 538–47 (2003).

195. Shyu, K. G., Chang, M. L., Wang, B. W., Kuan, P. & Chang, H. Cyclical mechanical stretching increases the expression of vascular endothelial growth factor in rat vascular smooth muscle cells. *J. Formos. Med. Assoc.* **100**, 741–7 (2001).
196. McIntosh, C. T. & Warnock, J. N. Side-specific characterization of aortic valve endothelial cell adhesion molecules under cyclic strain. *J. Heart Valve Dis.* **22**, 631–9 (2013).
197. Ranade, S. S. *et al.* Piezo1, a mechanically activated ion channel, is required for vascular development in mice. *Proc. Natl. Acad. Sci. U. S. A.* **111**, 10347–52 (2014).
198. Sucusky, P., Balachandran, K., Elhammali, A., Jo, H. & Yoganathan, A. P. Altered shear stress stimulates upregulation of endothelial VCAM-1 and ICAM-1 in a BMP-4- and TGF-beta1-dependent pathway. *Arterioscler. Thromb. Vasc. Biol.* **29**, 254–60 (2009).
199. Balachandran, K., Konduri, S., Sucusky, P., Jo, H. & Yoganathan, A. P. An ex vivo study of the biological properties of porcine aortic valves in response to circumferential cyclic stretch. *Ann. Biomed. Eng.* **34**, 1655–65 (2006).
200. Balachandran, K., Sucusky, P., Jo, H. & Yoganathan, A. P. Elevated cyclic stretch alters matrix remodeling in aortic valve cusps: implications for degenerative aortic valve disease. *Am. J. Physiol. Heart Circ. Physiol.* **296**, H756–64 (2009).
201. Starke, R. D. *et al.* Endothelial von Willebrand factor regulates angiogenesis. *Blood* **117**, 1071–80 (2011).
202. Lee, W. *et al.* Synergy between Piezo1 and Piezo2 channels confers high-strain mechanosensitivity to articular cartilage. *Proc. Natl. Acad. Sci. U. S. A.* **111**, E5114–22 (2014).
203. Li, J. *et al.* Piezo1 integration of vascular architecture with physiological force. *Nature* **515**, 279–82 (2014).
204. McHugh, B. J., Murdoch, A., Haslett, C. & Sethi, T. Loss of the integrin-activating transmembrane protein Fam38A (Piezo1) promotes a switch to a reduced integrin-dependent mode of cell migration. *PLoS One* **7**, e40346 (2012).
205. Hegen, A. *et al.* Efficient in vivo vascularization of tissue-engineering scaffolds. *J. Tissue Eng. Regen. Med.* **5**, e52–62 (2011).

206. Suh, K. Y., Seong, J., Khademhosseini, A., Laibinis, P. E. & Langer, R. A simple soft lithographic route to fabrication of poly(ethylene glycol) microstructures for protein and cell patterning. *Biomaterials* **25**, 557–563 (2004).
207. Miller, J. S. *et al.* Rapid casting of patterned vascular networks for perfusable engineered three-dimensional tissues. *Nat. Mater.* **11**, 768–74 (2012).
208. Ali, S., Saik, J. E., Gould, D. J., Dickinson, M. E. & West, J. L. Immobilization of Cell-Adhesive Laminin Peptides in Degradable PEGDA Hydrogels Influences Endothelial Cell Tubulogenesis. *Biores. Open Access* **2**, 241–9 (2013).
209. Jain, R. K. Normalization of tumor vasculature: an emerging concept in antiangiogenic therapy. *Science* **307**, 58–62 (2005).
210. Moon, J. J., Hahn, M. S., Kim, I., Nsiah, B. A. & West, J. L. Endothelial Morphogenesis. **14**, 1–7 (2008).
211. Julie E. Leslie-Barbick, Colette Shen, Christopher Chen, J. L. W. *et al.* Vascular Endothelial Growth Factor on Hydrogels Accelerates Endothelial Tubulogenesis and Increases Cellular Angiogenic Responses. *Tissue Eng. Part A* **17**, (2011).
212. Chen, J. & Simmons, C. A. Critical Roles for Matricellular , Matricrine , and Matrix Mechanics Cues. 1510–1524 (2011). doi:10.1161/CIRCRESAHA.110.234237
213. Puperi, D. S., Balaoing, L. R., O’Connell, R. W., West, J. L. & Grande-Allen, K. J. 3-Dimensional spatially organized PEG-based hydrogels for an aortic valve co-culture model. *Biomaterials* **67**, 354–64 (2015).
214. Johnson, L. M., Deforest, C. A., Pendurti, A., Anseth, K. S. & Bowman, C. N. Formation of three-dimensional hydrogel multilayers using enzyme-mediated redox chain initiation. *ACS Appl. Mater. Interfaces* **2**, 1963–72 (2010).
215. Tseng, H. *et al.* Anisotropic poly(ethylene glycol)/polycaprolactone hydrogel-fiber composites for heart valve tissue engineering. *Tissue Eng. Part A* **20**, 2634–45 (2014).



